10-31-2021

Prospect of harnessing solar energy, offshore wind energy and installing liquid air energy storage system to power Chittagong Port and design of a hybrid power system

Muhammad Abul Basar

WORLD MARITIME UNIVERSITY
Malmö, Sweden

PROSPECT OF HARNESSING SOLAR ENERGY, OFFSHORE WIND ENERGY AND INSTALLING LIQUID AIR ENERGY STORAGE SYSTEM TO POWER CHITTAGONG PORT AND DESIGN OF A HYBRID POWER SYSTEM

By

MUHAMMAD ABUL BASAR

A dissertation submitted to the World Maritime University in partial fulfilment of the requirements for the reward of the degree of

MASTER OF SCIENCE
in
MARITIME AFFARS

(MARITIME ENERGY MANAGEMENT)

2021

Declaration

I certify that all the material in this dissertation that is not my own work has been identified, and that no material is included for which a degree has previously been conferred on me.

The contents of this dissertation reflect my own personal views and are not necessarily endorsed by the University.

(Signature): MD.ABUL BASAR

(Date): 21st September 2021

Supervised by:
.....

Supervisor's affiliation**.....**

Acknowledgements

First of all, I convey shukria (Thank) to Almighty Allah for successful completion of my master's degree dissertation. At the same time, I thank my mother and wife for their kind support. I would like to convey my gratitude to my supervisor Professor Alessandro Schonborn, Assistant Professor, Maritime Energy Management, World Maritime University, Malmo, Sweden for his continued guidance in completion of my dissertation.

Special thanks to Professor Aykut I. Olcer, Department head, Maritime Energy Management, World Maritime University for his motivation. I also convey special thanks to Commodore Syed Ariful Islam, ex-Director General of Department of Shipping, Bangladesh for his support. Besides, my sincere gratitude to Commodore Abu Zafar Muhammad Jalal Uddin, Director General, Department of Shipping, Bangladesh for granting my leave to attend my master's degree.

Abstract

TITLE OF DISSERTATION: PROSPECT OF HARNESSING SOLAR ENERGY, OFFSHORE WIND ENERGY AND INSTALLING LIQUID AIR ENERGY STORAGE SYSTEM TO POWER CHITTAGONG PORT AND DESIGN OF A HYBRID POWER SYSTEM

Degree: **Master of Science**

KEYWORDS:

The Earth- ultimate dwelling place for about 7.9 billion human is being struck by one after another natural disasters and calamities. Entire human race is facing existential threat at the moment. Mankind already suffering globally from the deadliest virus ever known to forest fires, heatwaves, locust swarms, excessive rains, and floods. Global nations are all in agreement that majority of these disasters are linked to climate change. Hence, Climate change is a matter of serious concern at all levels of global environmental forum and discussions. Emission of GHGs in the atmosphere is accelerating the climate change. Unfortunately, international shipping is one of the contributors of this harmful GHG emissions to atmosphere. Global ports operation is a prominent source of this emission from international shipping. International Maritime Organization (IMO) is acting competently to reduce emission of pollutants from shipping through various environmental regulatory instruments. Technology innovators, scholars are developing innovative technologies for decarbonization of international shipping. Renewable energy applications are being developed and promoted as a solution in this regard. Energy generation technology from renewable wind and solar energy is well matured now while innovative ideas like liquid air energy storage system is being developed. Unlike other global nations, Bangladesh - an emerging developing country is considering reducing its carbon footprint by establishment of renewable energy solutions although very less study and data is available for specific high potential areas of Bangladesh. This research proposed and highlighted means to meet power demand of Chittagong port harnessing green energy from abundant offshore wind energy, solar energy and LAES system.

Table of Contents

List of Tables

List of Figures

Appendices

List of Abbreviations

AC : Alternating Current
BDC : Bottom Dead Centre
BPDB: Bangladesh Power Development Board
CPA : Chittagong Port Authority
DHI : Direct Horizontal Irradiance
DIFF : Diffuse Irradiance
DC : Direct Current
GDP: Gross Domestic Product
GHG : Green House Gas
GWC : Global Wind Atlas

GWC : Generalized Wind Climate data
GHI : Global Horizontal Irradiance
HEF: Heat Exchange Fluid
IMO : International Maritime Organization
IFC : International Finance Corporation
KWh : Kilowatt hour
LAES: Liquid Air Energy Storage
LCOE : Levelized Cost of Electricity
LCA : Life Cycle Assessment
LAEN : Liquid Air Energy Network
MPPT : Maximum Power Point Tracking
MEPC : Marine Environment Protection Committee
MWh: Megawatt hour
ORC : Organic Rankin Cycle
PVGIS: Photovoltaic Geographical Information System
PIV : Peak Inverse Voltage
RTE : Round Trip Efficiency
RTG : Rubber Tyred Gantry Crane
SBSTA: Subsidiary Body for Scientific and Technological Advice
SREDA: Sustainable and Renewable Energy Development Authority
STC : Standard Test Condition
TDC: Top Dead Centre
UNFCC: United Nations Framework Convention on Climate Change
UNSDG: United Nations Sustainable Development Goal
WNA: World Nuclear Association

Chapter - 1

1: Introduction

1.1: Background and History

Climate change is potentially a menacing threat to humanity and mother nature. Global governments-initiated action against climate change under the treaty of 'The 1992 United Nations Framework Convention on Climate Change (UNFCC)'. As a concrete climate action, the 2015 Paris Agreement, set the goal for global mean surface temperature to maintain well below 2°C above the mean of pre-industrial value while attempt to maintain temperature to 1.5°C (Lawrence & Schafer, 2019). Although strategic climate actions are in place, detrimental impacts of climate change on global humans, ecosystems, livelihoods increasing rapidly. As mentioned by UN Secretary General António Guterres in 2018 -

"*Climate change is moving faster than we are,*" (IPCC, 2018). IPCC 2019 report highlighted anthropogenic activities, burning of fossil fuels as responsible for the emission of carbon in the atmosphere which causes global warming. Under a business-as-usual scenario, the current global temperature of 1°C will increase to 1.5°C by the following decades which is a deviation from the track to maintain temperature well below 2°C (IPCC, 2019).

International shipping is one of the key contributors of this harmful GHG emission in the global atmosphere and global port operations are an integral part of it. In the 1995 UNFCC secretariat report, the contribution of international shipping to climate change was addressed, and Article 2(2) of the 1997 Kyoto Protocol mandated IMO for the parties of developed countries in addressing GHG emission from international shipping (Doelle & Chircop, 2019). Considerable measures have been undertaken by IMO so far on the issue and yet international shipping is responsible for about 3% of total global GHG emission (Ölcer et al, 2018). In April 2018, IMO MEPC adopted the "Initial IMO GHG Strategy" by resolution MEPC.304(72) which is marked as a milestone initiative that synchronizes with the 2015 Paris Agreement and UN Sustainable Development Goal 13 (UN SDG-13).

The Fourth IMO GHG study 2018 showed GHG emissions from the maritime sector have increased 9.6% from 977 million tonnes CO_2eq. in 2012 to 1076 million tonnes

CO_2eq in 2018 while according to The Third IMO GHG study in 2008, these emissions were 940 million tonnes CO_2eq (Psaraftis & Kontovas, 2021). Such an increasing trend of GHG emission indicates that international shipping is out of the line to meet the IMO initial GHG strategy to reduce GHG emission by 50% compared to the value of 2008 by the year 2050. Moreover, it is predicted that under a business-as-usual scenario, emissions from international shipping will increase from 50% to 250% by the year 2050 considering faster growth of seaborne trade in the future. In light of this, in its initial strategy, IMO proposed to include measures to improve global ports operation and development of energy-efficient infrastructures with regards to GHG emission reduction.

Bangladesh is an emerging and developing economy. In response to global climate awareness, the Government of Bangladesh also emphasized reducing GHG emissions arising from anthropogenic activities and developed a strategic plan to promote renewable energy. The Power division of The Government of Bangladesh released the “Renewable Energy Policy of Bangladesh” in November 2008. Energy policy 2008 of Bangladesh made a target to produce 10% of total electricity demand from renewable energy sources by 2020. Bangladesh has great potential of producing electricity from solar and wind energy (Islam et al, 2013).

Chittagong port is the busiest and largest seaport in Bangladesh. This port entirely depends on electricity supply from the national grid which mainly burns fossil fuel for electricity generation. Chittagong port is located adjacent to the Bay of Bengal where there is an unexplored potential for electricity generation from solar and wind energy. If these renewable energies are explored and integrated with the port grid, Chittagong port can become self-sufficient with power without depending on supply from the national grid.

1.1: Problem Statement

Chittagong is the busiest and largest seaport in Bangladesh which handles 92% of countries seaborne trade. The power demand for this port is met by two main sub-stations of 33/11KV capacity and twelve 11/0.4 KV electrical substations connected to the national grid. National grid power is mainly generated from fossil fuel sources. Besides, the port is equipped with one 2.5 MW and four 2.0 MW diesel generators

for backup power supply (SMP-CP, 2015). According to the strategic master plan for Chittagong port 2015, the port's maximum peak hour power demand is approximately 10 MW and the port's authority strategically decided to establish a new power plant of 30 MW capacity which will be upgraded to 50 MW later on. No mention is found regarding power generation from renewable energy sources despite the port is located close to the Bay of Bengal where there is potential scope to generate electricity from Solar and Wind energy.

The problem of harnessing these renewable energies in Bangladesh is that there is a lack of substantial data and literature in this regard. Study in this sector is essential to explore power generation potential from the Bay of Bengal using renewable energy sources. Comprehensive research to harness solar energy, offshore wind energy of the Bay of Bengal is urgent to demonstrate and motivate policymakers of Bangladesh which resultantly can pave the way to transform Chittagong port into a green port.

1.2: Research Aim and Objective

This study aims is to explore the potential for green electricity generation from renewable solar energy, offshore wind energy, and liquid air energy storage system for Chittagong port and integrate this green electricity with the port grid. To achieve this goal, the following research objectives are determined-

1. To study theories and technologies for green electricity generation from renewable wind energy, solar energy, and liquid air energy storage system.
2. To study the potential solar energy, wind energy available at Chittagong port area.
3. To provide sample calculations for the time-averaged operation of a renewable energy power plant to the meet total power demand of Chittagong port utilizing photo-voltaic panels, wind turbine, and liquid air energy storage system.
4. To design a grid-tie hybrid "Photovoltaic-Wind Turbine-Liquid Air Energy Storage(PV-WT-LAES) " electricity system to integrate green electricity generated from renewable energy sources with the port grid.

1.3: Research Questions

This research will strive to find answers to the below questions -

1. How much electricity can be produced from renewable wind and solar energy at Chittagong port and how much can be stored in a liquid air energy storage system to meet the emergency demand of Chittagong port?
2. How this green electricity generated by renewable wind energy, solar energy, and liquid air energy storage system can be connected with the port grid?
3. How much GHG emission can be saved if the above electricity generation system is installed at the Chittagong port?

1.4: Research Methodology

In this study, electricity generation from renewable energy of wind, solar and liquid air energy storage system is explored for the Chittagong port. For this purpose, at first, qualitative data describing energy production from wind, solar and liquid air energy storage systems is obtained through extensive literature study. At this stage, fundamental theory and mathematical equations for power and other required calculations related to these systems are established. Then, quantitative primary data was collected for selected locations from “Global Wind Atlas” (globalwindatlas.info) for wind energy and “Photovoltaic Geographical Information System (PVGIS)” (https://re.jrc.ec.europa.eu) database for solar energy. Details of this data collection process are described in section 3.2. Later on, the time-averaged probability distribution of wind speed occurrence is used to calculate the time-averaged power and energy production for the site based on data from the Global Wind Atlas for the chosen site at the Chittagong port. This calculation was performed in a computer program written in the “Python version 3.9.2” programming language. Details of wind energy calculations are described in section 3.1 of this literature.

PVGIS software is used for solar energy calculations. Details of solar energy applications are described in chapter 4.2. A LAES system is briefly discussed and analyzed in chapter 2.6 based on an extensive literature review. In chapter 5, the

design of a grid-tie hybrid “PV-WT-LAES” electricity system is established using simple mathematical formulas with the help of a Microsoft excel calculation sheet. Finally, the literature is concluded with discussions of calculation results, recommendations and limitations mentioned.

The flow chart of this research is as mentioned in figure 1 -

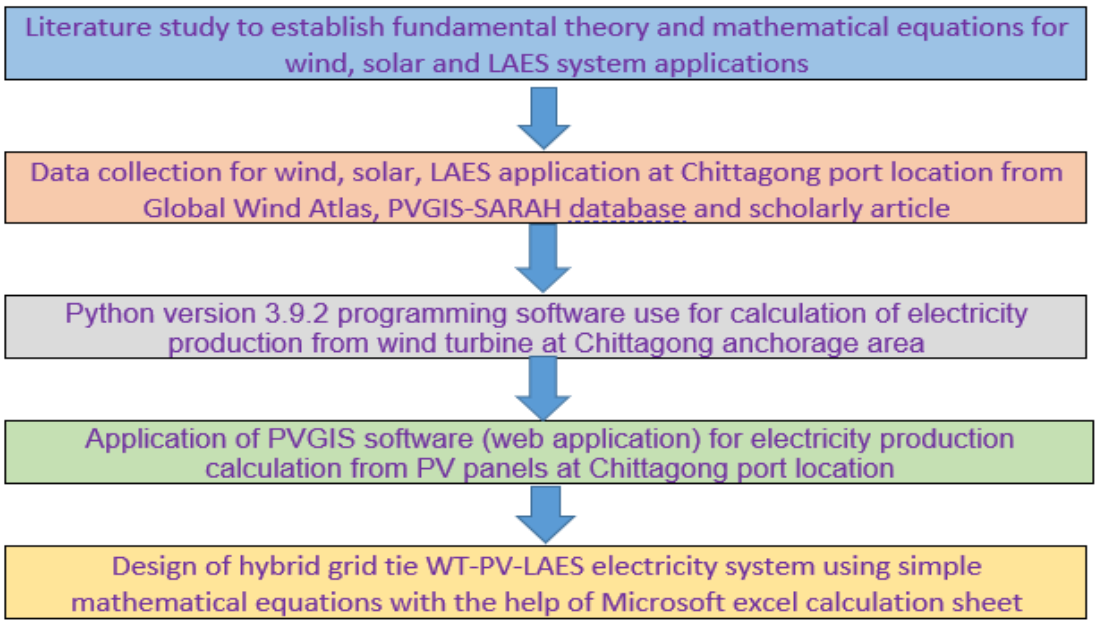

Figure 1: Flow chart of research methodology

Chapter - 2

2.0 : Literature Review

Bangladesh is a developing country with one of the world’s largest GDP growth rates. Energy is crucial for the development of Bangladesh which enables export-based industries, commerce to run un-interrupt. But Bangladesh is facing energy scarcity while day by day supply and demand gap for energy increasing. Approximately 70% of the total energy demand in Bangladesh is met by electricity production from natural gas. Unfortunately, countries natural gas reserve is not substantial and already started to import LPG, to supplement oil (Hydrocarbon unit, 2019). For sustainable development, Bangladesh must initiate power generation from renewable sources. Now, the status of renewable energy generation is very less than required. According to the Government hydrocarbon unit report, in the

year 2017-2018, Bangladesh produced 10958 MW of electricity of which 68% is produced from domestic sources (Coal, Natural gas, Hydropower), 24% generated by the use of petroleum fuels like furnace oil, diesel which is completely imported and 8% of total electricity were imported from India. This statistic demonstrates how significant it is for Bangladesh to harness renewable energy. In light of this, the Government of Bangladesh formulated the “Energy policy 2008” and targeted to generate 10% of the total energy production from renewable energy (GOB, 2008). Thereafter, enacted SREDA act 2012 was to establish the “Sustainable and Renewable Energy Development Authority (SREDA)” whose mandate is to promote renewable energy generation in Bangladesh. Despite governments intervention, electricity generation from renewable energy sources up to 2018 was only 570 MW out of 18,753 MW which is only 3% of the total power generation (Hydrocarbon Unit, 2019). The Pie chart in figure 2 shows clearly how negligible the share of power generation from RE sources in Bangladesh is-

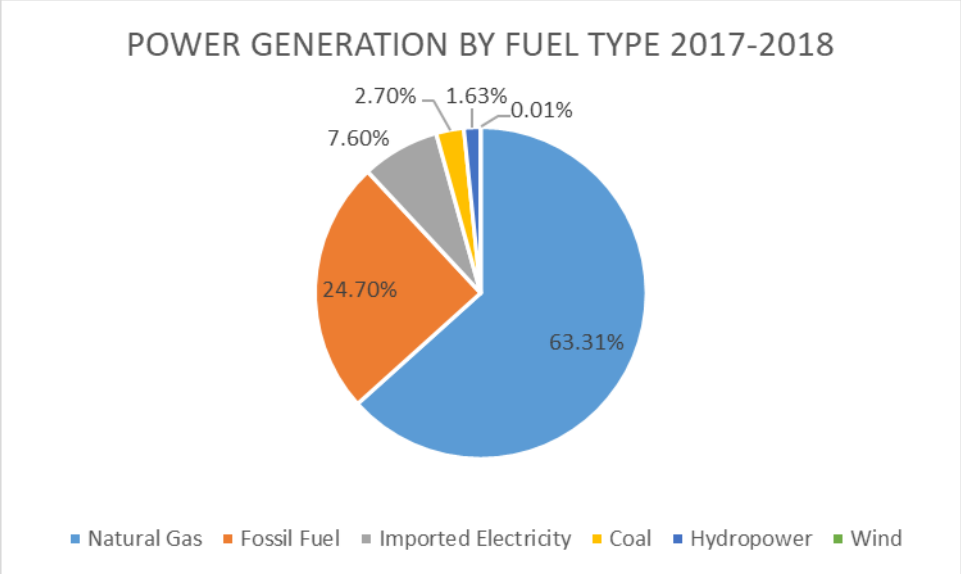

Figure 2: Bangladesh power generation by fuel type 2017-2018. Data collected from Hydrocarbon Unit, Bangladesh report 2019.

Bangladesh has potential RE sources although unexplored. Geographically the country is situated in a suitable location ($20^0 34'$ to $26^0 38'$ north latitude) to harness sunlight where solar irradiance is abundantly available throughout the year. Approximately 4 to 7 KWh/m^2/day solar energy is available in Bangladesh. Currently

very little of this energy is harnessed. A similar scenario exists concerning wind energy, despite its enormous potential. However, the government is currently planning to set up a pilot project by the seashore adjacent to Chittagong port to generate 20 MW of electricity by installing windmills. 200 MW power generation from wind energy will be considered upon the success of the 20 MW approved project. As the Government of Bangladesh is already strategically decided to harness wind energy and solar energy from seashore, this study aims to explore feasibility of powering Chittagong port from wind and solar energy only, although there are prospects for wave energy, geothermal energy and Biomass energy in this area. In the process of electricity generation from wind and solar energy, this study proposes integration of Liquid Air Energy Storage (LAES) system in a hybrid power system as a backup during unavailability or overcapacity of wind and solar energy. To understand the potential of electricity generation from renewable solar energy, wind energy, and liquid air energy storage system for Bangladesh, this section of the literature focused on a comprehensive literature review related to these topics.

2.1: Source of Solar Energy.

The sun, a paramount source of energy for almost all life that lives on Earth. It is 109 times bigger than Earth, mass more than 330000 times comparing to Earth. Sun is made of Hydrogen (Approximately 73%), Helium (Approximately 25%), a small quantity of Neon, Iron, Carbon, and Oxygen. Having extremely high temperature at its core, approximately 6000^0 Celsius together with exceedingly high gravitational force, the sun is capable to create nuclear fusion reaction by itself which generates tremendous energy. At the core of the Sun, proton-proton (p-p) chain reaction transforms Hydrogen into Helium. This is how Sun energy is produced which is then released in the form of light and heat at 3.846×10^{26} Joule per Second (Charbonneau, 2014).

Sunlight that we receive in the earth, is nothing but ultra-violate and infrared visible light which is a part of electromagnetic radiation that originated from the sun. In our upper atmosphere insolation (Incoming solar radiation) is about 174000 Terawatts whereas in the earth's surface where we live insolation level is about 3.5-7.5-kilowatt-hours per square meter per day.

2.2: Working principle of PV energy system.

PV panels are made by combining multiple solar cells. If photons hit any solar cells, electrons are separated from atoms. Solar cells are made combining P-type and N-type semiconductors which forms a P-N junction.

P-type semiconductors are doped with Boron and N-type doped with phosphorus to facilitate electrons free movement. When sunlight hit these silicon cells, photon excites electrons. Hence, electrons flow towards P-type silicon cells from N-type silicon cells that creates a positive charge on N-type cells and a negative charge on P-type cells. Electric field is created in this way by combining two different types of semi-conductors which move negative particles in one direction while positively charged particles move in other directions. Electric circuits are made by attaching conductors at the positive as well as the negative sides of the solar cells. If electrons pass through this circuit, this flow of electrons produces electricity. The solar array is made by wiring up many solar panels together. The larger the number of solar panels, the greater the electricity generation.

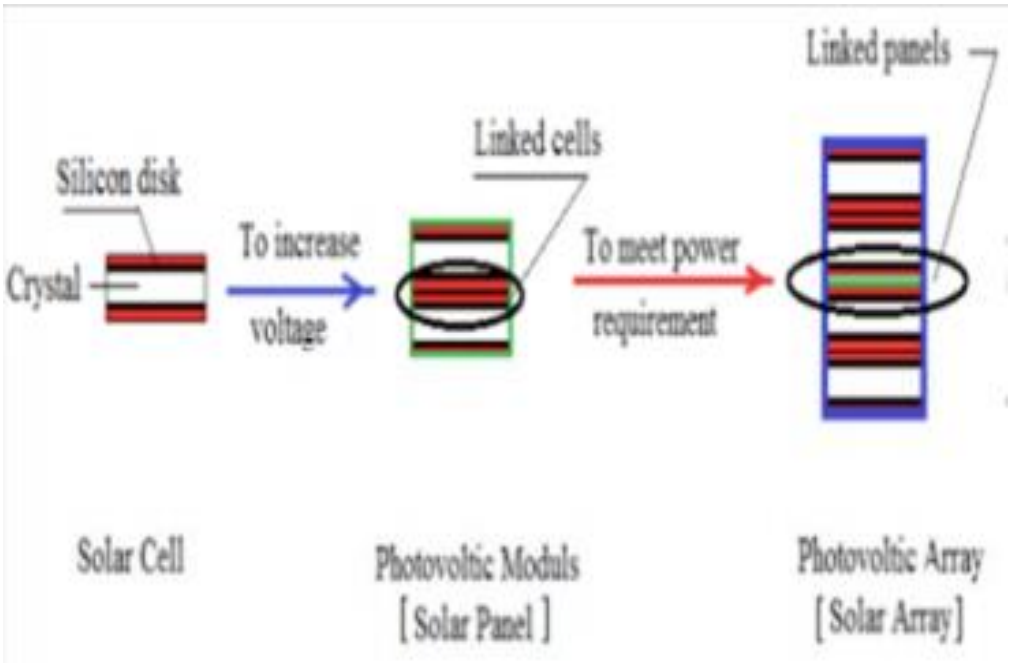

Figure 3: Formation of Solar cells, Solar Panel and Solar Array, Source- (Nyanya & Vu, 2019: Salem & Seddiek, 2017)

.

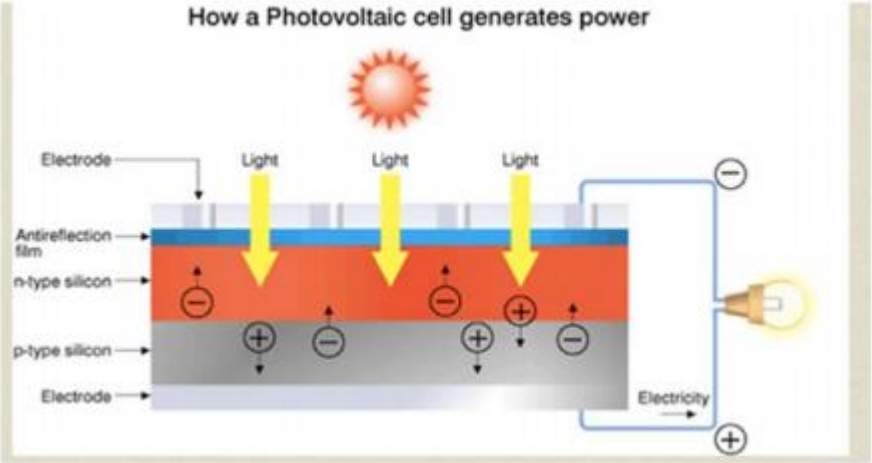

Figure 4: Photovoltaic effects in solar panel, Source- (Nyanya & Vu, 2019 : Bodel & Chiribuga, 2018).

For a better understanding of PV cell characteristics, an electrically equivalent simplified model can be used as in figure 5 -

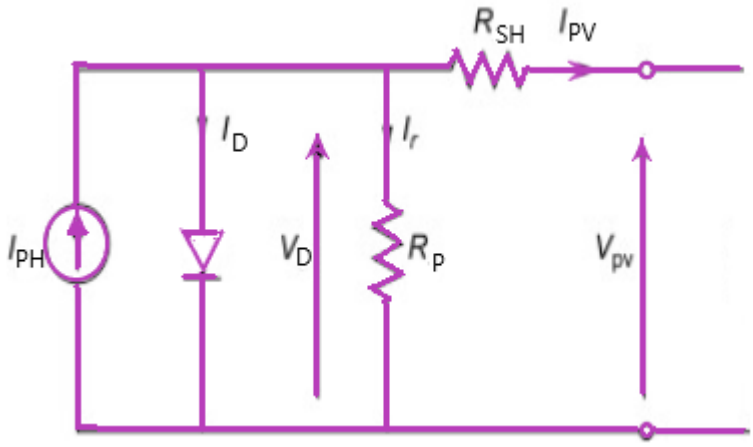

Figure 5: Equivalent circuit for a PV plant, reproduced from - (Rosa-clot & Tina, 2018)

In an equivalent model circuit like above, output current I and Output Volt V for a PV cell can be calculated using formulas below (Rosa-clot & Tina, 2018; Talukdar, 2018)-

$$I = I_{PH} - I_D - \frac{V_D}{R_{SH}}$$

$= I_{PH} - I_O\left(EXP(\frac{Q.V_D}{n.k.T}) - 1\right) - \frac{V_D}{R_{SH}}$

$= I_{PH} - I_O\{EXP(\frac{Q}{n.k.T}(V + R_S.I)) - 1\} - \frac{(V + R_S.I)}{R_{SH}}$ 1

(Rosa-clot & Tina, 2018; Talukdar, 2018)

And,

$V = V_D - R_S . I$ .....2 (Rosa-clot & Tina, 2018; Talukdar, 2018)

Where,

I_0 = Reverse saturation current

Q = Electron charge = 1.6 x 10^{-19} C

I_{PH} = Photocurrent in circuit A

I_D = Average current through diode

V_D = Voltage of Diode

R_{SH} = Equivalent Shunt resistance

k = Boltzmann constant = = 1.38×10^{-23} , J·K^{-1}

T= Temperature of Panel in K

R_S = Intrinsic series resistance (ohm)

When resistance is negligible, the solar cell output current can be calculated as below-

$I = I_{PH} - I_O(EXP(\frac{Q}{n.k.T} . V) - 1)$ 3

In open circuit condition, I = 0, in that case,

Open circuit voltage $V_{OC} = \left(\frac{n.k.T}{Q}\right) In\left(\frac{I_{PH}}{I_0} + 1\right)$

$= \left(\frac{n.k.T}{Q}\right) In\left(\frac{I_{PH}}{I_0}\right)$ 4

But when the circuit is in a shorted condition, the output voltage becomes zero, and average diode current is considered negligible, in that case,

Short circuit current, $I_{sc} = I = \frac{I_{PH}}{\left\{1+\frac{R_S}{R_{SH}}\right\}}$ 5

And PV panel output power is calculated by the below formula-

$P = V . I = \left\{I_{PH} - I_D - \frac{V_D}{R_{SH}}\right\} V$ 6

(Equation 3 to 6 sourced from Rosa-clot & Tina, 2018; Talukdar, 2018)

2.3: Optimise operation of PV system.

For maximum production of solar electricity from any PV system below mechanisms are vital-

1. Accurate PV surface tilt and azimuth operation of PV surface to increase incident solar irradiance.
2. Application of MPPT (Maximum Power Point Tracking) technique for extraction of photovoltaic electricity under varying ambient temperatures and solar irradiance.

For precise tilting and azimuth operation, sun trackers are used (Tang, Wu, & Li, 2018) which monitor sun path and sets PV panels perpendicular against solar irradiance. This way, input is maximized.

There is a direct relation between the power output of PV arrays with load current. Maximum power is achieved at a certain load current value.

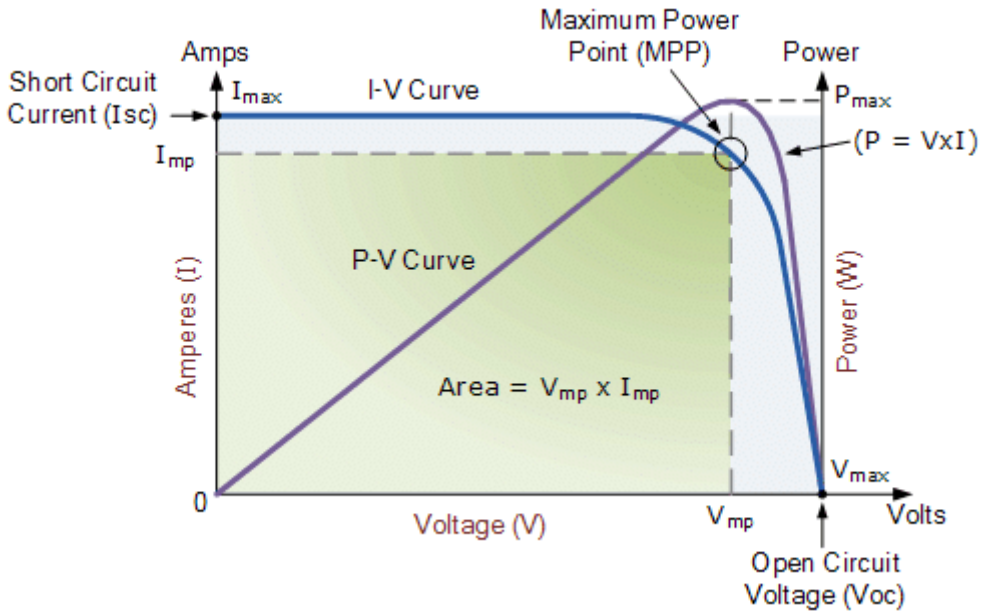

Figure 6: Typical PV panel Current-Voltage characteristics, Source from Jaffer (2018).

MPPT system operates PV panels at that specific load current at which maximum power can be achieved. This is done by using converters (DC-DC) in between

battery banks and solar panels. Alteration of converters driving duty signal causes a change of impedance which is sensed by PV arrays. In this way, the operating point attains the optimum power point position.

2.4: Theory of Solar Irradiation Angle Geometry

During the earth's orbital rotation around the sun, the North pole of the earth tilts 23.45^0 on 21 June towards the sun which is known as the summer solstice, and tilts 23.45^0 on 21 December away from the sun which is known as the winter solstice. As a result, the sun crosses the earth's sky much higher during the noon of June than the noon of December if seen from the northern hemisphere.

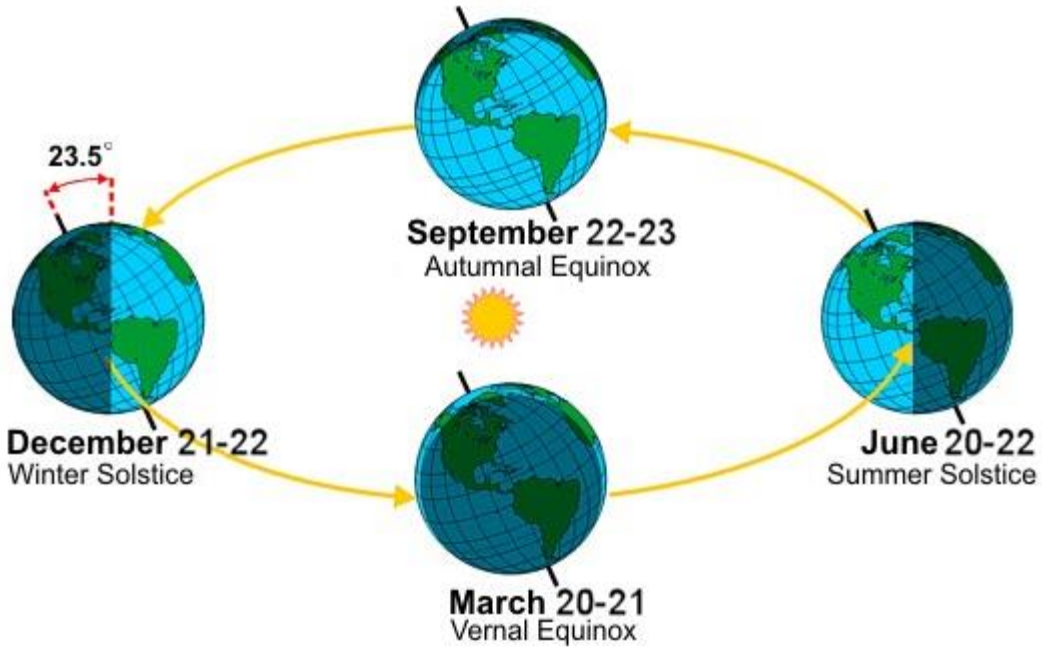

Figure 7: Seasonal configuration of earth and sun, source from- National oceanic and atmospheric administration(NOAA)

Yearly two times, the axis of the earth tilted neither toward the sun nor away from the sun. This causes an almost equal amounts of darkness and daylight at all latitudes. This phenomenon is known as Equinoxes. During this period, days are longer at higher latitudes as the sun takes long time to set and rise. During Equinox, even few a days before and after equinox, the day length at the equator is about 12 hours 6.5 minutes, at 30^0 latitudes 12 hours 8 minutes, at 60^0 latitudes 12 hours 16 minutes (NOAA).

2.4.1: Basic Solar Angles

The solar incidence angle changes around the year because of its rotation on the axis and elliptical orbit. To obtain maximum power from PV panels, sunlight should fall onto the panel at a steep angle. Hence, PV panel tilt angles should be altered monthly as well as seasonally (Karafil et al, 2015). Figure 8 showing various solar angles-

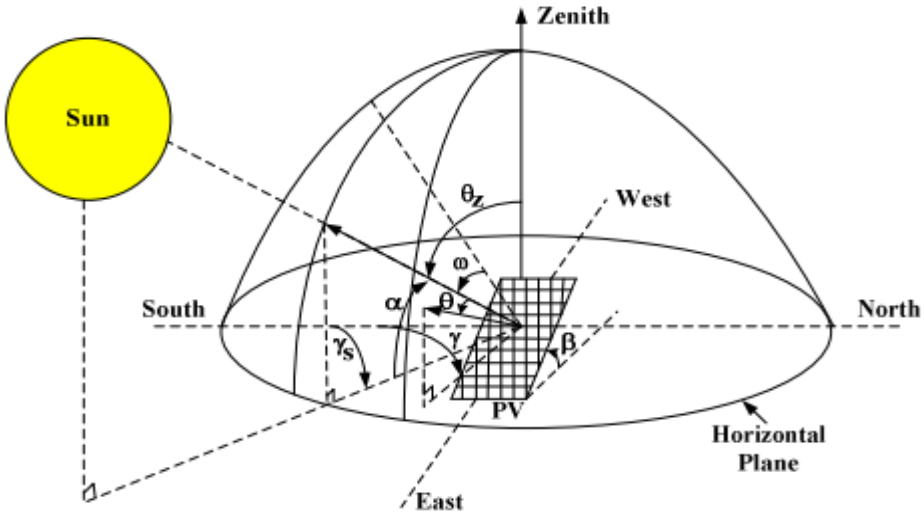

Figure 8: Solar Angles. Adapted from- (Karafil et al, 2015).

Angle form between the vertical axis of PV panel and line to the sun is Zenith angle (θ_z), its calculation depends on some other angle. θ_z is 0^0 at sunset, 90^0 during sunrise.

$$\theta_z = \cos\delta \times \cos\varphi \times \cos\omega + \sin\delta \times \sin\varphi \quad \text{(Karafil et al, 2015)}$$

φ is the Latitude angle that forms according to the equator centre and is used to state any location on the earth's surface. Symbol ω represents the hour angle or the time difference among noon and desired time of the day and is obtained multiplying the time difference with 15 fixed numbers. It is the angle form between the longitudes of the sunlight and the location.

$$\text{Hour Angle } \omega = 15 \text{ (solar time- 12)} \quad \text{……(Karafil et al, 2015)}$$

Solar Azimuth angle (γ_s) is formed between the north or south position of the sun to the solar direct radiation.

$$\gamma_S = \cos^{-1}\{ (\sin\alpha \times \sin\varphi) - \sin\delta / (\cos\alpha \times \cos\varphi) \} \quad \text{……(Karafil et al, 2015)}$$

α - represents the solar elevation angle between line to the sun and horizontal plan.

The solar elevation angle = 90 – zenith angle .....(Karafil et al, 2015).

The angle between the equator plan and sunlight is called 'Declination Angle (δ)'. The value of δ varies between -23.45^0 and 23.45^0, positive at North. On 21st June, the angle is at its highest point (23.45^0) and on 22nd December it is at its lowest point (-23.45^0). δ is calculated as below-

$$\delta = 23.45 \times \sin\left[360 \times \frac{(n+284)}{365}\right] \text{degree}$$ .....(Karafil et al, 2015)

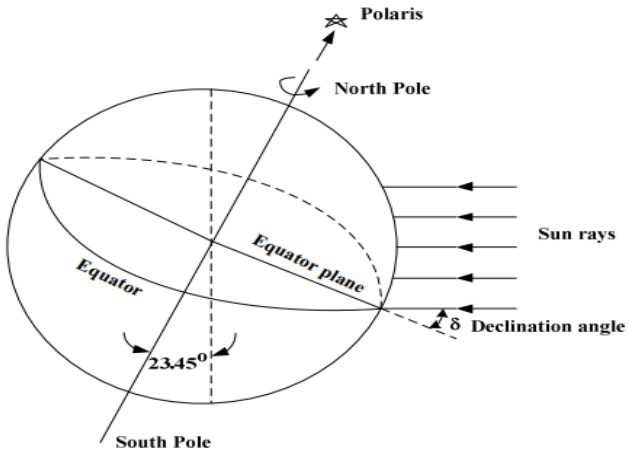

Figure 9: Solar Declination angle. Adapted from (Karafil et al, 2015).

Some other important formula in solar application is as below-

Apparent solar time (AST) = LST + {ET +4(Standard longitude – Local Longitude)}/60 .....(Karafil et al, 2015)

Where LST is local standard time, ET is the equation of time. AST is an hour.

2.4.2: PV Panel Annual Electricity Production Calculation

Instantaneous PV panel power production capacity can be calculated using the below formula (Alsayed et al, 2013; Talukdar, 2018)-

Open circuit voltage V_{oc} (t=0,1,2….24) = V_{oc} at standard temperature condition + K_v {T_c (t=0,1,2….24) – Reference Temperature} 33

Where K_v = Temperature co-efficient of V_{oc} in V/ ^{0}C (Alsayed et al, 2013)

Short circuit current I_{sc} (t=0,1,2….24) = I_{sc} at standard temperature condition + K_i {T_c (t=0,1,2….24) – Reference Temperature} x $\frac{PV\ panel\ Solar\ Irradiance\ (t=0,,1,2,..,24)\ in\ W/m2}{1000}$ 34

Where K_i = Temperature co-efficient of I_{sc} in A/ ^{0}C

(Alsayed et al, 2013)

In both the formula above, reference temperature is defined by manufacturer in ^{0}C and T_c (t=0,1,2,….24) = Site ambient temperature ^{0}C($\frac{cell\ nominal\ operating\ temp\ ℃ - 20}{800}$) x $PV\ panel\ Solar\ Irradiance\ (t = 0,,1,2,..,24)\ in\ W/m2$ …35

PV panel instantaneous power (hourly) can be calculated as below-

P_{pvh} = Inverter efficiency x Transformer efficiency x Fill factor x V_{oc} (t=0,1,2….24) x I_{sc} (t=0,1,2….24) …….36 (Alsayed et al, 2013)

Where Fill factor is applicable to PV panel which can be obtained from voltage-current characteristic curve of PV panel as below-

$$FF = \frac{maximum\ power\ point\ power}{\text{Open circuit voltage Voc (t=0,1,2....24)} \text{ x Short circuit current Isc (t=0,1,2....24)}} \quad \text{…..37}$$

(Alsayed et al, 2013)

PV panel daily power production can be calculated by the below formula-

E_{pvd} = Inverter efficiency x Transformer efficiency x FF x $\sum_{t=1}^{24} \text{Voc (t = 0,1,2 ....24) x Isc (t = 0,1,2 ....24)}$ …….38 (Alsayed et al, 2013)

For monthly power production below formula can be used-

E_{pvm} = E_{pvd} x total days of the month ……39 (Alsayed et al, 2013)

PV panel efficiency reduces with its age; hence the production of electricity also reduces. PV panel yearly lifetime average electricity production can be found using the below formula-

$$E_{pvavgy} = \frac{\text{Epvy} \sum_{t=o}^{\text{Npvl}\wedge -1} x \frac{100 - Mpv\ x\ t}{100}}{\text{Npvl}} \quad \text{……40 (Alsayed et al, 2013; Talukdar, 2018)}$$

Where Epvy is yearly electricity produced by a PV panel which is the summation of all 12 months of electricity production by a PV panel. M_{PV} is the gradient of derated efficiency curve per year. N_{pvl} is the lifetime of the PV panel.

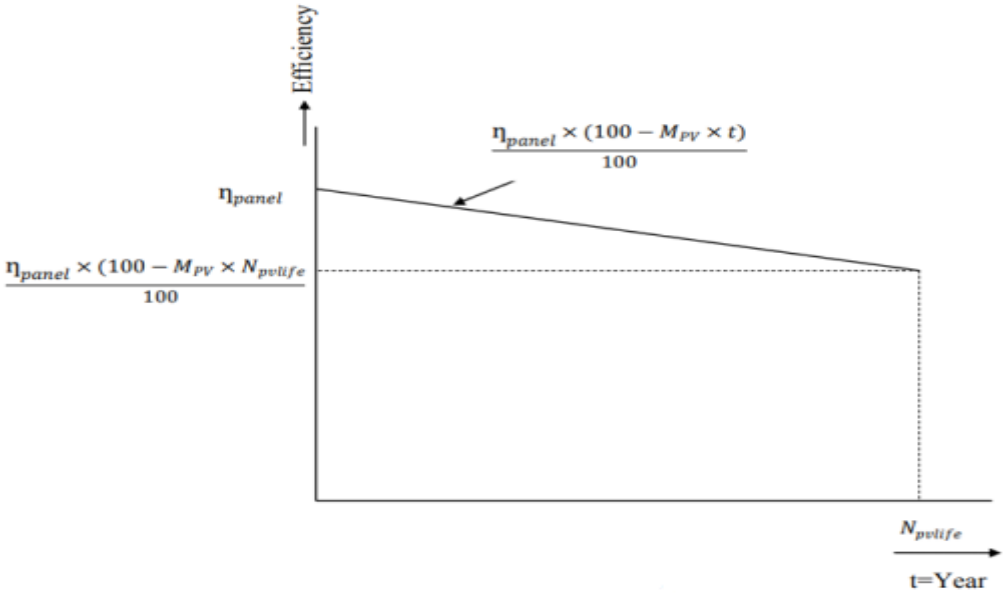

Figure 41: PV panel derated efficiency curve. Source- Alsayed et al, 2013; Talukdar, 2017.

Using formula 38, PV panel daily average electricity production can be obtained from below formula-

$$E_{pvd} = \frac{E_{pvavgy}}{365} \quad \text{.....41 (Alsayed et al, 2013; Talukdar, 2018)}$$

2.5: Fundamental theory of Wind Energy

Wind can be referred to as solar energy in an indirect form. The Sun provides Earth about 1.7 x 10^{14} Kilowatts of power as solar radiation. 1 to 2% of this radiation is transformed into wind energy. Radiation from Sun heats up the earth's surface unevenly causing a pressure gradient which results in cold airflow from the pole of the earth towards the equator. This is how Geostrophic Wind' or Global Wind' is formed. Global winds are available at higher altitudes. Earth's rotation causes the air mass to flow towards low-pressure region from high pressure region, this phenomenon is known as the Coriolis effect. Speed of the wind increases when the height from the ground increases due to the boundary layer effect and wind velocity with height follows the logarithmic pattern (Mathew et al, 2002).

2.5.1: Wind Probability Distribution

To determine the wind energy potential for a specific site, it is required to know the average wind speed of that site. Normally, wind energy potential of a location described using a a probability distribution function. To model wind speed climatology of a site, mostly 'Weibull Distribution' of wind speed and 'Wind Rose Diagram' is used.

The Weibull function represents the wind speed frequency distribution, and it is very useful in wind energy applications. Weibull distribution is expressed by 'Wind speed frequency curve' known as Probability Density Function and equivalent 'Wind speed duration Curve' known as 'Cumulative Probability Function' (Justus et al, 1978). For wind speed V, the probability density function is as below-

$$P(v) = \frac{k}{c}\left(\frac{v}{c}\right)^{k-1} exp\left(-\left(\frac{v}{c}\right)^{k}\right) \quad \text{.....7}$$

(Justus et al, 1978)

In the above equation, k and c are two Weibull parameters where k is the shape factor (dimensionless) and c is the scale factor (Units of speed). Their value depends on wind speed data and estimated basis wind data analysis. Few methods are available to calculate the value of k and c. A sample wind speed "Weibull Distribution Diagram" shown in figure 10 -

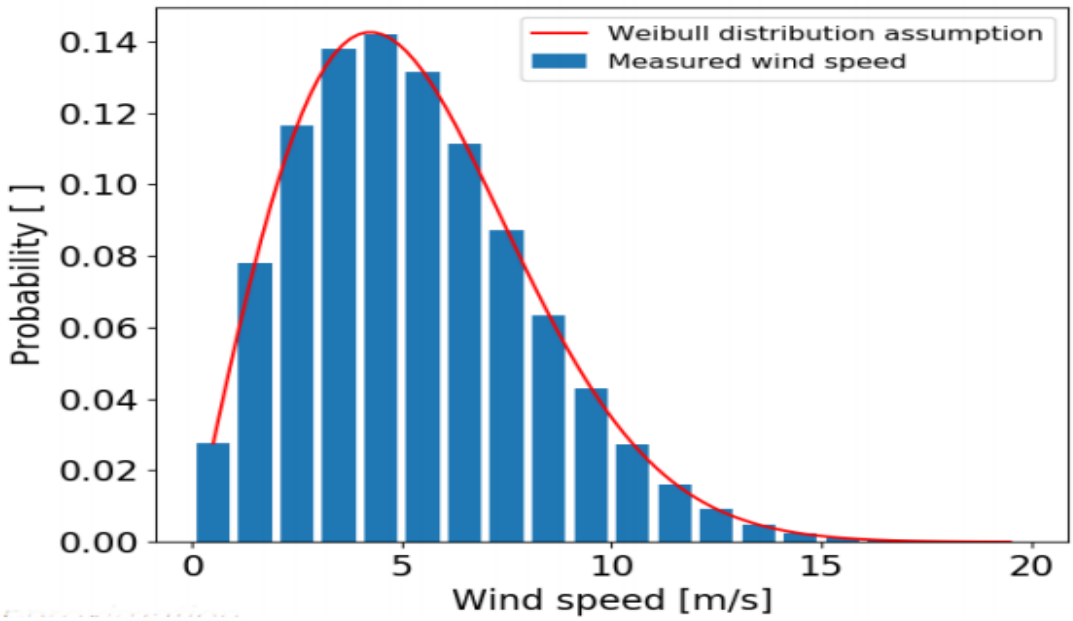

Figure 10: Sample wind speed Weibull Distribution diagram. Source- Schonborn (2021)

From Weibull distribution, two types of wind speeds can be obtained to estimate wind energy. One is 'Most occurring wind speed' and another one is 'Wind speed with highest wind energy' (Chang et al, 2003).

$$\text{Most occurring wind speed} = c\left(\frac{k-1}{k}\right)^{1/k} \quad \text{.....8}$$

$$\text{Wind speed with highest wind energy} = c\left(\frac{k+2}{k}\right)^{1/k} \quad \text{....9}$$

(Equation 8 &9 sourced from Chang et al, 2003)

Another important tool for describing wind speed climatology of a location is the 'Wind Rose Diagram' which displays the direction and magnitude of wind speed of a location for a period of time in a graphical representation. Wind speed frequency to a direction is obtained and the percentage of the wind speed frequency distribution is shown in a circle indicating the direction of wind flow. A typical wind rose diagram for Chittagong anchorage area is collected from 'Global Wind Atlas' for a location of 22.23^0 Latitude and -91.799^0 Longitude as shown in figure 11 -

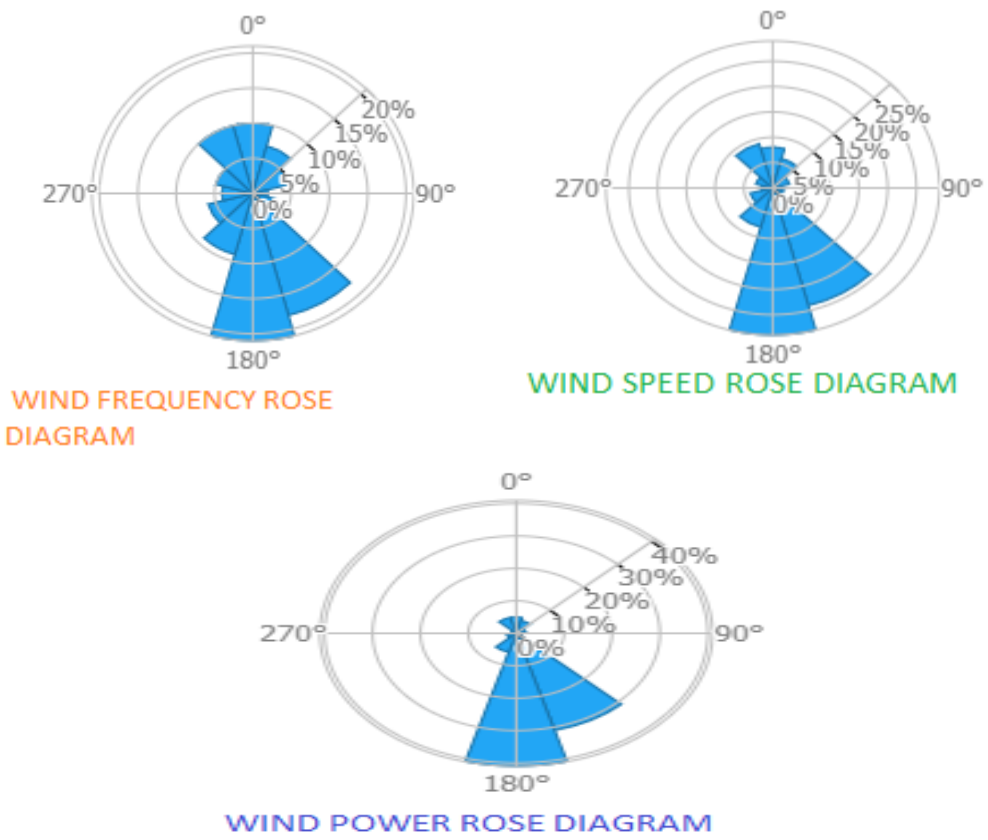

Figure 11: Wind Frequency, Speed and Power rose diagram for Chittagong anchorage area as collected from global wind atlas site.

2.5.2: Wind Turbine mechanisms

Wind turbines generate electricity by converting mechanical energy contained in wind into mechanical energy by rotational motion. The wind rotates turbine rotor blades and thus generator rotor coupled with it. When the generator rotor rotates inside armature windings, a magnetic field is created. According to Faraday's law, the alteration of magnetic field in armature winding due to relative motion between winding and magnetic field, voltage is generated in the armature winding.

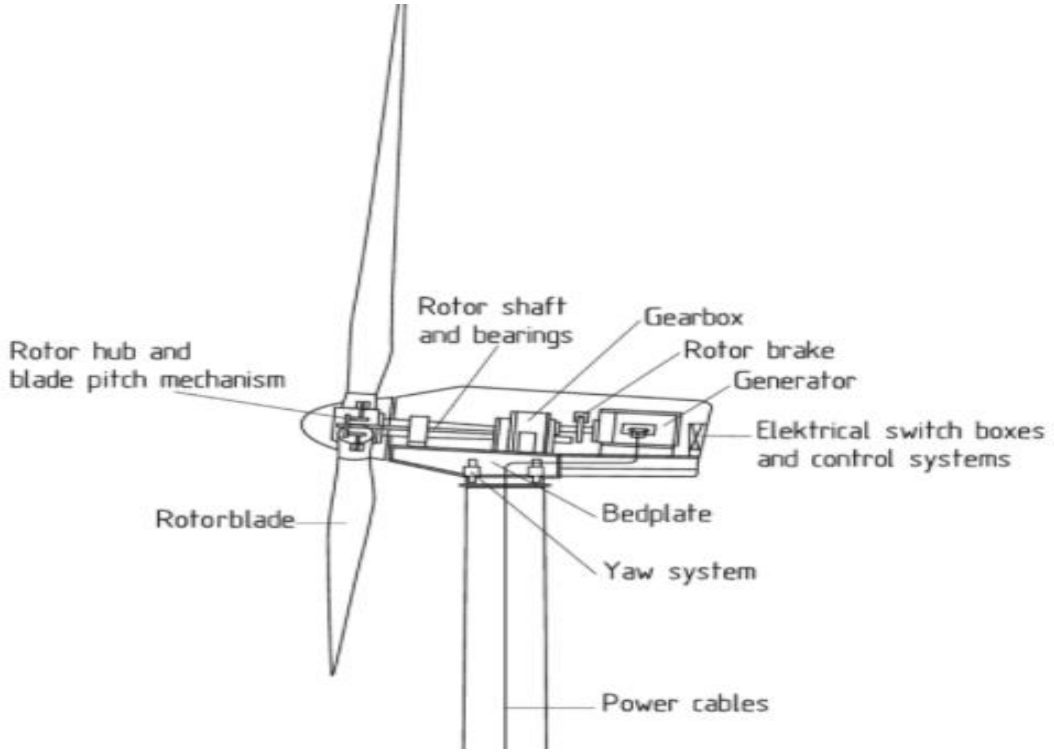

Figure 12: A typical Horizontal axis wind turbine structural components.

Source of figure - Hau, E. (2013). Wind Turbines.

2.5.2: Theory of Wind Turbine power, energy conversion, and Betz's Law

If we consider, an air of density ρ kg/m^3 with an initial velocity of V_{in} m/s and area of A_{in} m^2 approaches towards a turbine blade. Also, assume that velocity at blade is V, the area is A. Area of wind flow after turbine A_{out} while velocity after turbine $V_{out.}$

We know, the mass flow of air m = ρ A V kg

Kinetic energy per second = $\frac{1}{2}$ m v^2 = $\frac{1}{2}$ ρ A V^3 …. (Hau, E.,2013)

Hence, wind power becomes P_w = $\frac{1}{2}$ ρ A V^3 watt ……10 (Hau, E.,2013)

Mass flow before and after the turbine is same as per conservation of mass.

Before turbine wind power = $\frac{1}{2}$ x m x V_{in}^2 = $\frac{1}{2}$ ρ A V x V_{in}^2

After turbine wind Power = $\frac{1}{2}$ ρ A V x V_{out}^2

Hence, wind power converted by turbine = $\frac{1}{2}$ ρ A V (V_{in}^2 - V_{out}^2) …….11

Wind Force on rotor = F = m x a = m x $\frac{(V_{in} - V_{out})}{t}$

= $\frac{m}{t}$ x (V_{in} – V_{out})

= m (V_{in} – V_{out})

= ρ x A x V (V_{in} – V_{out}) ……. …….12

(Equation 11 & 12 source - Hau, E.,2013)

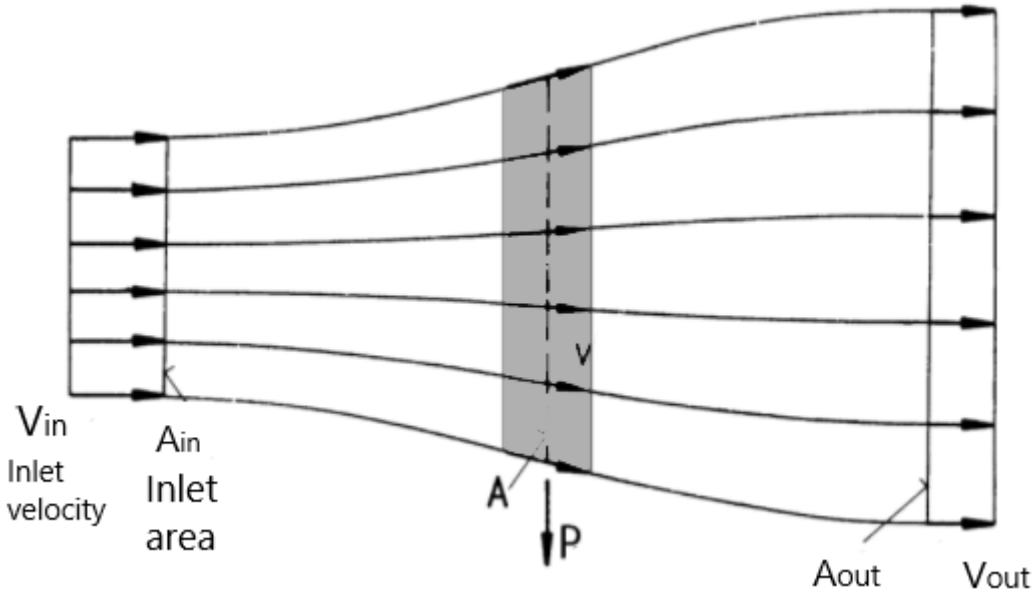

Figure 13 : Wind flow condition before and after wind turbine according to elementary momentum theory. Adapted from- Hau, E. (2013).

Therefore, Work done by turbine per second = W = F x V

= ρ A V (V_{in} – V_{out}) x V

= ρ A V^2 (V_{in} – V_{out}) ……13

= Power converted by Turbine

From figure 10 it is understood that V = $\frac{V_{in} + V_{out}}{2}$

If we put this value in equation 12, we get

Turbine power = $\frac{1}{2}$ ρ A x ($\frac{V_{in} + V_{out}}{2}$) x (V_{in}^2 - V_{out}^2)

= $\frac{1}{4}$ x V_{in}^3 x ρ A (1+$\frac{V_{out}}{V_{in}}$) x (1-$\frac{V_{out}^2}{V_{in}^2}$)

If we consider $\frac{V_{out}}{V_{in}}$ = b, then

Turbine power = $\frac{1}{4}$ x V_{in}^3 x ρ A (1+b) (1-b^2) ….14 (Equ.13 & 14 from Hau, E.,2013)

From this equation, after some re-arrangements, we obtain maximum turbine power as $P_{TMAX} = ½ \times V_{in}^3 \times \rho \times A \times \frac{16}{27}$ …….15 (Hau, E.,2013)

We know that,

wind turbine power coefficient C_p = Turbine output power / Input power of wind

$= P_{TMAX} / P_w$

$= (½ \times V_{in}^3 \times \rho \times A \times \frac{16}{27}) / ½ \rho A V^3$ (Hau, E.,2013)

Therefore, $C_P = 16/27 = 0.593$ = Wind turbine Maximum theoretical power co-efficient

This 16/27 expression is known as the Betz limit. It means theoretically wind turbines cannot capture kinetic energy over 59.3% from incoming wind.

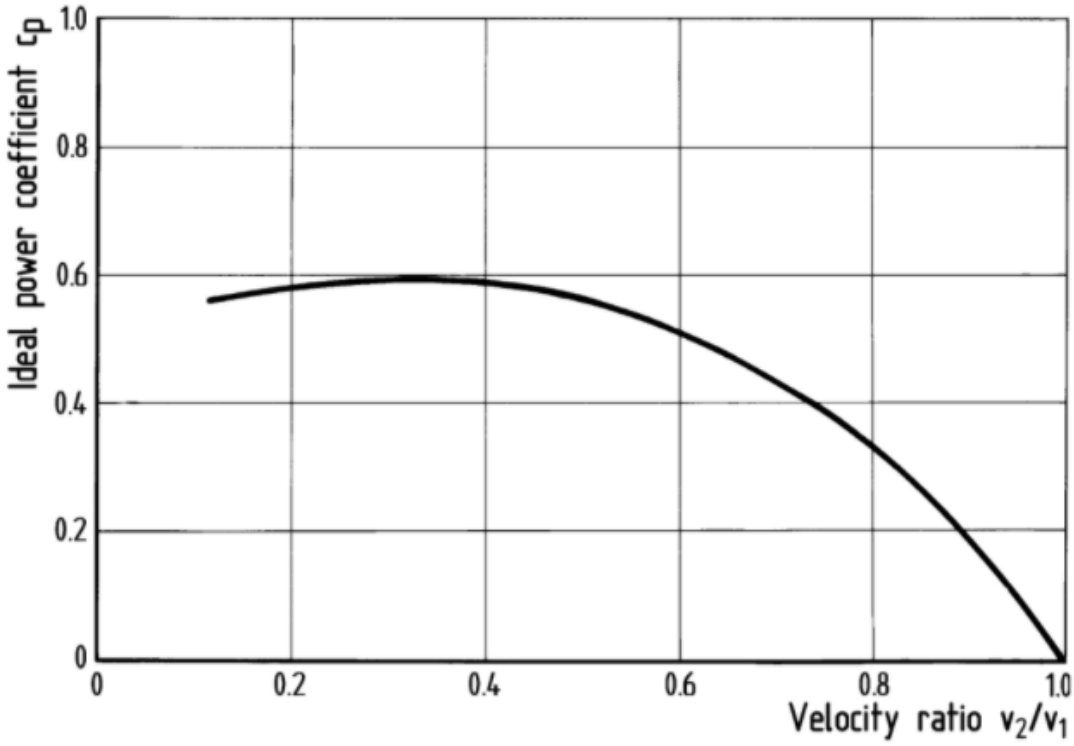

Figure 14: Power coefficient and velocity ratio graph before and after wind turbine. Source- Hau, E. (2013).

From the above equations, we learn that-

Power generated by a single turbine $P_T = ½ \times C_p \times \rho \times A \times V_{in}^3$ 16

Energy converted by a single turbine $E_T = P_T \times t$ …….17

(Equation 16 & 17 from Hau, E.,2013)

2.5.2: Wind Turbine characteristics

In theory, any wind turbine can capture a maximum 59.3% of wind energy according to Betz limit, but in practice power co-efficient for large wind turbines is between 0.45 to 0.50. According to momentum theory power generated by turbines from free stream airflow increases by the 3rd power of wind velocity and square of its diameter or linearly with the cross-sectional area. (Hau, 2013).

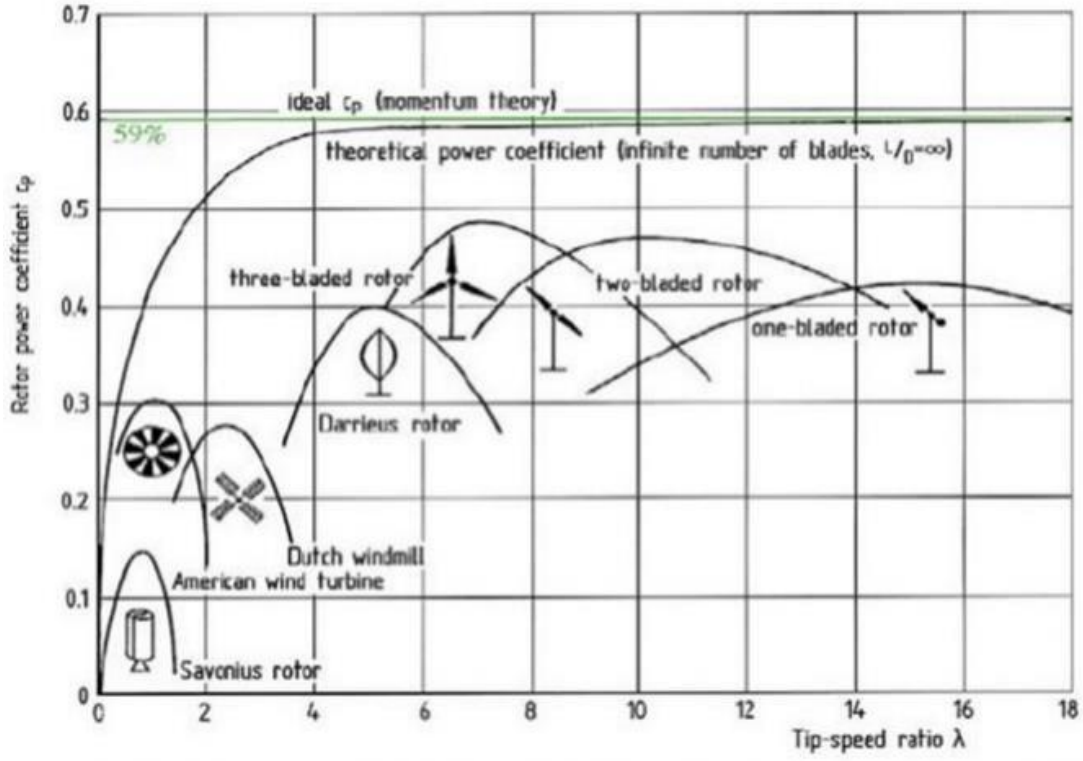

Figure 15: Power co-efficient and tip speed ratio of various wind turbines. Source- Hau, E., Wind turbines (2006), 2nd Ed., p.101

When the power co-efficient of the turbine reaches a maximum at 0.593, the wind velocity at the plan of flow of turbine amounts to 2/3 of undisturbed wind velocity and after turbine, it reduces to one third (Hau, 2013)

2.6: Liquid Air Energy Storage System (LAES)

In renewable energy applications, energy storage is considered to be an important aspect of electricity production. Energy demand varies throughout the day. Different types of electricity generation systems can be used to meet the demand. To balance

the grid supply and demand, energy management technologies are utilized. Energy storage can be considered as supply-side management (Lim et at, 2016). Renewable energy like wind and solar is location and weather dependant. As sunlight and wind availability is different at different seasons, the integration of these energies is always a challenge. LAES can work as a potential backup solution for some uncertain situations. When wind, solar output is low, LAES (Liquid Air Energy Storage) can generate electricity to balance the grid demand. Again, when there is high wind, high solar output, and excess electricity generation, LAES can absorb excess generation. LAES can utilize wasted off-peak renewal energy. This system produces liquid air during off-peak periods when demand is low, and energy is wasted. LAES supply this electricity during peak demand (Akhurst et al, 2013).

2.6.1: Economy of Liquid Air Energy Storage System

A few numbers of energy storage technologies are already available in the market while some other potential technologies are under development. The selection of suitable technology for a specific application depends on some characteristics like cost, energy density, power rating, and duration (Akhurst et al, 2013).

The table 1 shows the power rating and cost of different available competing energy storage systems as per liquid energy network, UK.

Among the available technologies mentioned in below table, pumped hydro storage and sodium sulphur batteries are commercially available at full scale, but they are very expensive.

System	Power Rating	Cost
Pumped hydro storage	100-5000MW	£1,000-1,300/kW
Sodium Sulphur Batteries	Up to 8 MW	£1,700-2,200/kW
Advanced Lead Acid	Up to 40 MW	£1,100-3,100/kW
Liquid Air Energy Storage	10-250 MW	£500-1,250/kW
Compressed air storage	5-400MW	£470-800/kW
Zn/Br redox batteries	Up to 2MW	£1,000-1200/kW
Vanadium redox batteries	Up to 3MW	£2,100-2,600/kW

Table 1: Energy storage technologies comparison. Data: Akhurst et al, 2013

Among all the technologies, compressed air storage is the cheapest, but this is not suitable for the Chittagong port considering geographic features. Salt Cavern is

required to store compressed air which is not suitable in the coastal area of Chittagong port. Hence, the closest competitor to compressed air storage is Liquid air energy storage which can be installed at Chittagong port economically. A 300 KWh LAES system is already successfully demonstrated by Highview Power Storage in Slough. Currently, a 10MWh capacity commercial plant is under development. Once this technology is applied more and more, the overall cost will be reduced.

In Chittagong port, installation of 2 MWh capacity of Liquid Air Energy Storage System will highlight port authority's commitment towards carbon-neutral tendency beside maintaining backup power source.

2.6.2: Cryo Energy System Description:

This study proposes the below discussed Cryo Energy System developed by Highview power storage to install at Chittagong port with 2 MWh capacity.

Cryo energy systems have three stages. Charging, storage, and discharging stage. In the charging stage, ambient air is compressed by the main air compressor and raised the pressure up to 5 to 8 bar absolute. Temperature is maintained to 20^0C by the evaporator. Air is then filtered in an air purifying unit to filter out carbon dioxide and water. Purified air is again compressed in RAC (Recycle Air Compressor) at 30 to 50 bar absolute pressure while the temperature is maintained at 20^0C by the evaporator. This high-pressure compressed air then passed through a series of heat exchangers known as 'Cool Box'. Very cold air outlet from cool box passes through the expansion valve where the air is expanded and condensed to a liquid. The temperature of this liquid is about -192^0 to -180^0 C and pressure drops to 1 to 5 bar absolute. Uncondensed air is returned via separator and a cool box to cool main high-pressure airflow. Part of the outlet air from a recycled air compressor is channelled to heat exchanger for cooling and expansion through a turbine. This is done to reduce energy consumption for air liquefaction and achieve optimum cooling. Very cold liquid air that is produced from the charging stage is stored inside a properly insulated tank.

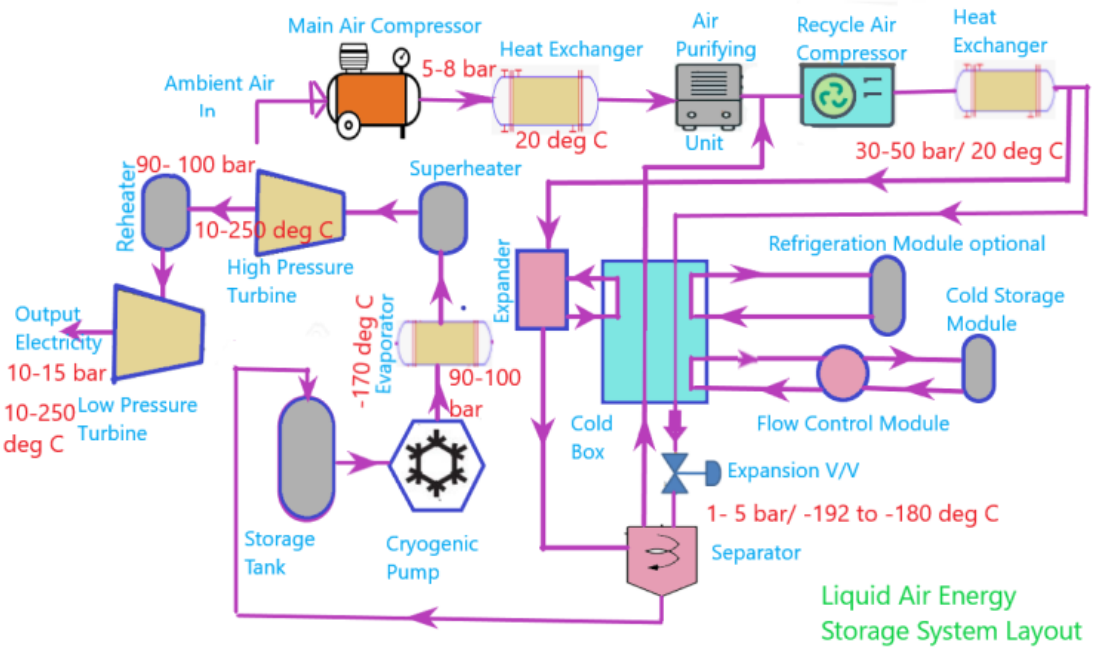

Figure 16: Diagram Liquid Air Energy Storage (LAES) system developed by Highview power company. Diagram made by the author (Idea from- Akhurst et al, 2013; Highview power storage).

When there is demand for electricity, discharging stage starts which follows the Rankine cycle principle. Cryo liquid pump increase the pressure of the flow up to 90 to 100 bar. Finally, warm high-pressure gas discharge from the cryogenic pump is expanded through a series of turbines to produce electricity.
The efficiency of the above system is typically 25%, but efficiency is increased up to 50-60% by recycling and storing thermal energy that is released during the power recovery process.

2.6.3: Dearman Cycle Working Principle :

A new generation of the cryogenic engines is being developed that operates on the “Dearman Cycle” which utilizes vaporization and expansion of liquid air.
This Dearman Cycle is explained below in a simple manner –

a. Return Stroke

During the return stroke, when the piston travels from BDC to TDC, a warm heat exchange fluid (HEF) is allowed to enter inside the engine cylinder. This HEF fills almost the entire dead volume of the cylinder.

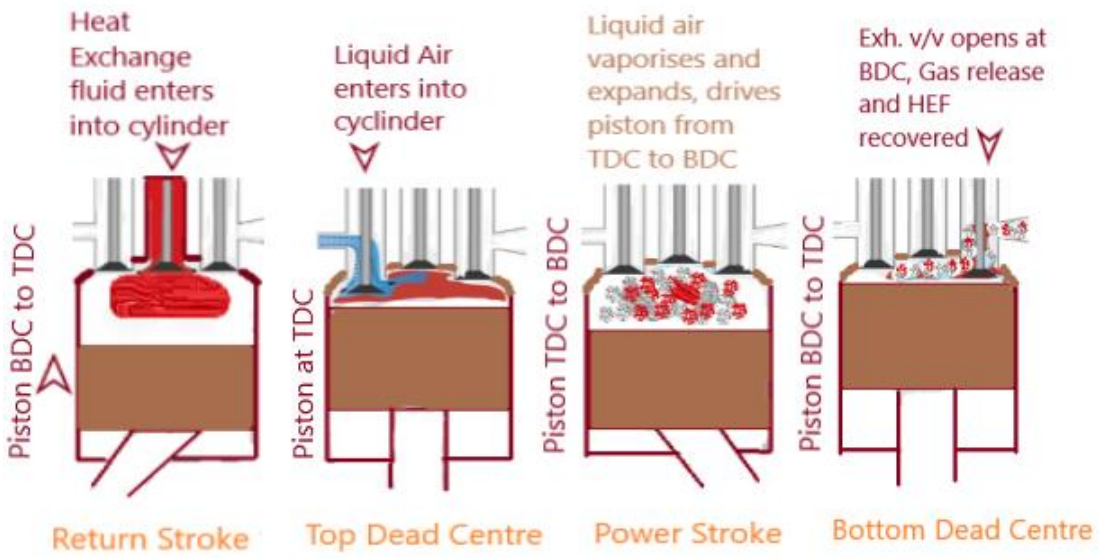

Figure 17: Schematic representation of Dearman Engine Cycle.

b. Top Dead Centre

At TDC, Liquid air is directly injected into the HEF. Due to a large temperature differential between HEF and liquid air, also a large surface area, hence, rapid heat transfer occurs between the fluids. It causes the vaporization of the cryogenic liquid and gives rise to pressure.

c. Power Stroke

When liquid air turns into gas due to vaporization, gas is expanded. This gas expansion drives the piston towards the BDC. During this entire period, direct contact heat transfer continues from HEF to expanding gases following the isothermal expansion principle. Hence, the gas expands but its temperature remains relatively constant.

d. Bottom Dead Centre

When piston at BDC, the exhaust valve is timed to open. As the exhaust valve opens, HEF and gas mixtures leave the cylinder. HEF is reused upon recovery from the exhaust stream and reheat. Gas is exhausted to the atmosphere.

2.6.4: Advantage of Dearman Engine:

Dearman engine appeared to be an attractive device capable of using liquid air as a zero-emission energy vector. Key features of the Dearman engine are as below-

- Cheapest zero-emission power system.
- Capable to use low-grade waste heat to increase efficiency.
- Fuel used is non-combustible, Generated exhausts are cool and clean
- Very low life cycle footprint
- Manufactured from simple recyclable materials and plastics, well-established process. Hence, low capital cost requirements.

2.6.5: Efficiency Improvement of Liquid Air Energy Storage System

Liquid air storage technologies are debated for low round trip efficiencies. Scholars have studied various solutions to improve round trip efficiencies of LAES. The table 2 highlights some key scholarly study findings for efficiency improvements together with sources-

Methods Proposed	Source
Air liquefaction by adding Claude cycle in cold box. Obtained 57% efficiency.	Morgan et al,2015
Comparison of Linde-Hampson, Collins, Claude cycle for cryogenic energy storage showed better cost-benefit in Claude Cycle.	Abdo et at, 2015
Impact of pressure loss, heat exchanger pinch-point temperature and turbine Isentropic efficiency.	Guizzi et al, 2015
Pebbles and rock for cryogenic energy storage as direct contact cold store.	Sciacovelli et al, 2017
Packed bed to store compression heat. Achieved round trip efficiency 50-60%.	Peng et al, 2016, 2018
Small scale air liquefaction cycle in microgrid. Obtained efficiency 25% with operating pressure 38 to 45 bar.	Borri et al, 2017
Hybrid energy storage system combining liquid and compressed air. Efficiency obtained 53%.	Kantharaj et al, 2015

Table 2: Different methods of improving RTE (Round Trip Efficiency) of LAES system as studied by scholars.

Recovering compression heat during the charging stage and liquid air cold energy in the discharging stage can improve the significant RTE of the LAES system. The cold energy loss from discharging cycle reduces round trip efficiency 7 times higher comparing heat energy loss of the charging stage. Recovering cold and heat energy and by utilizing this waste heat the RTE of LAES can be improved. Peng et al (2018) successfully shown improvement of efficiency up to 60% incorporating an Organic Rankine Cycle (ORC) with LAES. In this system, excess heat is utilized to generate power through the additional turbine. Working medium (R134a) of ORC is heated by using excess heat and thereafter cooled by using ambient cooling water.

2.6.6: Thermodynamic Calculations of LAES system

To conduct thermodynamic analysis of the figure of LAES layout, system is considered in steady-state and assumed heat loss from system components is nil. Also working medium R134a condensed in evaporator and condenser into a saturated state.

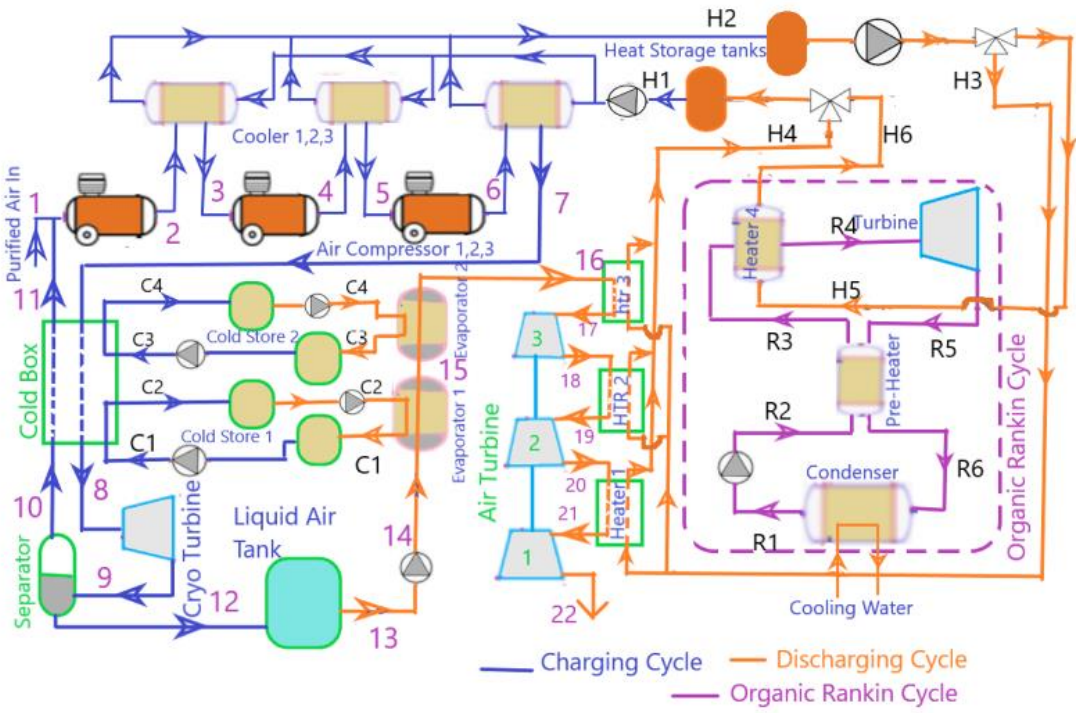

Figure 18: Layout of LAES system with Organic Rankin Cycle (LAES-ORC). Diagram made by Author (Idea from Peng et al, 2018).

During the charging stage, ambient air is compressed to high pressure in three stages via a multistage air compressor. Enthalpy of outlet air from each stage can be calculated using the below formula-

$$\text{Enthalpy} \quad H_{i+1} = H_i + \frac{H_{i+1,s} - H_i}{\eta_{compressor}} \quad \text{.....18} \quad \text{(Peng et al, 2018)}$$

Where, H_i = state i specific enthalpy
i = 1, 3 or 5
$\eta_{compressor}$ = Air compressor Isentropic efficiency
Subscript s refers the Isentropic compression.

High pressure compressed air is then directed to the cold box where the air is cooled by cold fluid, normally by propane and methanol. The mass flow rate of outlet cold air from the cold box can be calculated using below formula-

$$M_{air,ch} \times (H_7 - H_8) = (1-Y) \times M_{air,ch} \times (H_{11} - H_{10}) + M_{propane,ch} \times (H_{C2} - H_{C1}) + M_{methanol,ch} \times (H_{C4} - H_{C3}) \quad \text{.....19 (Peng et al, 2018)}$$

Where $M_{air,ch}$ = Air mass flow rate during the charging stage

$M_{propane,ch}$ = Propane mass flow rate during charging stage

$M_{methanol,ch}$ = Methanol mass flow rate during charging stage

Y = Liquid Air Yield

Cold compressed air of the cold box then sent to cryo turbine where expansion occurs at ambient pressure. Part of this air turns to liquid.

Two-phase air outlet enthalpy = $H_9 - H_8 - \eta_{cryo.turb} \times (H_8 - H_{9,s})$

.....20 (Peng et al, 2018)

Where $\eta_{cryo.turb}$ = Cryo turbine isentropic efficiency

During discharging, the Cryo liquid pump takes suction of liquid air from storage tank and pumps to high pressure. Enthalpy of this outlet air is-

$$H_{14} = H_{13} + \frac{H_{14,S} - H_{13}}{\eta_{pump}} \quad \text{.....21 (Peng et al, 2018)}$$

Where η_{pump} = Isentropic efficiency Cryo liquid pump.

In evaporators 1 and 2, propane and methanol recover the cold energy of liquid air. Outlet conditions of both evaporators are as below-

$$M_{air,di} \times (H_{15} - H_{14}) = M_{propane,di} \times (H_{C2} - H_{C1}) \quad \text{.....22 (Peng et al, 2018)}$$

Where $M_{air,di}$, $M_{propane,di}$ = Mass flow rate of air and propane during discharge

$$M_{air,di} \times (H_{16} - H_{15}) = M_{methanol,di} \times (H_{C4} - H_{C3}) \quad \text{.....23 (Peng et al, 2018)}$$

Where $M_{air,di}$, $M_{methanol,di}$ = Mass flow rate of air and methanol during discharge.

After evaporator, high-pressure air enters multi-stage air turbine via heater to produce electricity. Air outlet enthalpy after each stage of turbines can be calculated using below formula-

$$H_{i+1} = H_i - \eta_{turb} \times (H_i - H_{i+1,s}) \quad \text{.... .....24 (Peng et al, 2018)}$$

Where, η_{turb} = Air turbine isentropic efficiency. i = 17, 19 or 21

RTE, net output work during discharging, and net input work during the charging cycle can be obtained from the below formulas-

$$\eta_{RTE} = \frac{W_{AIR,OUT}}{W_{AIR,IN}} \quad \text{.....25}$$

$$W_{AIR,OUT} = (H_{17} - H_{18}) + (H_{19} - H_{20}) + (H_{21} - H_{22}) - (H_{14} - H_{13}) \quad \text{.....26}$$

$$W_{AIR,IN} = [\{M_{air,ch} \times \{(H_{17} - H_{18}) + (H_{19} - H_{20}) + (H_{21} - H_{22}) - (H_{14} - H_{13})\}] / M_{12} \quad \text{...27}$$

In ORC, R143a condensed to liquid in a condenser and then pumped to high pressure. Enthalpy of outlet R134a is as below-

$$H_{R2} = H_{R1} + \frac{H_{R2,S} - H_{R1}}{\eta_{pump}} \quad \text{.....28}$$

High-pressure R134a is heated to a high-temperature state in the heater by thermal oil. This R134a then enters to the turbine and produce electricity. Enthalpy of R134a after turbine can be calculated as below-

$$H_{R5} = H_{R4} - \eta_{turb} \times (H_{R4} - H_{R5,S}) \quad \text{.....29}$$

Per unit mass of liquid air output work can be calculated from below formula-

$$W_{ORC,OUT} = \{M_{ORC} \times ((H_{R4} - H_{R5}) - (H_{R2} - H_{R1}))\} / M_{AIR,DI} \quad \text{.....30}$$

Where M_{ORC} = R134a mass flow rate in ORC

(Formula 25 to 30 sourced from Peng et al, 2018)

During peak time, ORC generates electricity together with LAES discharging stage.

2.6.7: Thermodynamic Analysis of Liquid Air Energy Storage System

For thermodynamic analysis of the LAES system, simulation results of kinds of literature are compared and studied. Key findings of this comparison and studies are highlighted below-

2.6.7.1: Effect of Cold Room Temperature:

From the simulation of Peng et al, (2018), T-S diagram in figure 19 is obtained-

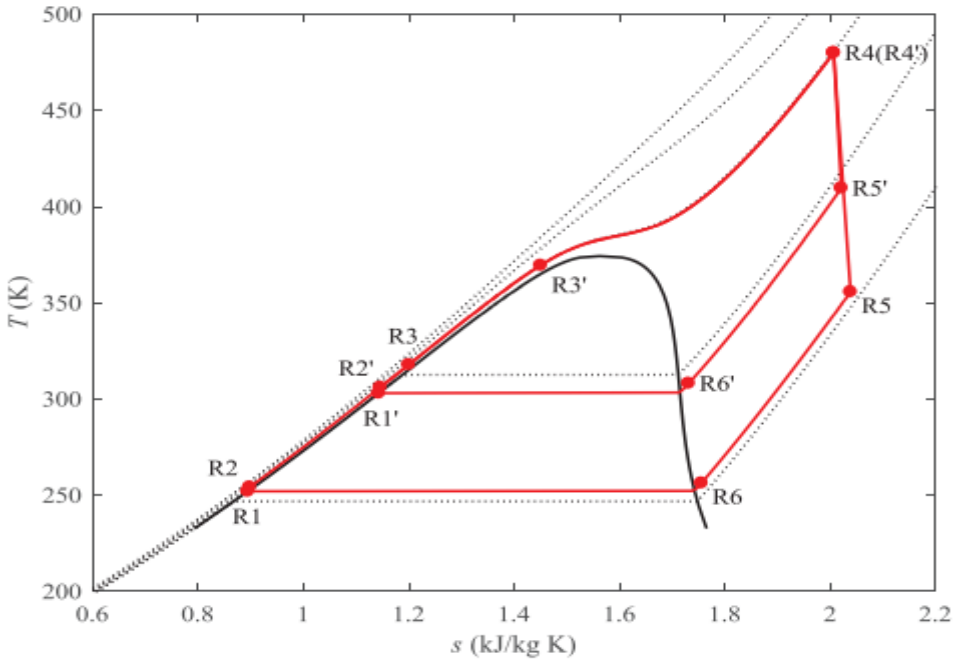

Figure 19: T-s diagram as obtained from simulation of Peng et al (2018) showing the effect of cold source temperature on ORC when R134a is working fluid.

This diagram was obtained upon simulation carried out by Peng et al (2018) and they claim that in an ORC when heat source temperature is the same, lower temperature cold source generates higher specific output power.

2.6.7.2: Exergy analysis of overall Liquid Air Energy Storage System

From the simulation of Guizzi et al (2015), work output and energy losses from the overall LAES plant were obtained as below figure. It is seen that exergy losses are maximum during storage or liquefaction and exergy losses are minimum due to heat rejection to the environment. The magnitude of exergy losses during the energy recovery section is also almost close to storage section losses.

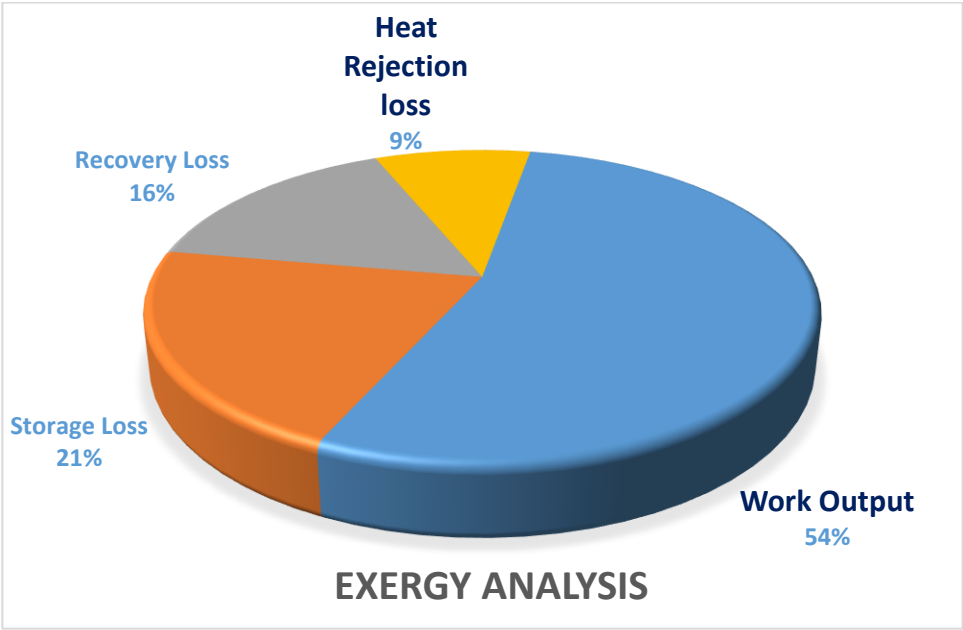

Figure 20: Exergy analysis of overall LAES plant as per the model of Guizzi et (2015).

2.6.7.3: Effect of Charging and Discharging Pressure

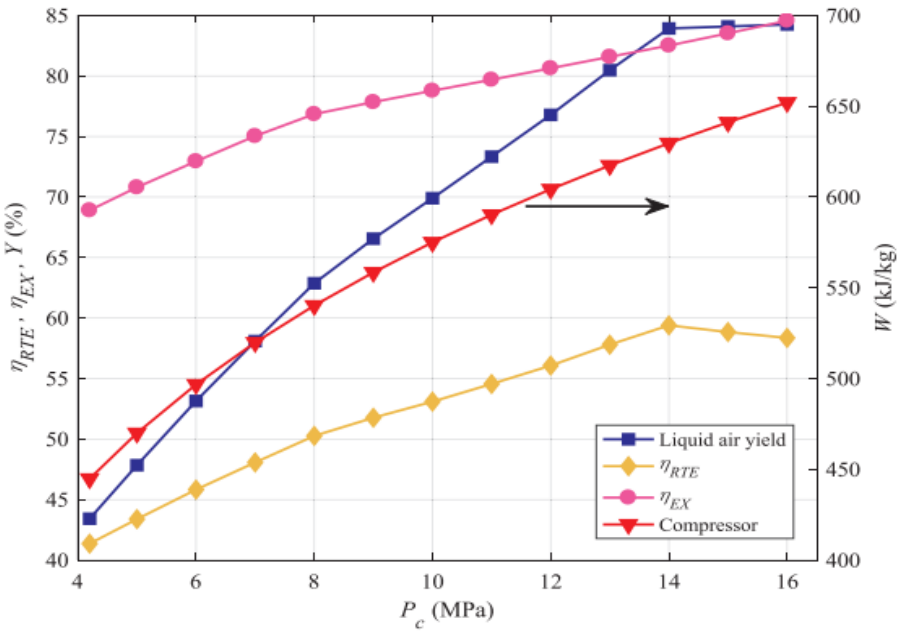

Figure 21: Impact of charging pressure on round trip efficiency (η_{RTE}), Exergy efficiency (η_{EX}), Liquid air yield (Y), compressor consumption as per the model of Peng et al (2018).

With the increase in charging pressure, liquid air yield increases up to certain pressure (14 MPa in this case) and then remains almost constant or reduces slightly. RTE follows the same trend. Whereas exergy efficiency and compressor electricity consumption increase continuously with the increase in charging pressure.

The figure 22 shows the effect of different discharge pressure on RTE. At relatively low charging pressure (4-8 MPa), RTE does not change that much. At charging pressure 8 to 14 MPa, RTE decreases gradually while discharging pressure increases. At 14 MPa charging pressure, RTE is maximum and above this high discharge pressure is beneficial for LAES.

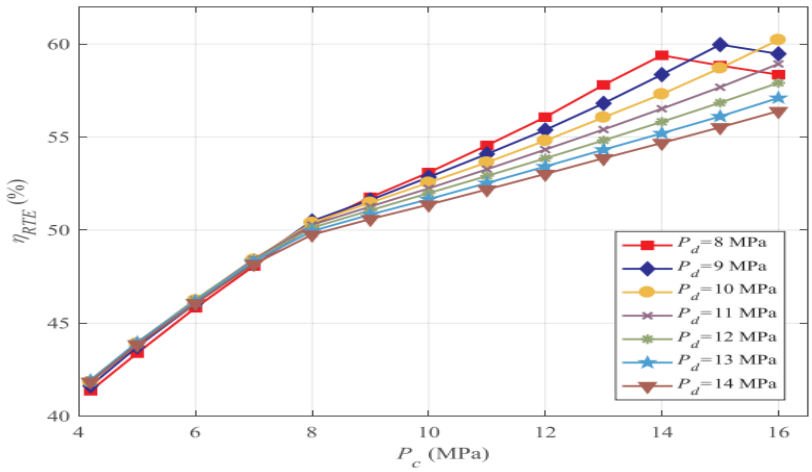

Figure 22: Effect of discharging pressure on round trip efficiency as per the model of Peng et al (2018).

2.6.7.4: Effect of Thermal Loss, Heat and Cold Recovery

In LAES, heat energy is stored in mediums like thermal oil, and cold energy is stored in mediums like propane and methanol. During storage, thermal dissipation to the environment causes energy losses. Both heat and cold energy loss cause a reduction of LAES performance. In the simulation of Peng et al (2018), it is seen that the decrease rate is 7 times higher in case of cold energy loss than heat energy loss.

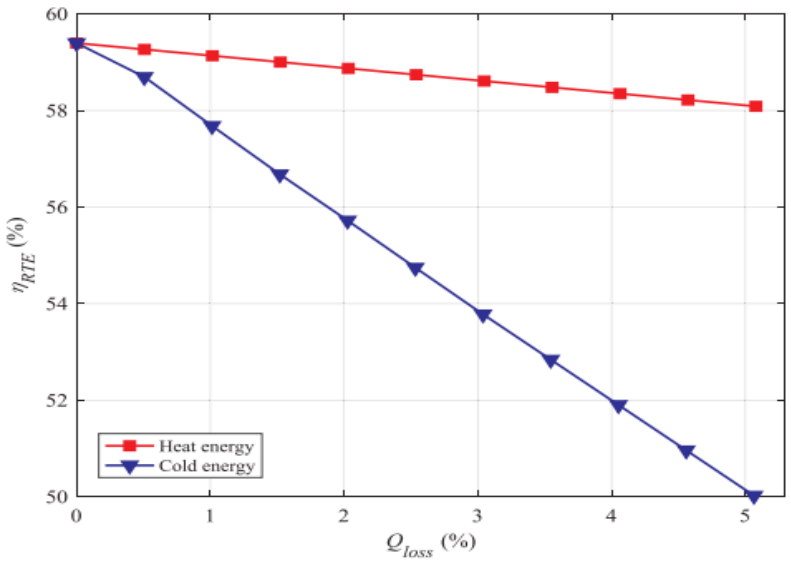

Figure 23: Effect of heat and cold energy losses during storage on Round Trip Efficiency of LAES system at Charging Pressure 14 MPa and Discharging Pressure 8 MPa in the simulation of Peng et al (2018)

Unlike thermal loss, heat recovery from compressed air during the charging stage and cold recovery from liquid air during discharging stage also affects the RTE of LAES. During charging, heat energy is generated due to the compression of ambient air which can be stored using a medium like thermal oil to use this heat during discharging cycle. The Simulation of Peng et al (2018) showed that about 20-45% excess heat of compression is wasted. The addition of the Organic Rankin Cycle (ORC) and Absorption Refrigeration Cycle (ARC) with LAES can make use of this wasted heat to improve the round-trip efficiency of LAES system.

Chapter 3

3.0: Methodology

3.1: Wind Power Calculation

The wind power converted by a wind turbine was calculated using equation P = ½*rho*Cp*A*v^3, where, rho is the density of the air, Cp is the power coefficient of the turbine, A is the rotor area of the turbine, and v is the instantaneous wind speed. This calculation was performed for every wind speed in steps of 1 m/s ranging from 0 m/s to 25 m/s. The power produced was multiplied by the number of

times in one year and the probability of this wind speed occurring, to obtain the amount of energy produced on average at that wind speed. The total energy produced in one year by the turbine was calculated as the sum of all energy produced at various wind speeds. This methodology was implemented in a computer program written in the Python 3.9.2 programming language. At first, the functions 'numpy' and 'matplotlib.pyplot' imported for calculation assistance in Python programming. Then Weibull 'A' and 'k' parameters for the proposed wind farm site were obtained from GWA 3.1 for roughness length 0.0 meter which is for sea surface level and at a reference height of 10 meters. Then the wind turbine selection was made, and specifications of turbine and windfarm were input into the computer program (Python). Turbine rotor diameter used as 90 m, power co-efficient C_p assumed as 0.45, and density of air considered as 1.2 kg/m^3. Total 7 units Vestas V90-2.0 MW turbine planned for the proposed wind farm. The maximum rating of wind turbine entered as 2 MW as mentioned in turbine manufacturers manual for this specific module.

After determining wind turbine and windfarm specifications, matrices of the probability of wind speed, turbine power, energy generation by turbine and time (number of hours) are set for calculating values for the range of 1 to 21 so that Python programming can calculate values from 1 up to 20 for each assigned variable. For this function created a 'for' loop in Python in range 1 to 21 which allowed repeating power calculation for various speed ranges. Wind speed array was formed that contains all different wind-speed values from 1 m/s to 20 m/s. Once the matrix was set, the probability of various wind speed occurrences using Weibull distribution was calculated using formula 8 putting the Weibull A and k parameters as obtained from GWA 3.1 indenting inside 'for' loop.

For calculating single turbine power generation for each wind speed in the 'for' loop, formula 16 is used assigning a maximum rating of a wind turbine to 2000 KW. This function provided the power generation capacity of a Vestas V90-2.0MW wind turbine at each wind speed from 1 m/s to 20 m/s in Watt at the proposed wind farm site. As the maximum power rating is fixed, the diagram did not display values more than 2MW.

Time assigned in the 'for' loop as per below formula-

$$t[i] = p[i]*24*365 \quad \text{where } i \text{ in range 1 to 21}$$

which calculated the possibility of the number of hours of various wind speeds per year [h/year].

After assigning time, energy generation by a single turbine was calculated using formula 17, inside the ‘for’ loop which provided an energy array containing energy values for each wind speed from 1 m/s to 20 m/s.

Then the total energy produced by a single turbine is calculated at all different wind speeds as the sum of energy produced at individual wind speeds in a megawatt-hour outside of the ‘for’ loop. This was done using a built-in summing function in the Python ‘numpy’ module using the below formula-

TotalEnergy = np.sum(Energy)

And total energy produced by the entire windfarm is calculated by multiplying the energy produced by one turbine by the number of turbines (7) in the wind farm.

In the end, Weibull diagram obtained by using Python function ‘matplotlib.pyplot’ for ‘probability (%) vs wind velocity (m/s)’, ‘Time (yearly hour) vs wind velocity (m/s)’, ‘Power (MW) vs wind velocity (m/s)’, ‘Energy (GWh) vs Wind velocity (m/s)’.

The entire Python programming sequence screenshot is shown below, and the data obtained is attached in appendix A.

```
# Wind power calculation program Anowara, Chittagong #
# This program calculates the yearly energy conversion of an offshore windfarm #
import numpy as np
import matplotlib.pyplot as plt
A = 7.28         # A-factor for Weibull distribution
k = 3.322        # k-factor for Weibull distribution
pi = 3.14159     # Define the value of pi
# Technical specification of the turbine
r = 126/2             # radius of the turbine rotor [m]
Area = r**2*pi       # Area of rotor [m2]
Cp = 0.50            # Turbine power coefficient  [ ]
rho = 1.2            # density [kg/m3]
Maxrating = 3450000 # Power rating of turbine [W]
# Specification of windfarm
N = 7          # Number of wind turbines in wind-farm
# Initialise matrices of zeros
Energy = np.zeros((21))      # Prepare matrix for energy values
Speed = np.zeros((21))       # Prepare matrix for wind-speed values
Pwt = np.zeros((21))         # Prepare matrix for wind-turine power values
p = np.zeros((21))           # Prepare matrix for probability values
t = np.zeros((21))           # Prepare matrix for time (number of hours) values
for i in range (1, 21):      # Create a loop that allows repeating
                               the power calculations for various wind-speeds
    v = i                  # Assign the iteration value 'i' as wind speed value
    Speed[i]=i             # Create an array that contains all different wind-speed values
    p[i] = (k/A)*(v/A)**(k-1)*np.exp(-(v/A)**k) # Probability of wind speed occurence
                                                  using Weibull distribution [ ]
    print(p)
        Pwt[i] = (1/2)*Area*Cp*rho*v**3   # Power of wind turbine [W]
        if (Pwt[i]>Maxrating):      # Checking if calculated power is larger than rated power
        Pwt[i]=Maxrating            # If calculated power is larger than rated power,
                                      assign rated power as maximum value
        print(Pwt)
     t[i] = p[i]*24*365         # Calculate the number of hours of this wind speed per year [h/year]
    Energy[i] = Pwt[i] * t[i]   # Calculate the energy produced at one particular wind-speed
                                      as the product of power and time [Wh/year]
    print(Energy)
TotalEnergy = np.sum(Energy)   # Calulate the total energy produced at all different wind speeds as
                                    the sum of energy produced at individual wind-speeds
TotalEnergyWindFarm = TotalEnergy * N  # Multiply the energy produced by one turbine by
                                         the number of turbines in the wind farm

print('The total energy produced by one turbine is', TotalEnergy/1000000, '[MWh/year]')
                                    # Output the total energy produced per year for one turbine
print('The total energy produced by the wind farm is', TotalEnergyWindFarm/1000000, '[MWh/year]')
                                    # Output the total energy produced for the entire wind-farm
# Plot results
# Plot probability versus wind speeds
plt.bar(Speed, p, color='violet')
plt.xlabel('Velocity [m/s]')
plt.ylabel('Probability [ ]')
plt.show()
# Plot number of hours versus wind speeds
plt.bar(Speed, t, color='purple')
plt.xlabel('Velocity [m/s]')
plt.ylabel('Time [hours/year]')
plt.show()
# Plot Turbine power versus wind speeds
plt.bar(Speed, Pwt, color='red')
plt.xlabel('Velocity [m/s]')
plt.ylabel('Power [W]')
plt.show()
# Plot Energy from one wind-turbine versus wind speeds

plt.bar(Speed, Energy, color='green')
plt.xlabel('Velocity [m/s]')
plt.ylabel('Energy [Wh]')
plt.show()
```

Figure 24 : Screenshot of Python programming for wind power calculations.

3.2: SOLAR Power Calculation

For solar irradiances data collection and PV power calculations, PV-GIS version 5 software has been used. PVGIS is a web application that is widely used for the estimation of photovoltaic system performance in Europe, Africa, a large part of Asia, and America. European Commission Joint Research Centre developed PVGIS in 2001. Besides many other services, this web application provides open access to monthly averages or daily profiles of solar radiation for wider geographical locations worldwide. In PVGIS 5, satellite data used for solar radiation calculations are obtained from the METEOSAT satellite which captured one image per hour.

To calculate solar radiation from satellites, the PVGIS-SARAH database has been used.

In the first step of the calculation, satellite images are used to determine the effect of clouds on solar radiation. Sun reflects incoming solar radiation; hence less radiation arrives at the ground. To calculate radiation reflectivity by clouds, satellite image pixels of the same time every day in a month are observed. The darkest pixels in a month are considered as a clear sky or no cloud day. Cloud reflectivity for other days of the month is then calculated relative to clear sky day for all hours of that day. Effective “cloud albedo” is calculated in this manner.

In the second step, the theory of radiative transfer in the atmosphere is used to calculate clear sky conditions solar radiation together with data of atmospheric aerosol content, ozone, and water vapor concentration. At last, cloud albedo and clear sky irradiance are used to calculate total radiation.

To obtain GHI, DHI for the location of Chittagong port and monthly PV energy production from selected PV panel, required input is fed into the PVGIS web application. Location is set to 22.313^0 Latitude and 91.808^0 Longitude. Crystalline Silicon-type PV technology is selected with an installed capacity of 1 KWp. System loss is considered 14%. Slop angle given 35^0 and Azimuth angle chosen as 0^0. With the provided inputs, the PVGIS-SARAH database used its in-built algorithms to calculate required outputs. In this manner, the monthly average GHI, DHI, and diffuse to global ratio for the location of Chittagong port for the entire year of 2016 is obtained.

Monthly average hourly GHI, DHI, DIFF for January to December were also calculated using PVGIS software and obtained required graphs. Finally, PVGIS calculated the average monthly global irradiation per square meter received by the PV module and average monthly electricity production from a PV module.
In addition to PV application calculations using PVGIS software, this study also highlighted appropriate theoretical formulas for required photovoltaic application calculations from peer-reviewed literature.

3.3: Liquid Air Energy Storage System (LAES)

For LAES, this literature conducted extensive scholarly article review which is included in the literature review chapter 2.6. At first, LAES details are described. Then brief discussion was carried out for thermodynamic calculations and analysis of LAES. Theoretical formula compiled for thermodynamic power calculation for a typical LAES. Measures to improve round trip efficiency of LAES were also highlighted. This study highlighted LAES incorporated with an Organic Rankin Cycle to install at Chittagong port to improve the efficiency of the overall plant as proposed by Peng et al (2018). Finally, the effect of various parameters on the RTE of LAES is indicated. Effect of cold room temperature, charging and discharging pressure, thermal loss, heat, and cold recovery is analyzed in this regard. In section 5.5 and 5.5.1, this study provided a logical explanation to use LAES as a backup power of Chittagong port and calculated the required capacity to be installed at Chittagong port using simple arithmetical formulas.

Chapter- 4

4 : Wind Energy Harnessing, Data Analysis, and Calculations

4.1: Site Selection for Wind Turbine

Chittagong port is located about 9 nautical miles away from the shoreline of the Bay of Bengal. Abundant wind energy available in the Chittagong port anchorage area can be harnessed by installing offshore wind turbines at the Bay of Bengal. Wind

turbines can be installed within 500 metres of distance from the shoreline of Patenga. A suitable location for wind turbines is shown in figure 25.

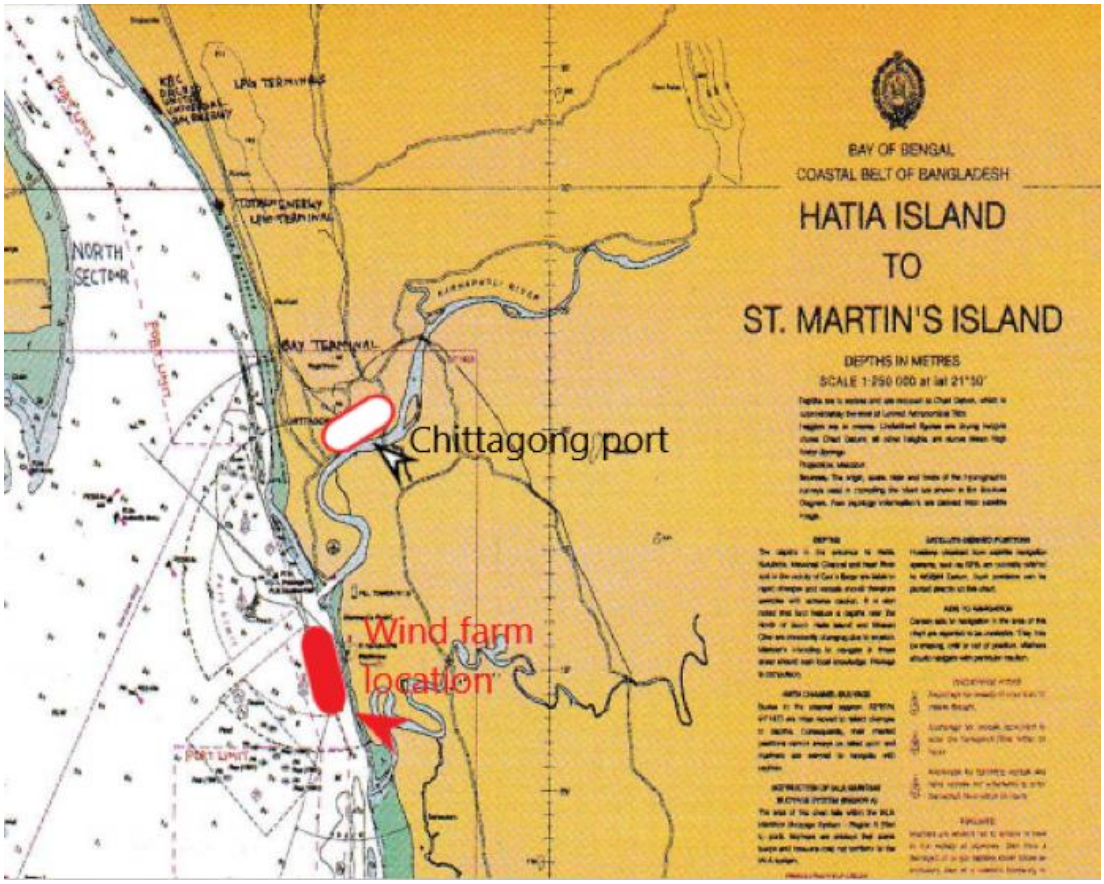

Figure 25: Location of the proposed windfarm, Chittagong port, and anchorage area. Photo source- CPA overview, 2020.

The proposed location is very close to the port and most of the Karnaphuli riverbank from farm location to port belongs to CPA. Power generated by wind turbines can be easily connected to the port grid by the port authority's own transmission lines. Besides, there are no markable infrastructures adjacent to the proposed location, hence wind turbine installation at this place will not obstruct any industrial or social activities.

4.1.1: Wind Data Collection for Proposed Wind Farm Site

Generalized Wind Climate (GWC) data for the location of 91^0 806' Longitude and 22^0 194' Latitude at the proposed windfarm site has been collected from Global

Wind Atlas (GWA) version 3.1. GWA is a web-based application that helps policymakers to identify high-wind areas for the generation of wind power at any location of the world. GWA 3.1 is the product of a partnership between The World Bank, International Finance Corporation (IFC), and the Department of Wind Energy of Technical University of Denmark. GWA 3.1 provides extensive location coverage from onshore to offshore up to 200 km from the shoreline. It also provides wind resource mapping at 250m horizontal grid spacing and also for the height of 10 m , 50 m, 100 m, 150 m, 250 m above sea level.

GWC climate data that is obtained from GWA 3.1 for the proposed wind farm site at Patenga offshore is shown partially in figure 14 with key features indication below-

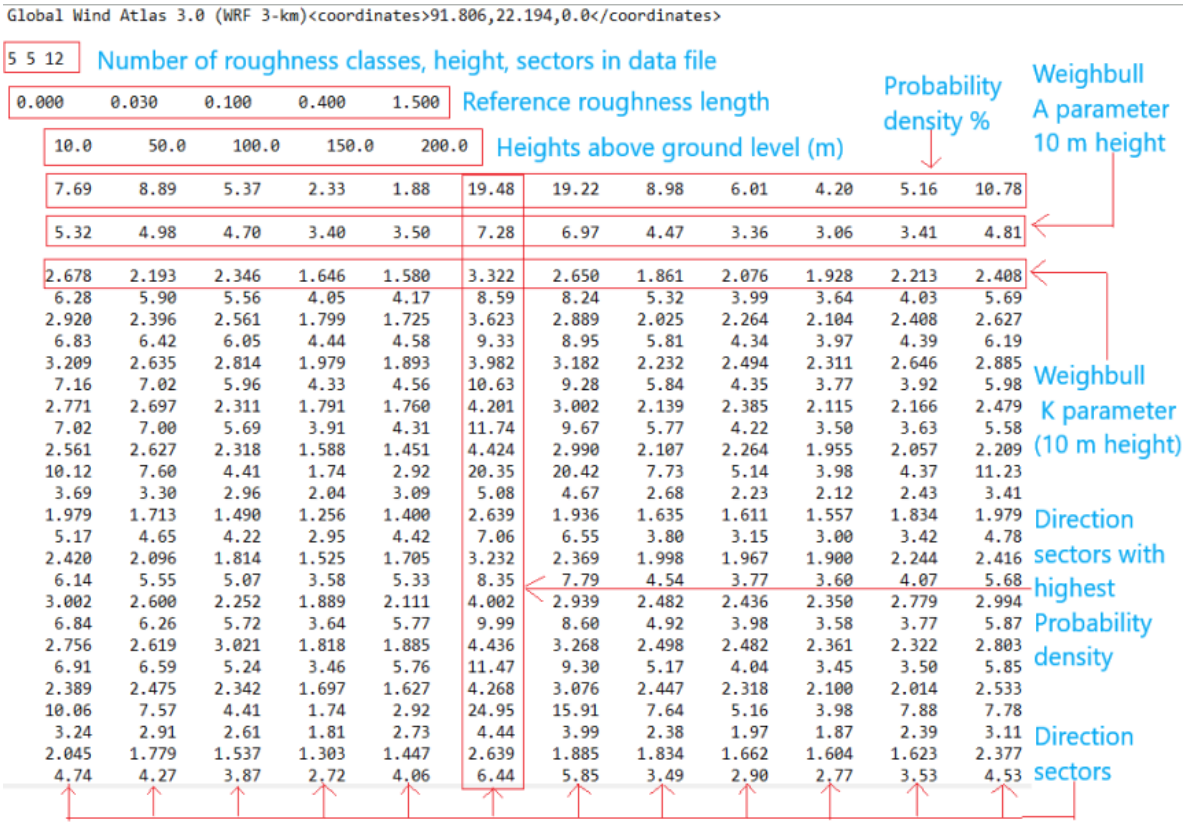

Figure 26: GWC data file for proposed wind farm site at Patenga with WRF 3 km for the coordinates of 91^0 806' Longitude and 22^0 194' Latitude. Source- GWA 3.1

Detailed meaning of values indicated in the GWC file by line can be found in figure 15 which is obtained from GWA 3.1-

Line	Contents
1	Global Wind Atlas 2.0 (WRF 9-km) ix: XXX, iy: YYY <coordinates>lat,lon,height</coordinates>
2	Number of roughness classes, heights and sectors in data set
	Values are: 5, 5 and 12
3	Reference roughness lengths [m]
	Values are: 0.00, 0.03, 0.10, 0.40, 1.50 m
4	Reference heights above ground level [m]
	Values are: 10, 50, 100, 150 and 200 m a.g.l.
5	Frequencies of occurrence for **reference roughness #1** (0 m)
6	Weibull A-parameters for reference height #1 (10 m) in [ms-1]
7	Weibull k-parameters for reference height #1 (10 m)
8-9	Weibull A- and k-parameters for reference height #2 (50 m)
10-11	Weibull A- and k-parameters for reference height #3 (100 m)
12-13	Weibull A- and k-parameters for reference height #4 (150 m)
14-15	Weibull A- and k-parameters for reference height #5 (200 m)
16-26	As lines 5-15, but for **reference roughness #2** (0.03 m)
27-37	As lines 5-15, but for **reference roughness #3** (0.10 m)
38-48	As lines 5-15, but for **reference roughness #4** (0.40 m)
49-59	As lines 5-15, but for **reference roughness #5** (1.50 m)

Figure 27: Details meaning of values by line of GWC data file. Source : https://globalwindatlas.info/about/faq

From figure 26, it is seen the A parameter for the proposed wind farm site at Patenga is 7.28 ms^{-1} and the K parameter is 3.322 at a maximum probability density of 19.48% for roughness length of 0.0 which is applicable for water bodies.

4.1.2: Wind Turbine Selection for Proposed Wind Farm

Multiple choices are available from different manufacturers for the selection of wind turbines. The selection of turbines involves various factors including budgetary capabilities, production scale, and so on. For this project, a Horizontal axis wind turbine is selected. VESTAS V90-2.0 MW of Wind Class IEC S/ IEC IIA wind turbine used during the calculation of this project. Specification of V90-2.0 MW horizontal axis turbine is given in table 2 -

Specifications	Value
Rated Power	2000 Kw
Wind Class	IEC S / IEC II A
Rotor Diameter	90 m
Swept Area	6362 m²
Cut in Wind Speed	4 m/s
Cut-out Wind Speed	25 m/s
Re-cut in wind speed	23 m/s
Frequency	50/ 60 HZ
Hub Heights	87 m
Blade length	44 m
Max Chord	3.9 m
Max Sound	104dB(A)

Table 3: Specification of Vestas V90-2.0 MW wind turbine. Source- Vestas wind system A/S, Denmark.

4.1.3: Wind Turbine Power Calculation

Power calculation process of the wind turbines are described in methodology chapter 3.1 of this document.

A small-scale wind farm consisting of 7 Vestas V90-2.0 MW wind turbines has been considered during calculation. Optimum number of wind turbines can be determined with the help of optimisation modelling, though this literature proposes 7 units turbine to install considering small energy demand of Chittagong port as well as port's anchorage area limitation. As this study focuses only to explore wind energy potential of the proposed site, turbine unit number is just a rational assumption to meet Chittagong port energy demand. Results obtained after calculating in the software are presented in the next sections -

4.1.3.1: "Wind Probability Density vs Speed" Weibull Diagram

This diagram shows the probability percentage of different wind speed in the proposed location. Percentage values of probable wind speed from 1 to 20 m/s at the proposed site as obtained from Python programming calculation is presented in figure 28. Figure 29 is the "Wind Probability and Wind Velocity

Weibull Diagram" as obtained from Python programming calculation for the proposed location.

```
[0.00000000e+00  4.53738039e-03  2.24104499e-02  5.52624699e-02
 9.90779283e-02  1.43132237e-01  1.72111749e-01  1.73171282e-01
 1.44640141e-01  9.87593073e-02  5.40301645e-02  2.31395009e-02
 7.56110839e-03  1.83390033e-03  3.20707292e-04  3.92292193e-05
 3.25249536e-06  1.76943983e-07  6.10915956e-09  1.29362677e-10
 1.62233471e-12]
```

Figure 28: Wind Probability density values (%) for wind speed from 1 m/s to 20 m/s at proposed wind farm site at Patenga, Chittagong anchorage as obtained from Python programming software 3.9.2.

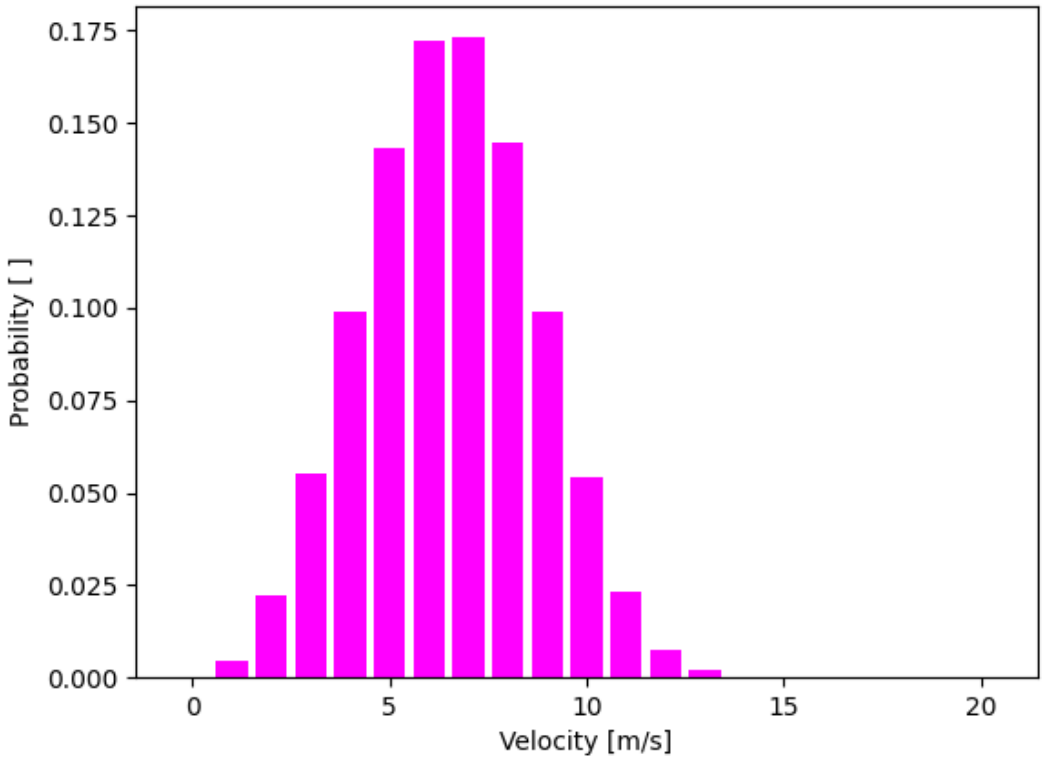

Figure 29: Wind Probability vs Wind Velocity Weibull Diagram of the proposed wind farm site

Figure 28 and 29 shows that in proposed wind farm site, probability of wind speed of 6 and 7 m/s is about 17% each, the probability for 5 and 8 m/s is about 14% each while there is 10% probability for a wind speed of 4 m/s and 9 m/s. Cut in speed of the selected wind turbine is 4 m/s. That means, more than 90% of the time of a year, this wind turbine will be able to generate electricity at the proposed location.

4.1.3.2: "Time vs Wind Speed" Weibull Diagram

This diagram shows how much time in hour in a year different wind speed from 1 to 20 m/s exists in the proposed location. Yearly "Time vs velocity' Weibull diagram for the proposed location as obtained from Python programming calculation is presented in figure 30 -

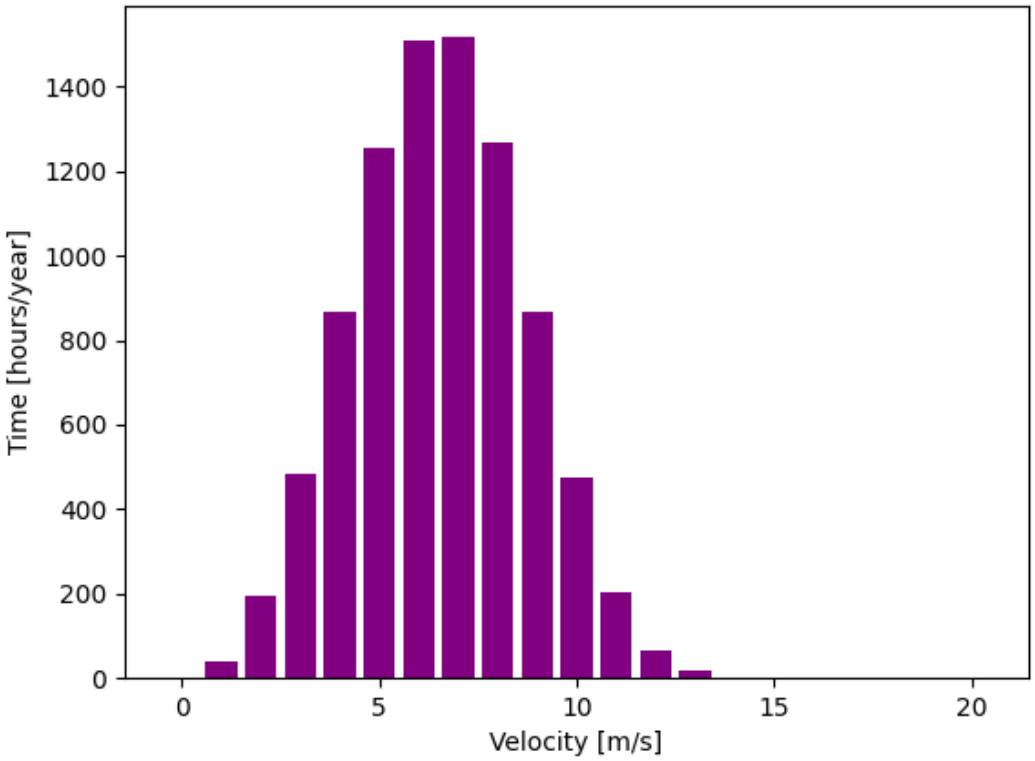

Figure 30: Time (hours/year) vs Wind Velocity (m/s) Weibull diagram for Patenga proposed wind farm site calculated in Python programming software basis data from GWA 3.1

Time and velocity diagram in figure 30 shows that at the proposed site yearly about 3000 hours (125 days) wind speed remains 6 m/s and 7 m/s, about 2600 hours (108 days) there is availability for 5 m/s and 8 m/s of wind speed while wind speed remains 9 m/s for more than 850 hours (35 days) and 10 m/s for about 500 hours (21 days). From this diagram we understand that about 10 months of the year wind turbine will remain productive at the proposed wind farm site.

4.1.3.3: Power vs Wind Speed Weibull Diagram

This diagram indicates how much power a Vestas V90-2.0 MW wind turbine will generate at different wind speed. Power generation values at different wind speed and power vs wind velocity Weibull diagram as obtained from Python calculation is presented in figure 31 and 32 -

```
[0.00000000e+00  1.71766433e+03  1.37413147e+04  4.63769370e+04
 1.09930517e+05  2.14708042e+05  3.71015496e+05  5.89158866e+05
 8.79444138e+05  1.25217730e+06  1.71766433e+06  2.00000000e+06
 2.00000000e+06  2.00000000e+06  2.00000000e+06  2.00000000e+06
 2.00000000e+06  2.00000000e+06  2.00000000e+06  2.00000000e+06
 2.00000000e+06]
```

Figure 31: Power generation (W) values by a single turbine at wind speed from 1 m/s to 20 m/s at Patenga proposed wind farm site calculated in Python.

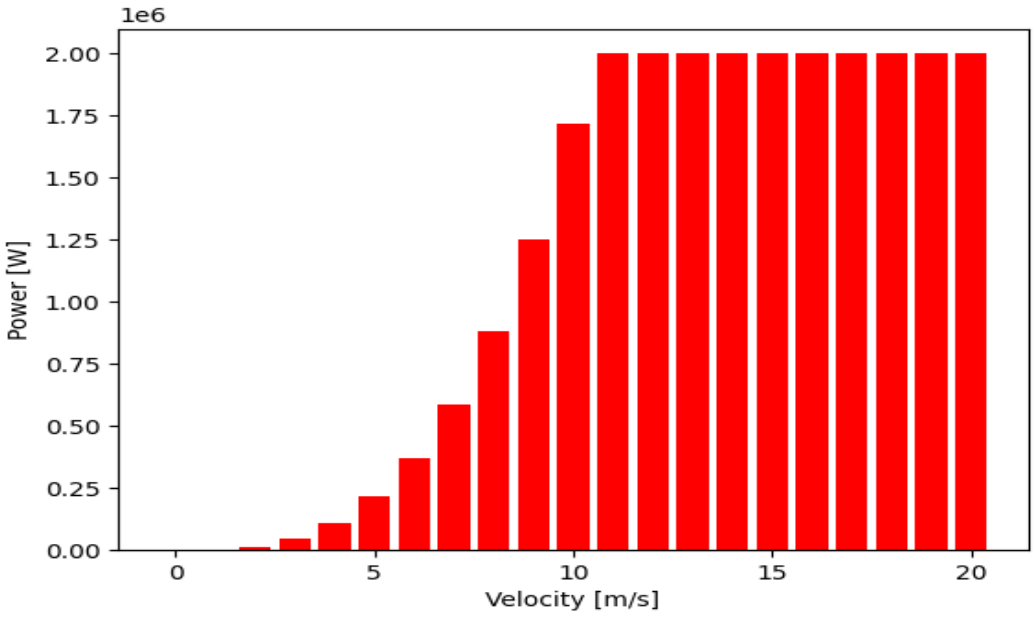

Figure 32: Power (MW) vs wind velocity (m/s) Weibull diagram for Patenga proposed wind farm site plotted in Python 3.9.2.

Figures 31 & 32 show that at only 11 m/s wind speed, Vestas V90-2.0 MW wind turbines reach their maximum power output of 2 MW. From figure 32, it is seen that if wind speed remains 9 m/s, then selected wind turbine will generate about 1250 kw electricity and at 10 m/s wind speed 1700 kw power will be produced while at 11 m/s and above this turbine will produce 2000 kw power. From figure 30, it is understood that more than approximately 7700 hours per year, wind turbines can generate electricity at various capacities at the proposed wind farm site. Which indicates, at least 10 months out of every 12 months, wind farm can produce electricity at this location. In figure 32, the power bar is flat from wind speed 11 m/s to 20 m/s as this is the power cut-out range for the selected wind turbines.

4.1.3.4: "Energy vs Wind Speed" Weibull Diagram

Values of energy array obtained at wind speed from 1 m/s to 20 m/s in Watt-hour and "Energy (GWh) vs Velocity (m/s)" Weibull diagram presented in figure 33 & 34 -

```
[0.00000000e+00  6.82727810e+04  2.69763362e+06  2.24510398e+07
 9.54111861e+07  2.69209187e+08  5.59379664e+08  8.93742469e+08
 1.11429762e+09  1.08329806e+09  8.12977813e+08  4.05404056e+08
 1.32470619e+08  3.21299338e+07  5.61879175e+06  6.87295921e+05
 5.69837188e+04  3.10005858e+03  1.07032475e+02  2.26643411e+00
 2.84233041e-02]
```

The total energy produced yearly by one turbine is 5429.90383487799 MWh.

The total energy produced yearly by the wind farm is 38009.32684414594 MWh

Figure 33: Values of energy (Wh) array and total annual energy produced by single turbine as well as entire windfarm at wind speed 1 m/s to 20 m/s as obtained from Python 3.9.2 programming calculation.

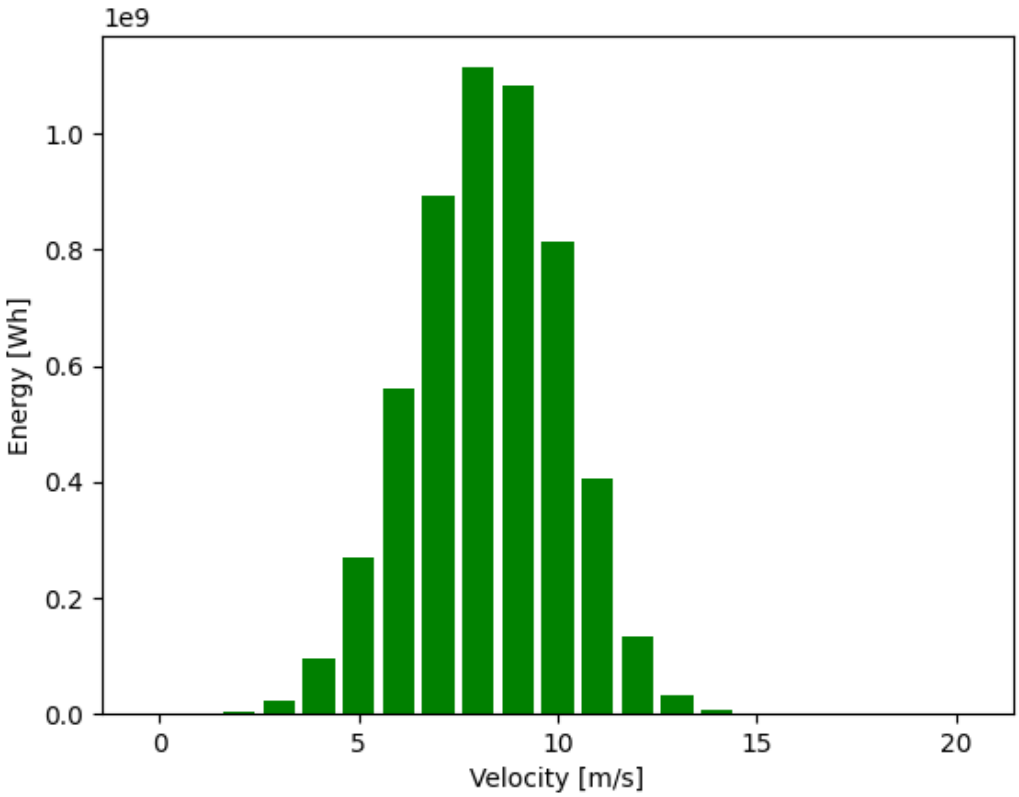

Figure 34: Energy (GWh) vs wind velocity (m/s) Weibull diagram for Patenga proposed wind farm site plotted in Python 3.9.2.

Calculation in Python showed in figure 33 that one wind turbine can produce a total of about 5430 MWh energy in one year considering all wind speed and entire wind farm can generate 38009 MWh energy yearly at the proposed wind farm site. According to figure 34, we understand that at only 8 m/s wind speed a Vestas V90-2.0 MW wind turbine will produce more than 1 GWh energy in a year.

4.2: Solar Data analysis and Photovoltaic power calculations

4.2.1: Location Data

Chittagong port has sufficient space for the installation of photovoltaic panels. Besides, ports warehouses rooftops, parking areas, and buildings can be utilized to fix the solar panels to generate at least 3 MW of electricity from Solar Energy. The location shown in the figure 35 within Chittagong port is chosen for solar plant

installation. Data is collected from European Commissions PV-GIS database which provides reliable solar data from all over the world using space satellites.

Site Location: Chittagong port, Bangladesh

Latitude : 22^0 318' , Longitude: 91^0 799' , Elevation: 7.0 m

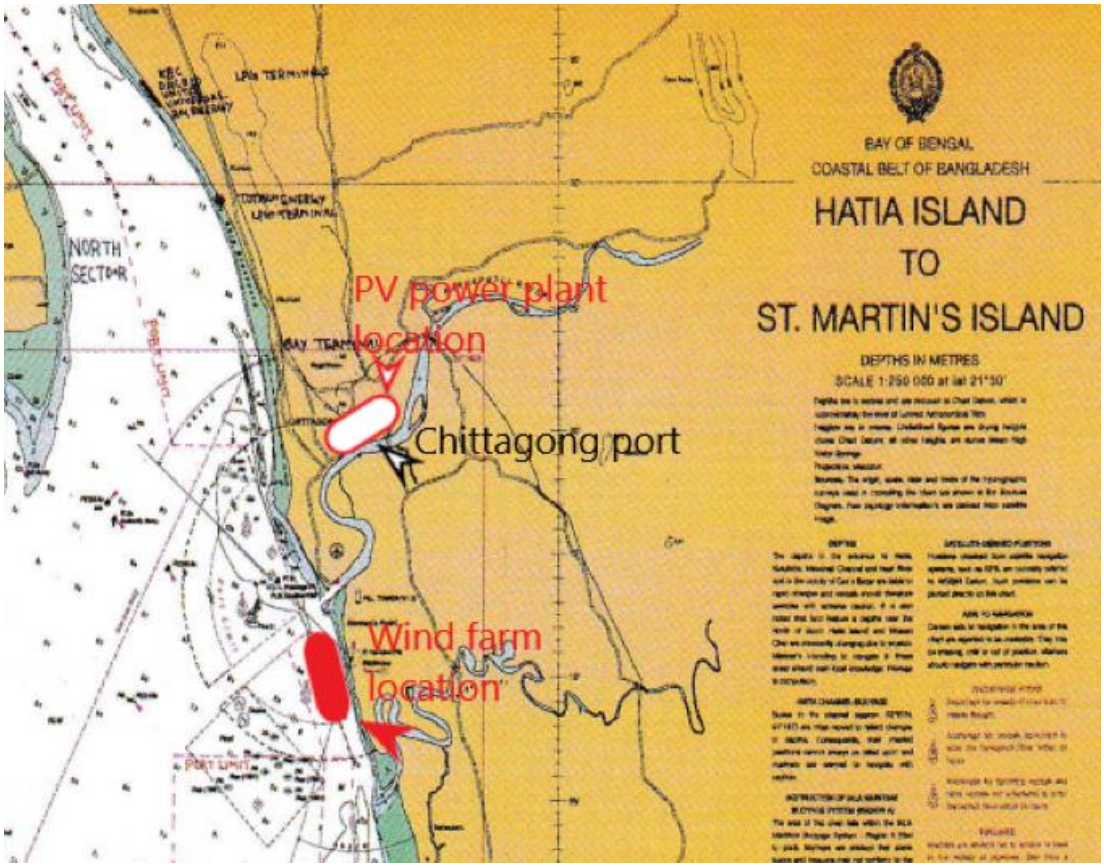

Figure 35: Location of Solar Plant within Chittagong port, Bangladesh. Source- CPA overview, 2020.

4.2.2: Monthly average GHI, DHI and Diffuse to Global Ratio for Chittagong Port

GHI is the total solar irradiance that incident on the horizontal plane of the earth surface and DIF is the diffuse solar irradiance incident on the horizontal plane of the earth surface. DHI is a direct solar irradiance incident on earth's horizontal plan. The monthly average DHI, GHI and diffuse to the global ratio for the location of Chittagong port is calculated using PV-GIS software for the year 2016 from January to December. Values are given in figures 36, 37 and table 4 -

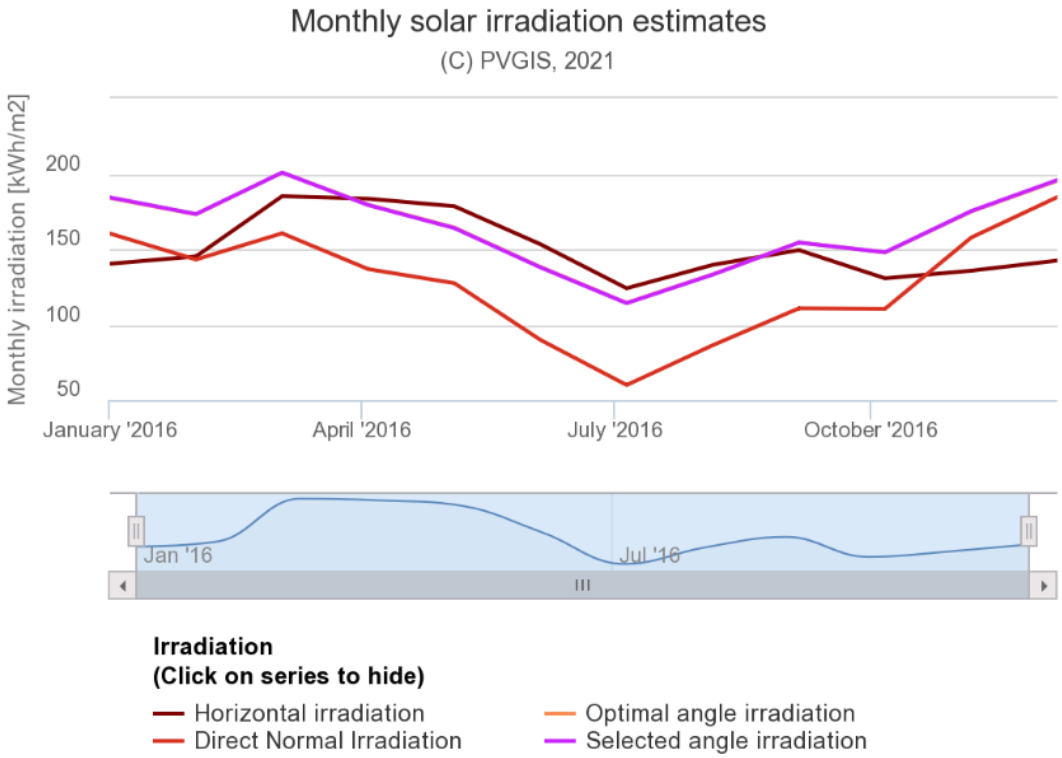

Figure 36: Monthly average GHI, DHI for Chittagong port for the year 2016 as calculated in PV-GIS software.

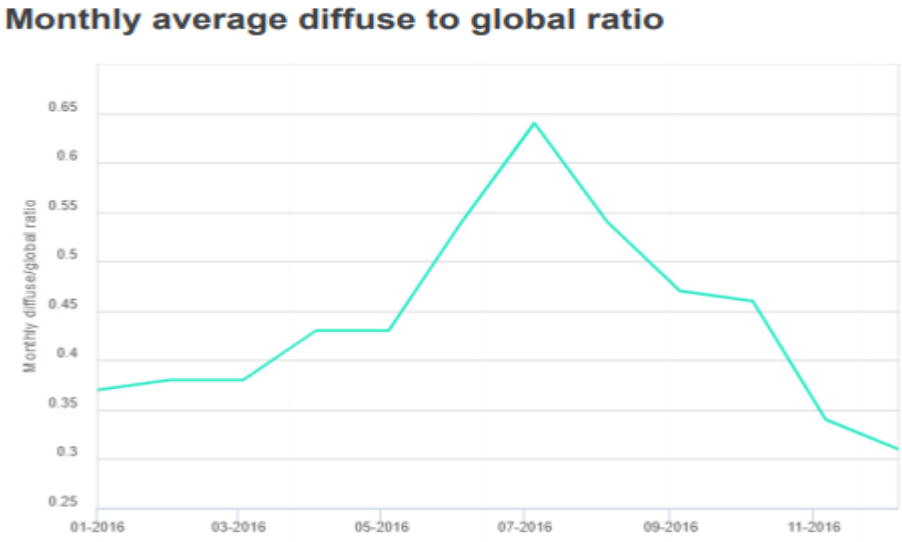

Figure 37: Monthly average diffuse to the global ratio for Chittagong port for the year 2016 as calculated in PV-GIS software.

Month	Monthly average GHI in KWh/m2	Monthly average DHI in KWh/m2	Diffuse/Global Ratio
January	140.29	160.32	0.37
February	145.16	143.11	0.38
March	185.08	160.48	0.38
April	183.4	136.74	0.43
May	178.4	127.42	0.43
June	153.2	89.8	0.54
July	124.05	59.92	0.64
August	139.57	86.31	0.54
September	149.34	110.75	0.47
October	130.65	110.45	0.46
November	135.68	157.64	0.34
December	142.42	184.48	0.31

Table 4: Monthly Average GHI, DHI, Diffuse/Global ratio for Chittagong port for the year 2016 as calculated in PV-GIS software.

From table 4 and figures 36, 37, it is seen that maximum monthly average GHI in 2016 for the Chittagong port area was 185.08 KWh/m^2 in March, and the minimum was 124.05 KWh/m^2 in July. The monthly average DHI found maximum of 184.48 KWh/m^2 in December and the minimum was 59.92 KWh/m^2 in July. In Chittagong, sufficient solar energy is available round the year, although the potential is less in June, July, and August.

4.2.3: Monthly Average Hourly GHI, DHI, DIF for Chittagong port

Within a day, PV output power changes with the change of solar irradiance. Electricity production of a PV panel is the summation of all hourly production within that particular day. To calculate hourly electricity production by a PV panel, it is required to consider hourly global solar irradiance incidents on the panels. Average monthly total GHI, DHI, DIF is required to convert to average hourly GHI, DHI, DIF. Hourly irradiation data can be obtained from daily average irradiation data according to the Liu-Jordan correlation equation below (Garg & Garg, 1987)-

$$GHI(hr) = \left\{\frac{\pi/24(cos\omega(hr) - cos\omega ss}{sin\ \omega ss - 2\pi\omega ss/360(cos\ \omega ss)}\right\} \times GHI(day) \quad \text{....31(Garg \& Garg, 1987)}$$

$$DIF(hr) = \left\{\frac{\pi/24(cos\omega(hr) - cos\ \omega ss}{sin\ \omega ss - 2\pi\omega ss/360(cos\ \omega ss)}\right\} \times GHI(day) \quad \text{...32 (Garg \& Garg, 1987)}$$

Where, hr = 0, 1,2,3……24 (denotes every hour of a day)

ω = Solar Hour angle

ω_{SS} = Sunset Hour Angle

Daily global, diffuse, and direct horizontal irradiance at Chittagong port location is calculated using PV-GIS software. Obtained values and graphs for all hours of January to June are presented in table (first 6 months in table 5, rest six months in table 6). All values from 2000 hours to 0500 hours are zero, hence not displayed in tables. All the values indicated in table 5 and table 6 are in W/m^2. The calculation process is described in Methodology chapter 3.2.

	January	February	March	April	May	June
Hour	GHI/DHI/DIF	GHI/DHI/DIF	GHI/DHI/DIF	GHI/DHI/DIF	GHI/DHI/DIF	GHI/DHI/DIF
5:00	0	0	0	0	0	0
6:00	0	0	0	19/0/18	37/0/36	33/0/32
7:00	6/2/03	42/19/22	79/22/56	119/29/88	111/18/90	88/9/77
8:00	263/149/111	286/161/121	291/135/151	319/142/171	281/109/166	211/58/149
9:00	515/330/179	544/350/186	544/321/213	523/286/227	453/215/229	348/131/209
10:00	735/508/217	769/538/221	757/496/249	708/435/260	598/330/256	469/207/251
11:00	895/649/234	917/664/240	904/623/265	825/533/276	684/402/269	548/261/275
12:00	968/718/237	987/727/246	960/676/268	857/566/276	704/412/278	572/274/285
13:00	947/698/236	986/730/242	931/654/262	825/545/265	684/402/269	550/261/278
14:00	848/617/219	891/650/228	835/574/247	735/480/242	612/355/245	478/209/259
15:00	669/468/193	716/505/200	664/434/220	576/349/216	469/249/211	396/170/217
16:00	440/289/145	491/323/161	450/270/172	390/212/171	312/142/164	267/89/172
17:00	166/98/66	229/132/94	213/104/105	181/71/106	148/42/103	133/23/107
18:00	0	0	11/2/09	25/0/24	35/0/34	42/0/41
19:00	0		0	0	0	0

Table 5: Hourly GHI, DHI, and DIF (Monthly average) for January to June for the location of Chittagong port from 0500 hours to 1900 hours as calculated in PV-GIS software.

Graphical representation of hourly irradiance values shown in table 5 is presented in Figure 38 for January to June as obtained from PV-GIS software calculations.

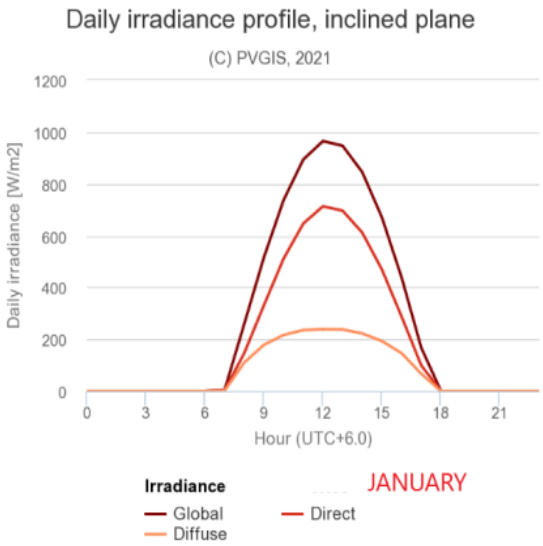
Daily irradiance profile, inclined plane
(C) PVGIS, 2021
Daily irradiance [W/m2]
Hour (UTC+6.0)
Irradiance
Global
Direct
Diffuse
JANUARY

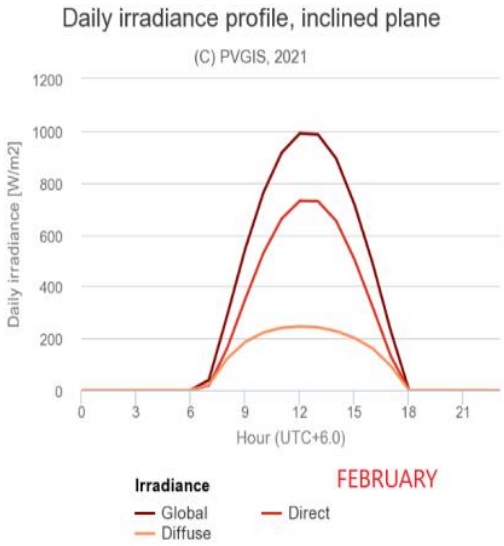
Daily irradiance profile, inclined plane
(C) PVGIS, 2021
Daily irradiance [W/m2]
Hour (UTC+6.0)
Irradiance
Global
Direct
Diffuse
FEBRUARY

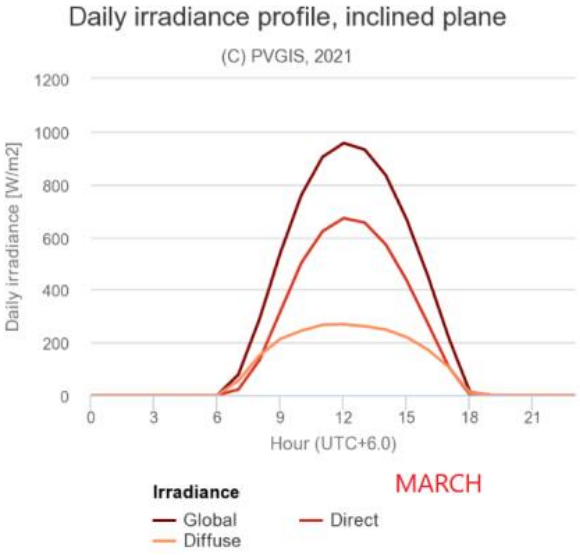
Daily irradiance profile, inclined plane
(C) PVGIS, 2021
Daily irradiance [W/m2]
Hour (UTC+6.0)
Irradiance
Global
Direct
Diffuse
MARCH

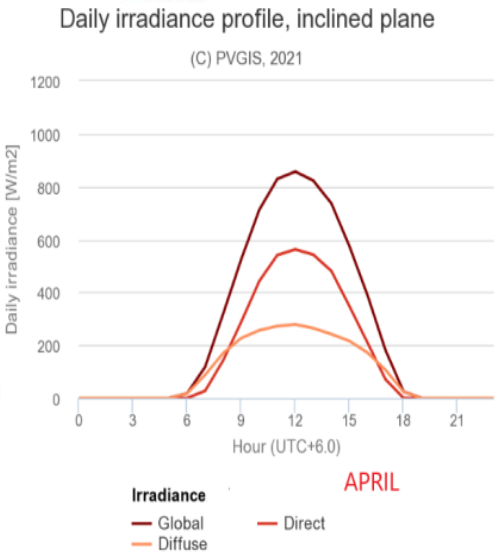
Daily irradiance profile, inclined plane
(C) PVGIS, 2021
Daily irradiance [W/m2]
Hour (UTC+6.0)
Irradiance
Global
Direct
Diffuse
APRIL

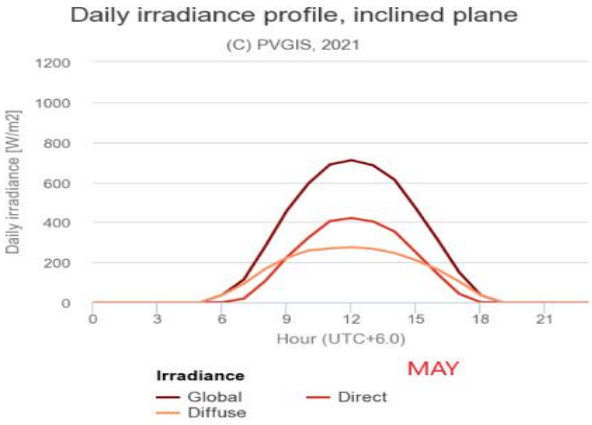
Daily irradiance profile, inclined plane
(C) PVGIS, 2021
Daily irradiance [W/m2]
Hour (UTC+6.0)
Irradiance
Global
Direct
Diffuse
MAY

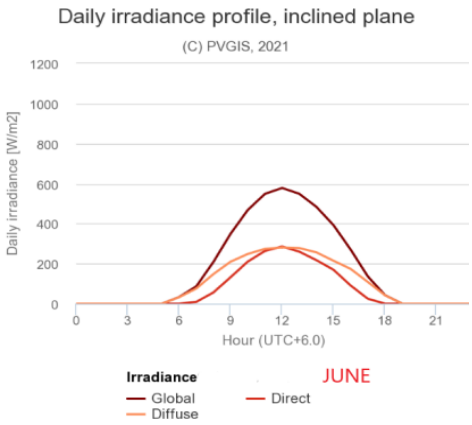
Daily irradiance profile, inclined plane
(C) PVGIS, 2021
Daily irradiance [W/m2]
Hour (UTC+6.0)
Irradiance
Global
Direct
Diffuse
JUNE

Figure 38: Graphical representation of hourly GHI, DHI, DIF values for the month of January to June

The table 6 shows the hourly GHI, DHI, DIF values in W/m^2 for the location of Chittagong port as obtained from the calculation of PV-GIS software-

	July	August	Sept.	Oct.	Nov.	Dec
Hour	GHI/DHI/DIF	GHI/DHI/DIF	GHI/DHI/DIF	GHI/DHI/DIF	GHI/DHI/DIF	GHI/DHI/DIF
5:00	0	0	0	0	0	0
6:00	28/0/28	23/0/22	15/0/14	1/0/1	0	0
7:00	78/9/67	72/11/60	90/23/65	111/43/66	115/58/56	52/30/22
8:00	189/51/134	195/59/132	245/103/137	323/183/135	370/225/141	305/180/122
9:00	319/116/196	342/133/202	425/218/199	522/332/182	623/428/187	539/355/178
10:00	439/178/252	485/226/250	579/329/240	682/448/223	810/590/209	748/531/207
11:00	518/227/280	588/291/285	672/379/281	771/519/240	908/673/222	899/669/218
12:00	558/254/293	623/297/314	696/393/291	758/492/254	914/669/231	947/713/221
13:00	551/252/288	617/297/308	692/407/273	717/456/250	859/624/223	913/686/215
14:00	504/230/264	563/271/281	608/349/248	621/393/218	745/537/199	811/601/199
15:00	405/168/229	439/189/241	471/257/205	478/295/176	565/388/170	629/452/169
16:00	271/88/177	285/94/186	292/135/152	292/165/123	335/213/118	385/257/123
17:00	149/29/116	147/32/111	118/36/80	85/34/49	64/36/27	87/55/31
18:00	46/0/45	35/0/34	4/0/4	0	0	0
19:00	0	0	0	0	0	0

Table 6: Hourly GHI, DHI and DIF (Monthly average) in W/m^2 for July to December for the location of Chittagong port from 0500 hours to 1900 hours as calculated in PV-GIS software.

The figure 39 demonstrates a graphical representation of table 6 values-

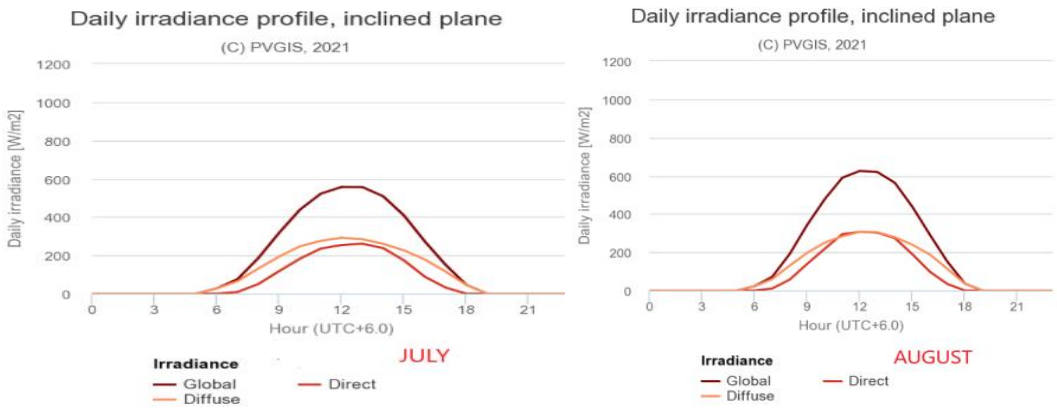

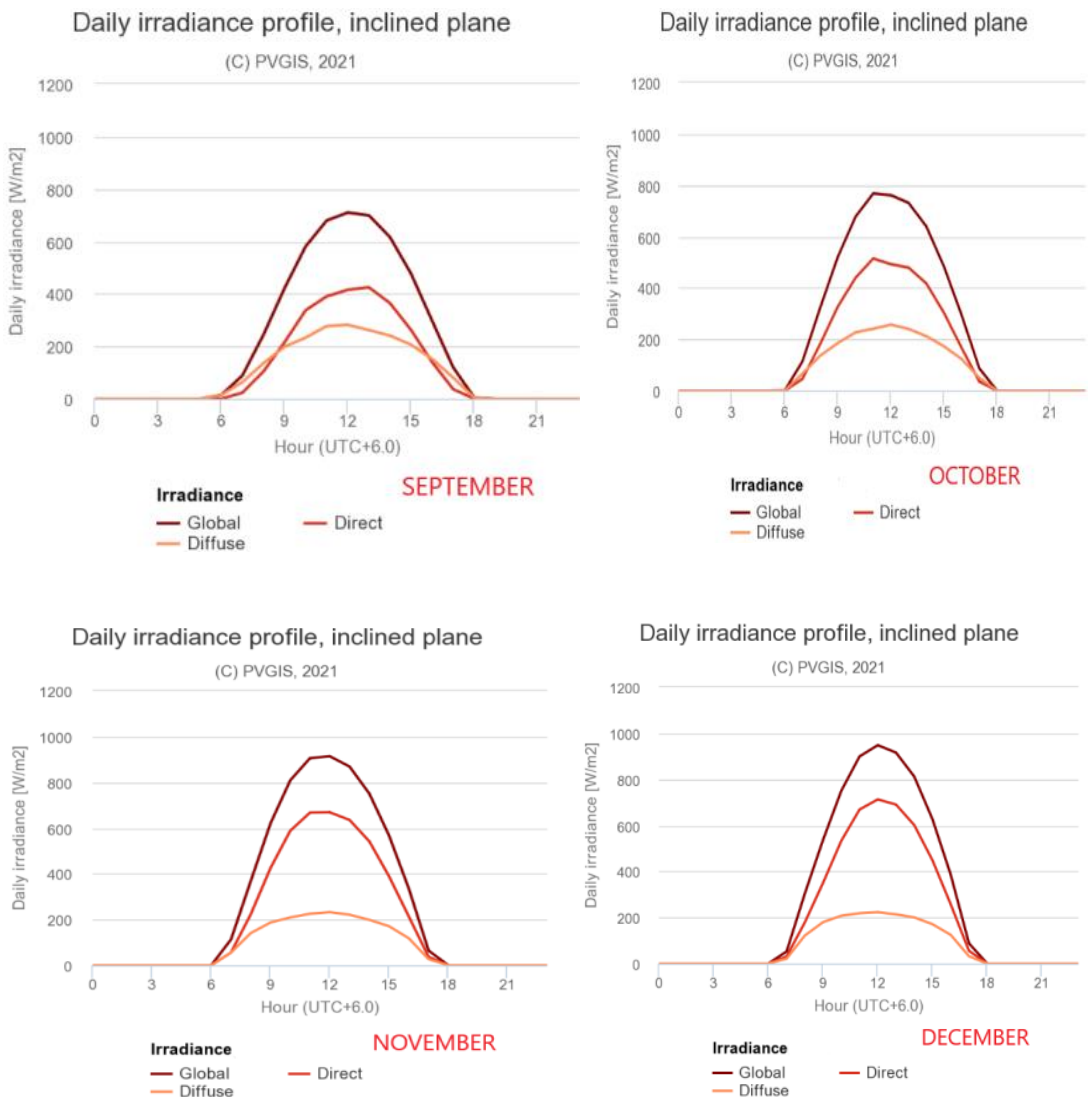

Figure 39: Graphical representation of hourly GHI, DHI, DIF values for July to December as obtained from PV-GIS software calculation.

Figure 38 and figure 39 show that the beginning and end months of the year have maximum hourly solar irradiance while middle months have lower potential. These graphs also indicates that throughout the year solar panels will be able to generate electricity at the proposed location.

4.2.4: Selection of Photo-Voltaic Panel

There are various types of Photo-voltaic panels available of different capacities manufactured by different companies. A suitable PV system can be selected considering budgetary, logistics, and requirements constraints. In this document,

HiDM5 CS1-Y 400MS all-black high-density mono parc module PV panel made by Canadian Solar is selected for calculation. Specification of this PV panel is as shown in table 7 -

Specification	Data
Cell-Type	Mono-Crystalline
Dimensions	2021 *996 *35 mm (79.6 *39.2 *1.38 in)
Maximum power P_{max}	400 W
Operating Voltage V_{mp}	43.5 V
Open Circuit Voltage V_{oc}	52.3 V
Operating Current I_{mp}	9.20 A
Short Circuit Current I_{sc}	9.90 A
Module Efficiency	19.9%
Temperature co-efficient P_{max}	-0.37%/^{0}C
Temperature co-efficient V_{oc}	-0.29 % / °C
Temperature co-efficient I_{sc}	0.05 % / °C

Table 7: Specification of HiDM5 CS1-Y 400MS PV panel selected for Chittagong port Solar power plant as obtained from manufacturer Canadian Solar specifications brochure.

The above values are applicable under standard test conditions of Irradiance of 1000 W/m^2, spectrum AM 1.5, and cell temperature of 25^0 C.

Current-temperature curves for the above PV panel is shown in the below figure-

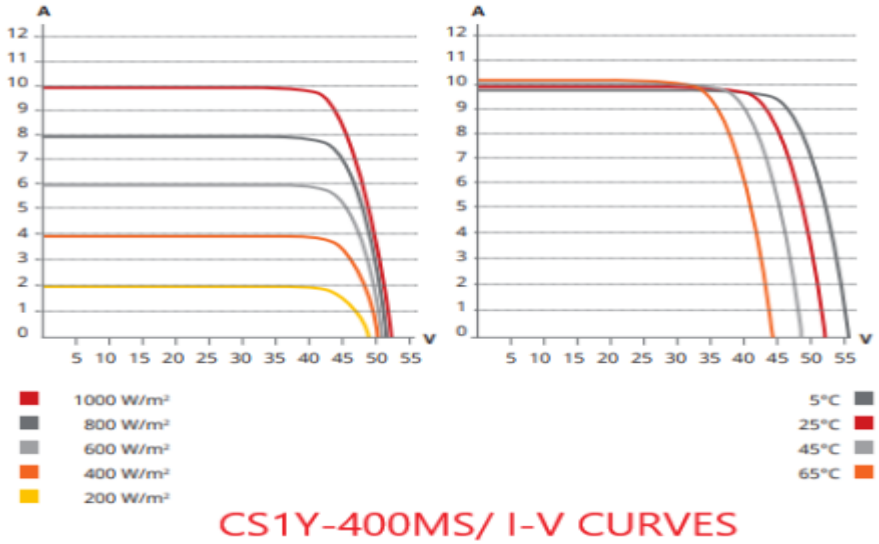

Figure 40: HiDM5 CS1-Y 400MS photo-voltaic panel Current-Voltage curves as obtained from Canadian Solar specifications module.

4.2.5: Photo-Voltaic Panel Power Output and Required Number of PV Panels Calculation

For this project, the monthly average electricity generation capacity has been calculated using PV-GIS software. Details of the calculation process is described in methodology chapter 3.2. Figure 42 shows the monthly average sum of global irradiance received by the given PV module system and figure 43 shows the monthly average electricity production by PV module in KWh as obtained from PV-GIS software calculation for the location of Chittagong port.

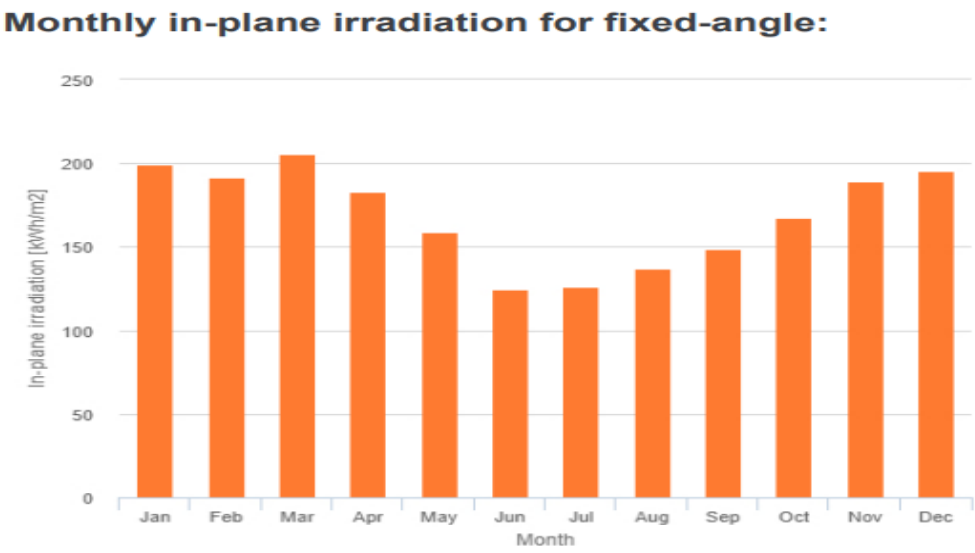

Figure 42: PG-GIS calculation result of the average monthly sum of global irradiation per square meter [kWh/m²] received by the modules of the given system at Chittagong port.

According to figure 42, monthly average in-plane irradiation for the fixed angle of selected PV panel is maximum of about 210 KWh in March and minimum of about 130 KWh in June.

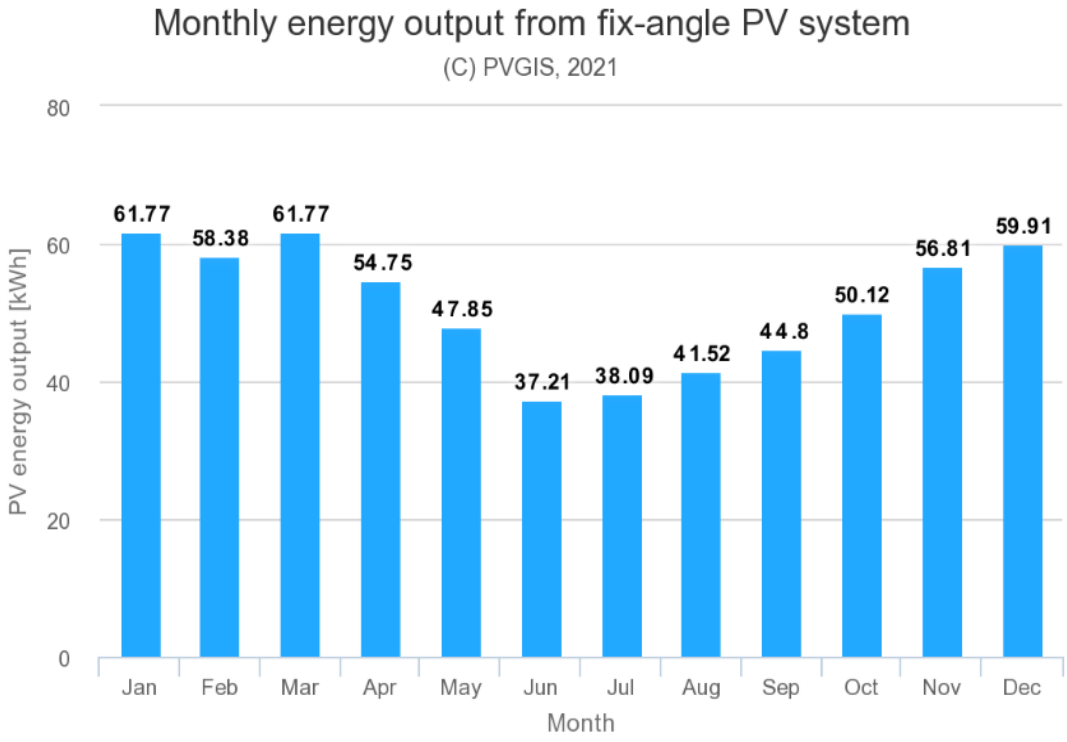

Figure 43: PV-GIS calculation result of average monthly electricity production from the given system [kWh] at Chittagong port location.

As per figure 43, the selected fixed angle PV panel produces average monthly maximum of 61.77 KWh energy in January and March. The lowest monthly average energy production is 37.21 KWh. According to PV-GIS software calculation,
In the 1st year, total electricity production by a single Canadian Solar HiDM5 CS1-Y 400MS PV-module in the Chittagong port location is 612.98 KWh which is the summation of 12 months of production by a single panel.
Average daily electricity production in a year according to equation 29 = 612.98/365 = 1.68 KW/day.
If the plan is to produce 3 MWh energy from photovoltaic installations, then the required number of PV panels is = 3000/0.07 = 42857.14 units.

4.2.6: GHG Emission Calculation as Measure of Environmental Performance

Equivalent Carbon-Dioxide (eq.CO_2) is a basis to evaluate the environmental performance of the electricity generation system. Eq CO_2 refers to an amount and it compares environmental impacts of different GHGs basis their Global Warming Potential (GWP). This study prefers to calculate the emission of eq.CO_2 considering Life Cycle Assessment (LCA) of the electricity generation system. LCA is conducted in four-stages to calculate eq.CO_2 as described in the table 8 -

Stage Name	Scope of eq.CO_2 emission calculation
Metallurgical Stage	Extraction of resources, Material processing, Finishing of final products. Composition, production, fabrication, finishing of silicon cells, inverters, glass, required electronics, blade, gear, rotor, turbine, tower and other components for wind, PV and LAES module are considered in this stage.
transportation and Construction stage	Transportation of PV-WT-LAES module components to power plant site. Fitting of modules with balance of systems including infrastructures, wiring, components inter-connections. GHG emission calculation includes fossil fuel consumptions for transportation and consumptions during processing of balance of systems materials.
Operation stage	Periodical maintenance, Inspections, cleaning and replacements of parts- consumable items of PV-WT-LAES modules.
Decommissioning stage	Recycle, disposal, deconstruction process

Table 8: Life Cycle Assessment stages and scope of eq.CO_2 emission calculations

According to many LCA studies over various PV and WT systems, electricity generation from the WT module emits average of 34.11 g eq. CO2/kWh while PV module emits average of 49.91 g eq. CO2/ kWh (Nugent et al, 2014; Talukdar, 2017).

Emission of eq.CO_2 for 1 KWh national grid electricity generation in Bangladesh can be calculated as below-

Emission for 1 KWh grid electricity generation

$$= \frac{total\ daily\ emission\ of\ eq.CO_2\ for\ 1\ unit\ grid\ electricity\ generation\ from\ different\ fuels}{Total\ daily\ grid\ electricity\ generation\ from\ all\ fuels}$$

(Nugent et al, 2014; Talukdar, 2017)

$$= \frac{EL_{G.D} \times EM_{G/KWh} + EL_{O.D} \times EM_{O/KWh} + EL_{C.D} \times EM_{C/KWh} + EL_{HYD.D} \times EM_{HYD/KWh}}{EL_{total.D}}$$

$$= \frac{\{(101.74\times10^6\times499) + (26.10\times10^6\times733) + (3.46\times10^6\times888) + (2.15\times10^6\times26)\}}{133.45\times10^6}$$

= 547.24 g eq.CO_2

Where, $EL_{G.D}$ = Daily electricity generation from gas in Bangladesh

= 101.74×10^6 KWh (BPDB, 2017)

$EM_{G/KWh}$ = Emission of eq.CO_2 for generation of 1 KWh electricity from gas = 499 g/KWh (WNA, 2017)

$EL_{O.D}$ = Daily electricity generation from Oil in Bangladesh

= 26.10×10^6 KWh (BPDB, 2017)

$EM_{O/KWh}$= Emission of eq.CO_2 for generation of 1 KWh electricity from Oil = 733 g/KWh (WNA, 2017)

$EL_{C.D}$ = Daily electricity generation from Coal in Bangladesh

= 3.46×10^6 KWh (BPDB, 2017)

$EM_{C/KWh}$= Emission of eq.CO_2 for generation of 1 KWh electricity from Coal = 888 g/KWh (WNA, 2017)

$EL_{HYD.D}$ = Daily electricity generation from Hydro power in Bangladesh

= 2.15×10^6 KWh (BPDB, 2017)

$EM_{HYD/KWh}$ = Emission of eq.CO_2 for generation of 1 KWh electricity from Hydro power = 26 g/KWh (WNA, 2017)

$EL_{total.D}$ = Total daily electricity generation in Bangladesh from all fuels

Similarly, Emission for 1 KWh electricity generation from PV-WT-LAES system

$$= \frac{total\ daily\ emission\ of\ eq.CO_2\ for\ 1\ unit\ electricity\ generation\ from\ PV-WT-LAES\ system}{Total\ daily\ electricity\ generation\ from\ PV-WT-LAES\ system}$$

(Nugent et al, 2014; Talukdar, 2017)

$$= \frac{EL_{PV.D} \times EM_{PV/KWh} + EL_{WT.D} \times EM_{WT/KWh} + EL_{LAES.D} \times EM_{LAES/KWh}}{EL_{PV-WT-LAES.D}}$$

$$= \frac{\{(3000\times49.91) + (10000\times34.11) + (1000\times547.24)\}}{14000}$$

= 74.14 g eq.CO_2

Where, $EL_{PV.D}$ = Daily electricity generation required from PV panels

= 3 MWh = 3000 KWh

$EM_{PV/KWh}$= Emission of eq.CO_2 for generation of 1 KWh electricity from PV

= 49.91 g/KWh (Nugent et al, 2014)

$EL_{WT.D}$ = Daily electricity generation required from WT module

= 10 MWh = 10000 KWh

$EM_{PV/KWh}$= Emission of eq.CO_2 for generation of 1 KWh electricity from WT

= 34.11 g/KWh (Nugent et al, 2014)

$EL_{LAES.D}$ = Daily electricity generation required from LAES module

= 1 MWh = 1000 KWh

$EM_{PV/KWh}$= Emission of eq.CO_2 for generation of 1 KWh electricity from LAES

= 547.24 g/KWh (Considering grid generation emission)

$EL_{total.D}$ = Total daily electricity generation from PV-WT-LAES system

= 3000 + 10000 + 1000 = 14000 KWh

Saving of daily emission by installing PV-WT-LAES = 547.24 – 74.15

= 473.09 g eq.CO_2

Therefore, from the above two calculations, it is seen that installing -PV-WT-LAES electricity generation system at Chittagong port will save GHG emission of 473.09 g eq.CO_2 for 1 KWh of electricity generation.

Chapter 5

5.0: Design of Port Grid-Tie PV-WT-LAES Electricity System

In chapter 4.2.5., we have already calculated PV panel electricity production capacity and a number of PV panels required to meet the 3 MW power demand. In this chapter, the design approach to connect photovoltaic systems, wind turbine electricity systems and liquid air energy storage system with the port grids will be discussed.

5.1: Requirements of PV Inverters

PV inverters are electrical converters that convert solar panels Direct Current (DC) output into a utility frequency Alternating Current (AC) so that current can be fed to the commercial electrical grid. Sinusoidal wave inverter should be used as PV plant to be interfaced with port grid. For extraction of maximum PV electricity, inverters should be embedded with a maximum power point tracking facility. Figure 44 shows how PV panels are connected with MPPT and Inverter in an off-grid system.

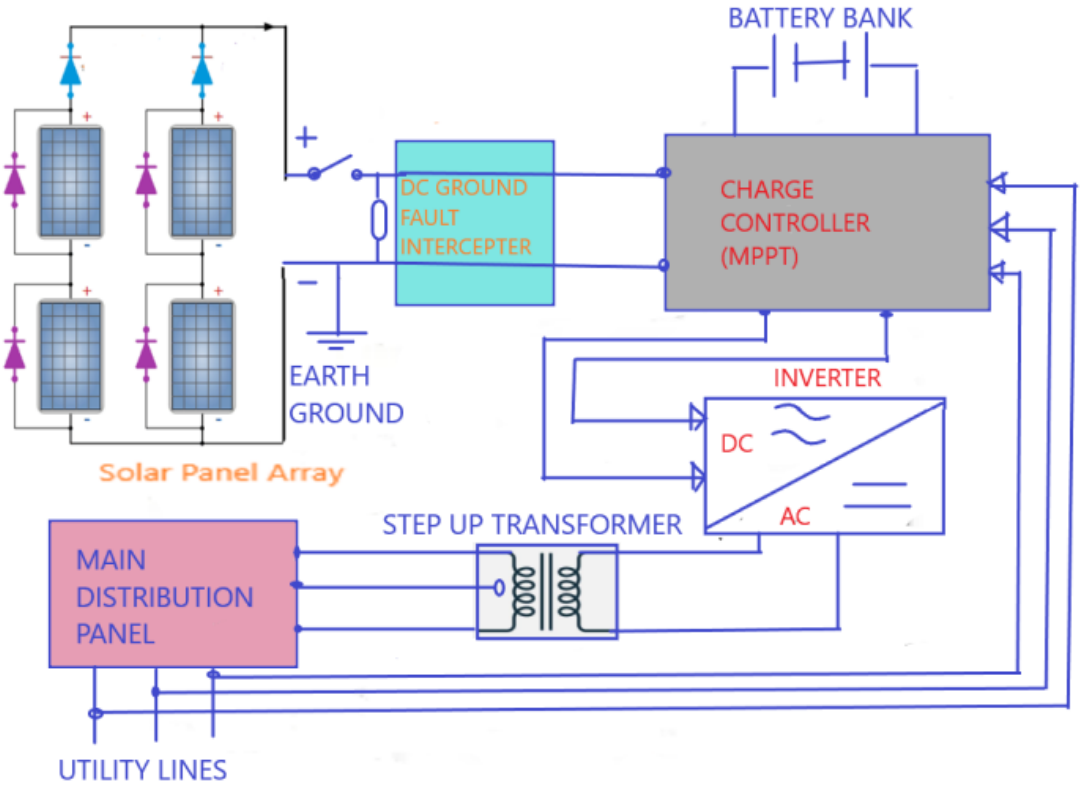

Figure 44: Typical simple off-grid PV system with Inverter circuit diagram. Reproduced by the author from 'https://solar.smps.us/off-grid.html'

Specification of selected grid-tie PV inverter for this project is as table 9 -

Description	Value
Type	3 x 330TS-SV Multi MPPT 990kw
Manufacturer	Solarmax, Germany
Rated Power	990 KW
Number of String (MPPT embedded)	9 nos
Inverter string rated power	110 KW/String
Inverter efficiency	0.95
Inverter maximum MPP voltage	800 V
Inverter minimum MPP voltage	450 V
Inverter string maximum DC voltage	900 V
Inverter string minimum DC voltage	450 V
Inverter output Voltage	280 V, 3-phase

Table 9 : Specification of grid tie inverter selected for project. Source- Talukdar, 2017.

Maximum power rating of PV inverter under record maximum solar irradiance at record minimum temperature can be found from below formula (Alsayed et al, 2013)-

PV inverter power rating = Max PV power under highest irradiance and lowest temperature = N_P X { V_{OC} + K_V (T_{MIN} + ($\frac{NT-20}{800}$) X G_H – T_R } X { I_{SC} + K_I (T_{MIN} + ($\frac{NT-20}{800}$) – T_R)) X G_H/1000 } X FF ……42 (Alsayed et al, 2013)

= 13307.23 KW

Where, Standard Test Condition (STC) = Ambient temperature 25^0C, exposure of irradiance 1000 W/m^2

N_P = Number of PV panels = 42857 units

V_{OC} = Open circuit voltage under standard test condition = 52.3 V

I_{SC} = Short circuit current under standard test condition = 9.90 A

K_V = Open circuit voltage temperature coefficient in V/^{0}C = -0.29 V/^{0}C

K_I = Short circuit current temperature coefficient = 0.05 A/^{0}C

NT = Operating cell nominal temperature = 46^0 C

T_{MIN} = Lowest ambient temperature recorded over few years = 4^0 C

G_H = Highest day peak solar irradiance recorded over few years in W/m^2

= 950 W/m^2

T_R = Manufacturer reference temperature = 25^0 C

FF = Fill Factor = 0.747

Total number of central inverters = Ceiling ($\frac{total\ power\ of\ pv\ inverters}{power\ of\ each\ inverter}$) (Talukdar, 2017)

= Ceiling ($\frac{13307.23}{990}$) = 13 ……43

5.2: Requirements of Transformer

The transformer is used in the PV-Wind electricity system to step up inverter output voltage. Transformer primary is connected with inverter output and transformer secondary is connected to the grid.

Transformer rating can be found from below formula-

$P_{trans.pv} = P_{pv.plant} \times \eta_{inv.pv} \times \frac{1}{power\ factor}$ (Talukdar, 2017)

Where, $P_{trans.pv}$ = Power rating for PV transformer

$P_{pv.plant}$ = PV plant maximum instantaneous power

$\eta_{inv.pv}$ = PV inverter efficiency

For wind turbine system transformer, wind turbine module output terminal is connected with transformer low tension side and transformer high-tension side is connected with the grid. It is necessary to ensure the same high-tension voltage and low tension of the transformer with grid voltage and wind turbine module voltage. The transformer LT side and WT output terminal voltage remain 3-phase, 400V, and transformer HT side – grid voltage is 3-phase, 33000V. Wind turbine transformer maximum rated power can be calculated from wind turbine module power curve as below-

$P_{trans.wt} = (P_{max.wt} + P_{max.pv}) \times \frac{1}{power\ factor}$ ……44 (Talukdar, 2017)

= (14 +3) x $\frac{1}{0.90}$ = 18.9 MVA

Where, $P_{max.wt}$ = Total power of wind turbine system = 14 MW

$P_{max.pv}$ = Total power of PV system = 3 MW

So, the proposed PV-WT-Grid hybrid electricity system transformer's apparent power rating should be 18.9 MVA.

5.3: PV System Electrical Connection

A large size multi-string central inverter of capacity up to 500 KW is suitable for this 3 MW project. Every string of a multi-string inverter is connected with A number of series-connected PV panels. During connection of PV panel string with an inverter, it should be confirmed that voltage generated by PV panel string is less than the allowed maximum input voltage of the inverter. Also, string MPP voltage and current should remain within the inverters safe range (Myrzik & Calais, 2003).

In the selected MPPT embedded 3 x 330TS-SV inverter, there are 9 input string terminals. According to equation 43, the required number of central inverters for this project is 13 units.

Therefore, total inverters input string terminal of this project = 13 x 9 = 117

Maximum number PV panels that can be connected with single inverters input string terminals = $\frac{42857}{117}$ = 366 units

Each inverter's input string terminals connected power rating = $\frac{Inverter\ total\ power}{117}$

= $\frac{13307}{117}$ = 113.74 kw

Each PV panel maximum power point voltage can be calculated for record lowest temperature and highest irradiance exposure as below (Talukdar,2017;Yang et al, 2003)-

$$V_{MPP.MAX} = V_{MPP.PANEL}\left[1 + 0.05391\ log\left(\frac{G_H}{G_{STC}}\right)\right] + K_V\left(T_{MIN} - T_{REF}\right) \quad \text{.....45}$$

$$= 43.5\left[1 + 0.05391\ log\left(\frac{950}{1000}\right)\right] - 0.29\ (4 - 25)$$

$$= 37.29\ V$$

Where, $V_{MPP.PANEL}$ = MPP voltage of PV panel under STC = 43.5 V (From table 6)

Other values are as defined in equation 1.

In the same way, each panel lowest MPP voltage can be calculated as below-

$$V_{MPP.MIN} = V_{MPP.PANEL}\left[1 + 0.05391\ log\left(\frac{G_{MIN}}{G_{STC}}\right)\right] + K_V\left(T_{MAX} - T_{REF}\right) \quad \text{.....46}$$

(Yang et al, 2003; Talukdar,2017)

$$= 43.5\left[1 + 0.05391\ log\left(\frac{50}{1000}\right)\right] - 0.29\ (45 - 25)$$

$$= 34.65\ V$$

Where, G_{MIN} = Minimum solar irradiance that allows MPP trackers to function suitably = 50 W/m^2

$T_{MAX.A}$ = Highest ambient temperature recorded = 45^0 C

Equation 5 is applicable for lowest irradiance exposure and highest temperature recorded. To find out open circuit voltage of each PV panel at record highest irradiance exposure and lowest temperature, below formula can be used (Talukdar,2017; Alsayed et al, 2013)-

$$V_{OC.H} = V_{STC.OC} + K_v (T_{MIN.A} + (\frac{NT-20}{800}) \times G_H - T_{REF}) \quad \text{.....47}$$

$$= 52.3 + (-0.29) ((4 + (\frac{46-20}{800}) \times 950 - 25)$$

$$= 49.44 \text{ V}$$

Similarly, open circuit voltage at record lowest irradiance exposure and highest temperature can be calculated as below-

$$V_{OC.MIN} = V_{STC.OC} + K_v (T_{MAX.A} + (\frac{NT-20}{800}) \times G_{MIN} - T_{REF}) \quad \text{.....48}$$

(Alsayed et al, 2013)

$$= 52.3 + (-0.29) ((45 + (\frac{46-20}{800}) \times 50 - 25)$$

$$= 46.03 \text{ V}$$

Where, $V_{STC.OC}$ is PV panel open circuit voltage at standard test condition as obtained from PV panel specifications. Other values are as mentioned in equation 1. Number of PV panels that can be connected in series in a string can be calculated as below (Kerekes, 2013) –

$$\text{Maximum panel in series per string} = \text{MIN} [\text{floor} (\frac{V_{IN.MAX.MPP}}{V_{MPP.MAX}}) , \text{floor}(\frac{V_{OCDC.MAX}}{V_{OC.H}})] \quad \text{....49}$$

(Kerekes, 2013)

$$= \text{MIN} [\text{floor} (\frac{800}{37.29}) , \text{floor}(\frac{900}{49.44})]$$

$$= \text{MIN} [21, 18]$$

$$= 18$$

Where, $V_{IN.MAX.MPP}$ = Inverter maximum MPP voltage = 800 V (From specification)

$V_{OCDC.MAX}$ = Inverter string maximum DC voltage = 900 V (Specification)

$V_{MPP.MAX}$ = 37.29 V (From equation 4)

$V_{OC.H}$ = 49.44 V (From equation 6)

Similarly,

Minimum panel in series per string = MAX [ceiling($\frac{V_{IN.MIN.MPP}}{V_{MPP.MIN}}$) , ceiling($\frac{V_{OCDC.MIN}}{V_{OC.MIN}}$)]

(Kerekes, 2013)

= MAX [ceiling ($\frac{450}{34.65}$) , floor($\frac{450}{46.03}$)]

= MAX [13, 10]

= 13

Where, $V_{IN.MIN.MPP}$ = Inverter minimum MPP voltage = 450 V (From specification)

$V_{OCDC.MIN}$ = Inverter string minimum DC voltage = 450 V (Specification)

$V_{MPP.MIN}$ = 34.65 V (From equation 5)

$V_{OC.MIN}$ = 46.03 V (From equation 7)

From the above calculations, it is seen that maximum of 18 PV panel units or minimum of 13 PV panel units can be connected in series in an inverter string. For this project, 16 PV panel units can be selected to connect in series in a string practically.

Strings of series connected PV panels are connected in parallel with each inverters input string terminal.

Total parallel strings = $\frac{Maximum\ PV\ panel\ number\ in\ single\ inverter\ input\ string\ terminal}{PV\ panel\ number\ connected\ in\ series\ in\ single\ string}$

(Kerekes, 2013; Talukdar, 2017)

= $\frac{366}{16}$ = 23 (Rounded up)

The below figure shows a schematic diagram of series-connected 16 PV panels and 23 parallel connections with each inverter string terminal for this project together with blocking diodes and bypass diodes arrangements.

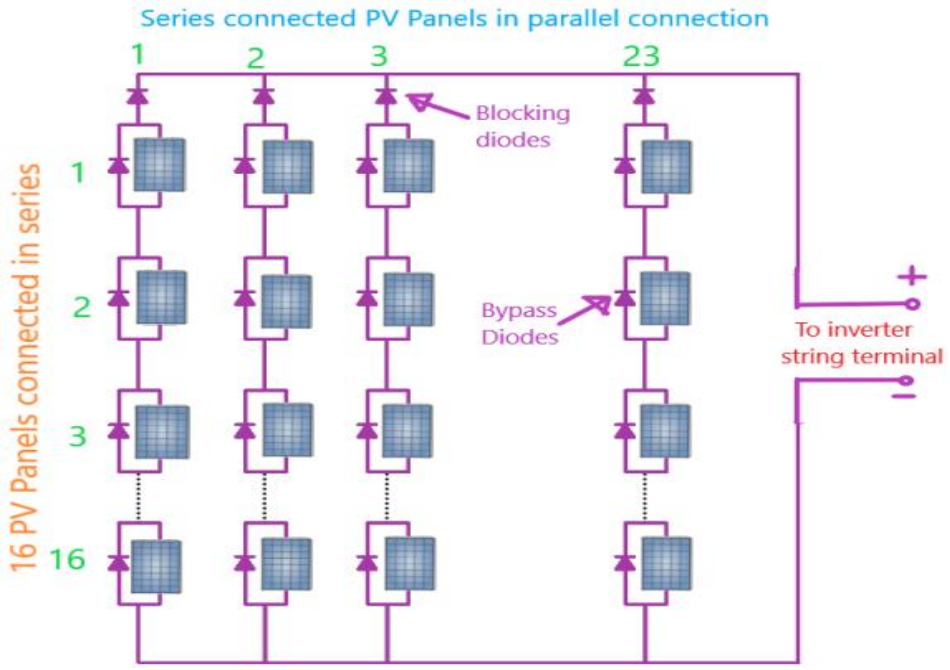

Figure 45: Series and parallel connection of PV panels with each inverter string terminal for this project. Reproduced by the author. Basic circuit source- Talukdar, 2017; Saravanan et al, 2019.

5.4: Blocking Diodes and Bypass Diodes Applications

Diodes are two terminal electronic devices. The Main function of the diode is to direct electrical current flow in one direction only. It means they allow only unidirectional flow of current. This property of diodes is extremely useful in PV plants. Blocking diodes and bypass diodes are extensively used in PV installations. Blocking diodes allow current flow from solar panel to the inverter but prevent reverse current flow from the inverter to the solar panel. This way, blocking diodes safeguards PV panels from unwanted damage from reverse power.

Bypass diodes maintain the reliability of the solar system in case of solar panel failure. In a multi-string panel, if one panel becomes faulty, it bypasses the faulty panel and provides an alternative path for current to flow.

Bypass diodes are connected in parallel with each PV panel to shunt the current around it, but the blocking diodes are connected in series in a string.

Peak Inverse Voltage (PIV) of blocking diode should be higher than inverter maximum string voltage and for bypass diode, PIV should be higher than panel maximum open-circuit voltage.

Blocking diode PIV ≥ ($V_{OC.H}$ x PV panel in series in a string)

PIV ≥ (49.44 X 16)

PIV ≥ 791 V

Bypass diode PIV ≥ $V_{OC.H}$

PIV ≥ 49.44 V

Panel string maximum possible short circuit current for this PV installation is as below (Talukdar, 2017; Alsayed, 2013)-

$I_{sc.string.max} = \{(I_{SC.STC} + K_i(T_{MAX.A} + (\frac{NT-20}{800}) \times G_H - T_{REF})) \times \frac{G_H}{1000} \}$

$= \{(9.90 + 0.05(45 + (\frac{46-20}{800}) \times 950 - 25)) \times \frac{950}{1000} \}$

= 11.82 A

Therefore, the blocking diode and bypass diode current rating for these PV installations should be greater than 11.82 A.

5.5: LAES as Backup Power for Chittagong Port

The weather of the region is governed by the monsoon. Wind flows from south to south-east direction during the period from April up to September. For a small period, time wind flows easterly direction. From November to January, the wind turns to the northerly and north-easterly direction. In February and March, wind changes its flows via westerly direction and settles from southerly to south easterly. During a year, wind speed of more than 20 knots (Beaufort scale 5) prevails for 6% of the time while 0.1% of the time wind speed remains more than 30 knots (Beaufort scale 7). Although this prevailing weather condition in Bangladesh is favourable for power generation from renewable wind and solar energy, for a period of 1 to 2 months of the year, power generation from renewable sources may experience low productivity. During this period, managing a backup power source for Chittagong port is essential to make ports normal power demand. LAES electricity system is a potential solution in this respect which can be utilized as emergency power of Chittagong port when no other power source is available for a certain period as well as it can add power to regular peak hour power demand. For this to happen, LAES

system capacity needs to be established upon calculation of actual port energy demand. Although the peak energy demand of the port is claimed to be only 10 MWh, the actual energy requirement is likely to be more than this. This is because Chittagong port is growing faster every year. Chittagong port ranked 87th in the year 2009 among the world's 100 top busiest container handling ports while this port ranked 58th in the year 2020 (Lloyds List, 2020). To determine the required capacity of LAES, it is essential to calculate the energy consumption of the cargo and container handling equipment's of the Chittagong port.

5.5.1: LAES capacity calculation

The below table shows the cargo and container handling equipment details of Chittagong port as of 2019 and calculated the approximate energy demand based on rational assumptions.

Equipment Name	Capacity (ton)	Quantity (Actual)	Approximate Unit energy consumption (KWh)	Total Energy Demand (MWh)
Quay gantry crane	40	14	250	3.5
Yard rail mounted gantry crane	40	01	250	0.25
Rubber tyred gantry crane	40	41	250	10.3
Mobile harbor crane	84	03	500	1.5
Mobile Crane for Cargo handling	10-50	38	200	7.6
4 high straddle carrier	40	48	250	12.0
2 high straddle carrier	40	02	250	0.5
Reach Stacker	45	11	250	2.7
Forklift truck	42	03	250	0.75
Reach stacker	07	09	50	0.45
Forklift spreader	16	09	80	0.72

Table 10: Approximate energy demand as calculated based on container and cargo handling equipment's statistics of Chittagong port.

According to the above table, the approximate energy demand for container and cargo handling equipment's is about 40 MWh if all the equipment's are used at a time at full load which is unlikely. Due to the long period of clearing and forwarding formalities of containers and cargoes, excess traffic of hinterland connectivity, lack

of stevedores and labours, it is more likely that approximately 50% of the time port operation remains idle. Besides, the electricity consumption estimated above is just a rational assumption based on 100% load operation. Considering the above, peak hour energy demand for container and cargo handling equipment's can be assumed at about 20 MWh currently. Basis these assumptions, it is advisable to set up an LAES system with a capacity of 10% of the total peak hour energy demand of the port.

Required LAES capacity for Chittagong port = $\frac{10 \times 20}{100}$ MWh

= 2 MWh

Therefore, if 2 MWh capacity LAES system is installed at Chittagong port, this system can easily supply power to below equipment's for 12 hours peak hour port operations while can be charged at off-peak period of rest 12 hours-

- Quay gantry crane to connect with LAES = 2 units = 2 × 250 KWh
  = 0.5 MWh
- Rail mounted gantry crane to connect with LAES = 1 units = 0.25 MWh
- RTG crane to connect with LAES = 2 units = 2 × 250 KWh = 0.5 MWh
- Straddle carrier to connect with LAES = 2 units =2 × 250 KWh = 0.5 MWh
- Reach stacker to connect with LAES = 1 units = 0.25 MWh

If the above equipment's is provided emergency connections with LAES system, they can be operated in case of total power loss using the storage energy of the LAES system for up to 12 hours. In addition, LAES can run above equipment's during the regular peak hour periods with the stored energy charged during off-peak period and save potential energy loss. Multiple 300 KWh capacity LAES systems developed by Highview company can be integrated to produce 2 MWh energy or even a complete 2 MWh capacity LAES system can be installed.

Number of 300 KWh capacity Highview LAES system required = $\frac{2000}{300}$ = 6 units

Section 5.5.2 shows the schematic diagram of the proposed WT-PV-LAES Hybrid Power System.

5.5.2: Schematic Diagram of WT-PV-LAES Hybrid Power System

Figure 46 shows how wind energy, solar energy, and liquid air energy storage system can be integrated into Chittagong port-

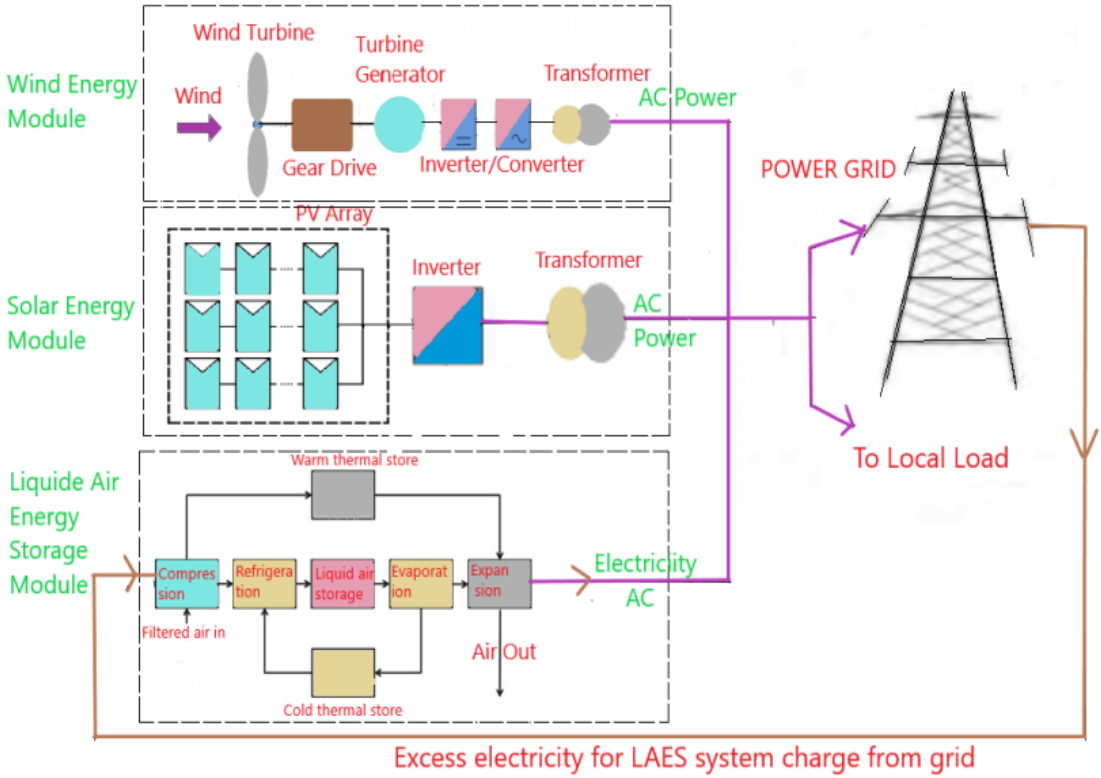

Figure 46 : Schematic diagram of WT-PV-LAES hybrid power system for Chittagong port. Diagram is drawn by the author combining from various sources schematics. (Gareth & Mathew, 2014; Vecchi et al, 2021; Huang, 2009; Talukdar, 2017)

Chapter 6

6.0: Discussion of Findings, Limitations, and Recommendations:

6.1: Findings

This literature is successful to find answers to its research questions. Electricity generation potential from wind energy and solar energy, LAES system has been explored for Chittagong port and anchorage area. A simplified design for a hybrid PV-WT-LAES electricity system was also developed. Number and specification of

required major components like a wind turbine, PV panel, inverter, transformer, diodes, the electrical connection have been established. Key findings of this study are as below-

- Generalized wind climate data as obtained from the global wind atlas shows that the Chittagong anchorage area has potential wind energy availability from which sufficient green electricity can be generated by installing horizontal axis wind turbines that can meet the entire power demand of Chittagong port. If “Vestas V90-2.0” MW wind turbine is installed, it can produce electricity for about 11 months a year. Calculation using Python programming language software shows that one wind turbine can produce about 5430 MWh energy per year and an entire wind farm consisting of 7 horizontal axis wind turbines can generate 38009 MWh energy yearly at the proposed wind farm site. Hence, as Chittagong port is a low energy consuming port (Energy demand only 10 MWh), the entire power demand of the port can be met by developing a medium scale offshore wind turbine plant at Chittagong port anchorage area.
- Bangladesh is a coastal riverine country with six seasons where tropical monsoon impacts the local weather. Hence, wind and solar energy availability vary throughout the year. As seen from wind power calculation, wind turbines will remain non-operational for about one to two months a year. Normally, December, January, and February are the winter months of Bangladesh. During wintertime, wind availability is less but solar irradiance is maximum during winter months. Figure 38 and 39 of this literature shows the GHI, DHI, DIF data of Chittagong port as obtained from European Commissions PV-GIS SARAH database. The solar irradiance graph of 12 months in figure 38 and 39 shows that Chittagong port has a high potential to produce electricity from the photovoltaic power plants. Therefore, during winter when less wind is available, PV power plants can meet the partial power demand of the port. Again, during stormy and rainy days in May-June-July-August, when solar irradiance is less, then wind turbine will have maximum wind availability to produce electricity. Hence, combining wind and solar power plants can ensure port electricity supply round the year.

- This research developed a design for a photovoltaic power plant of 3 MWh capacity for Chittagong port. Calculation of PV power from PV panel for the location of Chittagong port using PV-GIS web application software shows that installing a single Canadian Solar HiDM5 CS1-Y 400MS PV-module in Chittagong port location can produce 612.98 KWh electricity per year with a daily production rate of 1.68 KWh. If only 42857 units of similar PV panel is fitted together, 3 MWh electricity can be produced from solar energy at Chittagong port. As Chittagong port possesses a big area, much more PV panels can be accommodated within the port premise without interrupting existing infrastructures and a 5 to 10 MWh capacity stand-alone solar power plant can be installed at Chittagong port to meet its power demand from renewable solar energy.
- If wind and solar power plant described in this study combined, they will generate more electricity than the port need. This excess electricity can be made useful if the LAES electricity system is fitted with a PV-WT electricity system. At night or during the off-peak periods when energy demand is low and energy is wasted, the LAES system will use this excess electricity to produce liquid air. During peak period and when PV-WT system is unable to produce sufficient electricity, LAES will use this liquid air to produce electricity to balance the supply and demand of the port. Just using a 2 MWh capacity LAES system, Chittagong port can sustain its 10% energy demand for about 12 hours. Highview power company already successfully demonstrated a 300 KWh capacity LAES system, and 10 MWh capacity plant is under development. For Chittagong port, a 2 MWh capacity LAES system can be considered to install as a power backup solution of the port.
- This research successfully demonstrated that the entire energy demand of low energy consuming Chittagong port can be met from renewable energy sources. Solar energy module, wind energy module, and liquid air energy storage module can be integrated (as in figure 46) with the national grid. This grid-tie PV-WT-LAES electricity system is a realistic environment-friendly energy solution for Chittagong port which can supply additional electricity to the national grid. Even if hybrid PV-WT-LAES electricity remains low productive for one or two months due to weather uncertainty,

this system will enable the port to meet its power demand from the national grid in case of emergency. This study has successfully demonstrated the design approach of a grid-tie PV-WT-LAES electricity system for Chittagong port.

6.2: Limitations

This study mainly focused on technical aspects, processes and design of electricity generation from renewable wind, solar energy, and liquid air. This study could not verify economic and social constraints and impacts of electricity generation from these renewable energy sources for Chittagong port. Analysis of economic and social aspects itself an extensive task, hence recommended to conduct further research in these aspects. Besides, this literature did not identify the annual average electricity share among solar energy module, wind energy module, LAES module, and the national grid. Levelized cost of electricity (LCOE) was not addressed within the scope of the study. This study could not determine actual energy consumption of Chittagong port cargo and container handling equipment's, consumption of all this equipment's given in this study is just rational assumptions.

6.3: Recommendations

Bangladesh is an emerging shipping nation. The value of total import and export of the country stands at about 78 billion USD per year (DOS, 2021). The majority share of this import and export is accomplished via Chittagong port. Chittagong port growing twice as fast as the nation. Chittagong port ranked 58th among the world's top 100 busiest container handling ports in 2020 (Lloyd's list, 2020). To improve the overall image of Chittagong port globally, the authority should focus on reducing the carbon footprint of the port operations. Although financial requirements of hybrid grid- tie PV-WT-LAES electricity system are not addressed in this study, it is in the authors confident that Chittagong port can switch its power production from fossil fuel to entirely on renewable energy sources like grid-tie PV-WT-LAES electricity system comfortably within its financial reserve and budget. Investment in green electricity generation to meet the port's power demand will highlight the port authority's commitment towards de-carbonization of the port and will ensure the

transition of the port into a green and smart port. For this to happen, the following recommendations are suggested-

- Harnessing renewable wind energy, solar energy is a solution towards reducing carbon footprint from power generation process. Until today major share of Bangladesh's total power generation is from fossil sources that is environmentally harmful. Recent inclination of the Government of Bangladesh is a positive approach in promoting renewable power generation. While the Government is currently considering generation of 200 MW electricity generation from wind energy in the same region where Chittagong port belongs, port authority can demonstrate leadership in this field by switching its power profile entirely to green renewable power through installation of grid tie hybrid PV-WT-LAES system. By becoming first mover in harnessing renewable energy in the region, Chittagong port can secure public funding for their greening project when the Government has already approved it's planning to harness renewable energy through the planning commission.
- Although there is certain benefit of GHG emission reduction while using renewable energy technologies, initial installation cost is likely to be higher. But yet, there exists better economy of renewable technologies in the long run due to lower maintenance and operating costs. Besides, tendency of the Government of Bangladesh to subsidise renewable energy harnessing from public funding can lessen initial economic burden to install renewable power plant. As this literature mostly and comprehensively demonstrated technical feasibility of harnessing renewable energy in Chittagong port, therefore economic, social, and environmental criteria of installing hybrid grid-tie PV-WT-LAES electricity system at Chittagong port shall be evaluated extensively.
- Port authority shall include renewable energy policy and secure, allocate the required budget in its 30-year Strategic Master plan for the conversion of Chittagong port into a green port.
- Port authority shall initiate a pilot trial of small-scale offshore wind turbine power plant of 10 MW capacity at port anchorage area, install 3 MW

capacity PV power plant and 2 MW capacity LAES electricity system to meet its power demand.

- Cargo and container handling equipment's energy inventory shall be made to improve the overall energy efficiency of the port.
- Multi-criteria optimization of the hybrid grid-tie PV-WT-LAES electricity system shall be conducted where economic, environmental, and social criteria are optimized to identify the optimal sharing among the systems.

References

Abdo, RF., Pedro HT., Koury RN., Machado, I., Coimbra, CF., Porto, MP., (2015). Performance evaluation of various cryogenic energy storage systems. *Energy 2015. 90, 1024-32.* http://refhub.elsevier.com/S0306-2619(18)30496-3/h0060

Akhurst, M., Arbon, I., Ayres, M., Brandon, N., Bruges, R., Cooper, S., ... & Wilks, M. (2013). Liquid Air in the energy and transport systems: Opportunities for industry and innovation in the UK.

Alsayed, M., Cacciato, M., Scarcella, G. and Scelba, G., (2013). Multicriteria Optimal Sizing of Photovoltaic-Wind Turbine Grid Connected Systems. *IEEE Transactions on Energy Conversion.,* Vol.28 , Issue. 2 , pp. 370-379.

Borri, E., Tafone, A., Romagnoli, A., Comodi, G., (2017). A preliminary study on the optimal configuration and operating range of a “microgrid scale” air liquefaction plant for Liquid Air Energy Storage. *Energy Conversion and Management.* Volume 143, Pages 275-285. ISSN 0196-8904. https://doi.org/10.1016/j.enconman.2017.03.079.

Gareth. B, Matthew, B., (2014). The application of liquid air energy storage for large scale long duration solutions to grid balancing. *EPJ Web of Conferences. 79. 03002. 10.1051/epjconf/20137903002.*

Chang, T. J., Wu, Y. T., Hsu, H. Y., Chu, C. R., & Liao, C. M. (2003). Assessment of wind characteristics and wind turbine characteristics in Taiwan. *Renewable energy*, *28*(6), 851-871.

Charbonneau, P. (2014). Solar Dynamo Theory. *Annual Review of Astronomy and Astrophysics, Vol 52, 255–257*.

Doelle, M., Chircop, A., (2019). Decarbonizing international shipping: An appraisal of the IMO’s Initial Strategy. *Review of European, Comparative, & International Environmental Law*, 28(3),268-277. https://doi.org/10.1111/reel.12302

Guizzi, GL., Manno, M., Tolomei, LM., Vitali, RM., (2015). Thermodynamic analysis of a liquid air energy storage system. *Energy. Volume 93, Part 2, Pages 1639-1647, ISSN 0360-5442.* https://doi.org/10.1016/j.energy.2015.10.030.

Garg, H.P., Garg, S.N., (1987). Improved correlation of daily and hourly diffuse radiation with global radiation for Indian stations. *Solar & Wind Technology*. Volume 4, Issue 2, Pages 113-126. ISSN 0741-983X. https://doi.org/10.1016/0741-983X(87)90037-3.

Hau, E. (2013). Wind turbines: fundamentals, technologies, application, economics. *Springer Science & Business Media*.

Hossen, M.A., Rafiq, F., Kabir, M.A., Morshed, M.G., (2019). Assessment of water quality scenario of Karnaphuli river in terms of water quality index, South-Eastern Bangladesh. *American Journal of Water Resources. 2019, 7(3), 106-110 doi:10.12691/ajwr-7-3-3.*

Huang, N., (2009). Simulation of Power Control of a Wind Turbine Permanent Magnet Synchronous Generator System (2013). Master's Theses (2009 -). Paper 215. http://epublications.marquette.edu/theses_open/215

http://www.bpdb.gov.bd/bpdb/pdb_utility/maxgen/dailygen_archive/3363report.pdf

IPCC, (2018). Global Warming of 1.5°C. *An IPCC Special Report on the impacts of global warming of 1.5°C above pre-industrial levels and….* [Masson-Delmotte, V., P. Zhai, H.-O. Pörtner, D. Roberts, J. Skea, P.R. Shukla, A. Pirani, W. Moufouma-Okia, C. Péan, R. Pidcock, S. Connors, J.B.R. Matthews, Y. Chen, X. Zhou, M.I. Gomis, E. Lonnoy, T. Maycock, M. Tignor, and T. Waterfield (eds.)]. In Press.

IPCC, (2019). Climate Change and Land: *an IPCC special report on climate change, desertification, land degradation, sustainable land management, food security, and greenhouse gas fluxes in terrestrial ecosystems* [P.R. Shukla, J.Skea, E. Calvo Buendia, V. Masson-Delmotte, H.-O. Pörtner, D. C. Roberts, P.Zhai, R. Slade, S. Connors, R. van Diemen, M. Ferrat, E. Haughey, S. Luz, S.Neogi, M. Pathak, J. Petzold, J. Portugal Pereira, P. Vyas, E. Huntley, K.Kissick, M. Belkacemi, J. Malley, (eds.)]. In press.

Islam, Md. Shariful et al., (2013). Feasibility Study of Wind Power Generation in Bangladesh: A Statistical Study in the Perspective of Wind Power Density and Plant Capacity Factor. *International Journal of Renewable Energy Research, Vol. 3, Issue. 3.*

J. M. A. Myrzik, And M. Calais, (2003). String and Module Integrated Inverters for Single- Phase Grid Connected Photovoltaic Systems - A Review*. 2003 IEEE Bologna Power Tech Conference, June 12th-26th, Bologna, Italy*.

Justus, C. J., Hargraves, W. R., Mikhail, A., Graber, D., (1978). Methods for estimating wind speed frequency distributions. *Journal of Applied Meteorology 17 (1978) 350-353.*

Jaafer, A., (2018). Design and Construction of a Tracking Device for Solar Electrical Systems. *The Journal of Scientific and Engineering Research. 5. 225-236*.

Kerekes., Tamas., Koutroulis, Eftichis., (2013). An Optimization Method for Designing Large PV Plants. *IEEE Journal of Photovoltaics.* April 2013, VOL. 3,NO. 2, pp.814- 822

Kantharaj, B., Garvey, S., Pimm, A., (2015). Thermodynamic analysis of a hybrid energy storage system based on compressed air and liquid air. *Sustainable*

Energy Technologies and Assessments. Volume 11, Pages 159-164. ISSN 2213-1388. https://doi.org/10.1016/j.seta.2014.11.002.

Karafil, A., Özbay, H., Kesler, M., Parmaksiz, H., (2015). Calculation of Optimum Fixed Tilt Angle of PV Panels Depending on Solar Angles and Comparison of the Results with Experimental Study Conducted in Summer in Bilecik, Turkey. 10.1109/ELECO.2015.7394517.

Lim, Y., Al-Atabi, M., & Williams, R. A. (2016). Liquid air as an energy storage: A review. *Journal of Engineering Science and Technology*, *11*(4), 496-515.

Mars Bodell, J., & Tapia Chiriboga, C. (2018). Techno-economic analysis of the Local System Operator concept in a multi-dwelling unit in Sweden: A parametric sizing and optimization of a PV-battery system with EVs equipped with vehicle-to-home application.

Morgan, R., Nelmes, S., Gibson, E., Brett, G., (2015). Liquid air energy storage – Analysis and first results from a pilot scale demonstration plant. *Applied Energy. Volume 137, 845-853, ISSN 0306-2619.* https://doi.org/10.1016/j.apenergy.2014.07.109.

Morgan, R., Nelmes, S., Gibson, E., Brett, G., (2015). An analysis of a large-scale liquid air energy storage system. *Energy 2015. 93,1639-47.* http://refhub.elsevier.com/S0306-2619(18)30496-3/h0055.

Mathew, S., Pandey, K.P., Anil, K.V., (2002). Analysis of wind regimes for energy estimation. *Renewable Energy, Berlin Heidelberg .2002, pp 381-399.*

Nugent, Daniel., Sovacool, Benjamin K., (2014). Assessing the lifecycle greenhouse gas emissions from solar PV and wind energy: A critical meta-survey. *Energy Policy.* Vol. 65, pp. 229–244.

Olcer, A. I., Kitada, M., Dalaklis, D., & Ballini, F. (2018). Trends and Challenges in Maritime Energy Management. *Springer International Publishing AG*. http://ebookcentral.proquest.com/lib/wmulib-ebooks/detail.action?docID=5379937.

Overview, 2020. Chittagong Port Authority, Chattogram. http://www.cpa.gov.bd/

Peng, H., Shan, X., Yang, Y., Ling, X., (2018). A study on performance of a liquid air energy storage system with packed bed units. *Applied Energy*. Volume 211, Pages 126-135. ISSN 0306-2619. https://doi.org/10.1016/j.apenergy.2017.11.045.

Psaraftis, H.N.; Kontovas, C.A. (2021). Decarbonization of Maritime Transport: Is There Light at the End of the Tunnel? *Sustainability 2021.* 13, 237. https://doi.org/10.3390/su1301 0237.

Rosa-Clot, M., Tina, G.M., (2018). Introduction to PV Plants. *Submerged and Floating Photovoltaic Systems. Chapter-3, P 33-64*. ISBN 9780128121498. https://doi.org/10.1016/B978-0-12-812149-8.00003-X.

Sciacovelli, A., Vecchi, A., Ding, Y., (2017). Liquid air energy storage (LAES) with packed bed cold thermal storage – From component to system level performance through dynamic modelling. Applied Energy. Volume 190, Pages 84-98, ISSN 0306-2619. https://doi.org/10.1016/j.apenergy.2016.12.118.

Salem, Ahmed.M & Seddiek, I., (2016). Techno-Economic Approach to Solar Energy Systems Onboard Marine Vehicles. *Polish Maritime Research. 23. 10.1515/pomr-2016-0033.*

Saravanan, S., Kumar, R.S., Prakash, A., Chinnadurai, T., Tiwari, R., Prabaharan, N., Babu, B.C., (2019). Chapter 8 - Photovoltaic array reconfiguration to extract maximum power under partially shaded conditions, by Rajeev Kumar Chauhan, Kalpana Chauhan. Distributed Energy Resources in Microgrids. Academic Press. Pages 215-241, ISBN 9780128177747. https://doi.org/10.1016/B978-0-12-817774-7.00008-9.

Song, Yongduan & Wang, Bikun & Li, Bin & Zeng, Yu & Wang, Lei. (2013). Remotely monitoring offshore wind turbines via ZigBee networks embedded with an advanced routing strategy. Journal of Renewable and Sustainable Energy. 5. 10.1063/1.4773467.

S. B. Kjaer, J. K. Pedersen, F. Blaabjerg, (2005) .A Review of Single-Phase Grid-Connected Inverters for Photovoltaic Modules. *IEEE Transactions on Industry Applications, September/October 2005, Vol. 41, No. 5.*

Talukdar, A. (2017). Multicriteria optimization of design of a grid interfaced PV-wind power system. Department of electrical and electronic engineering. Bangladesh University of engineering and technology. [Masters Thesis.]

Vecchi, A., Li, Y., Ding, Y., Mancarella, P., Sciacovelli, A., (2021). Liquid air energy storage (LAES): A review on technology state-of-the-art, integration pathways and future perspectives. Advances in Applied Energy. Volume 3, 100047. ISSN 2666-7924. https://doi.org/10.1016/j.adapen.2021.100047.

World Nuclear Association, (2017). Comparison of Lifecycle Greenhouse Gas Emissions of Various Electricity Generation Sources. [Online]. www.worldnuclear.net/uploadedFiles/org/

Yang, A.B., Shen, H., Liao, X., (2003). Computer-aided design of PV/wind hybrid system. *J. Renewable Energy, 2003;Vol. 28 ,pp.1491-1512.*

Appendices

1. Python wind power calculation results screenshot

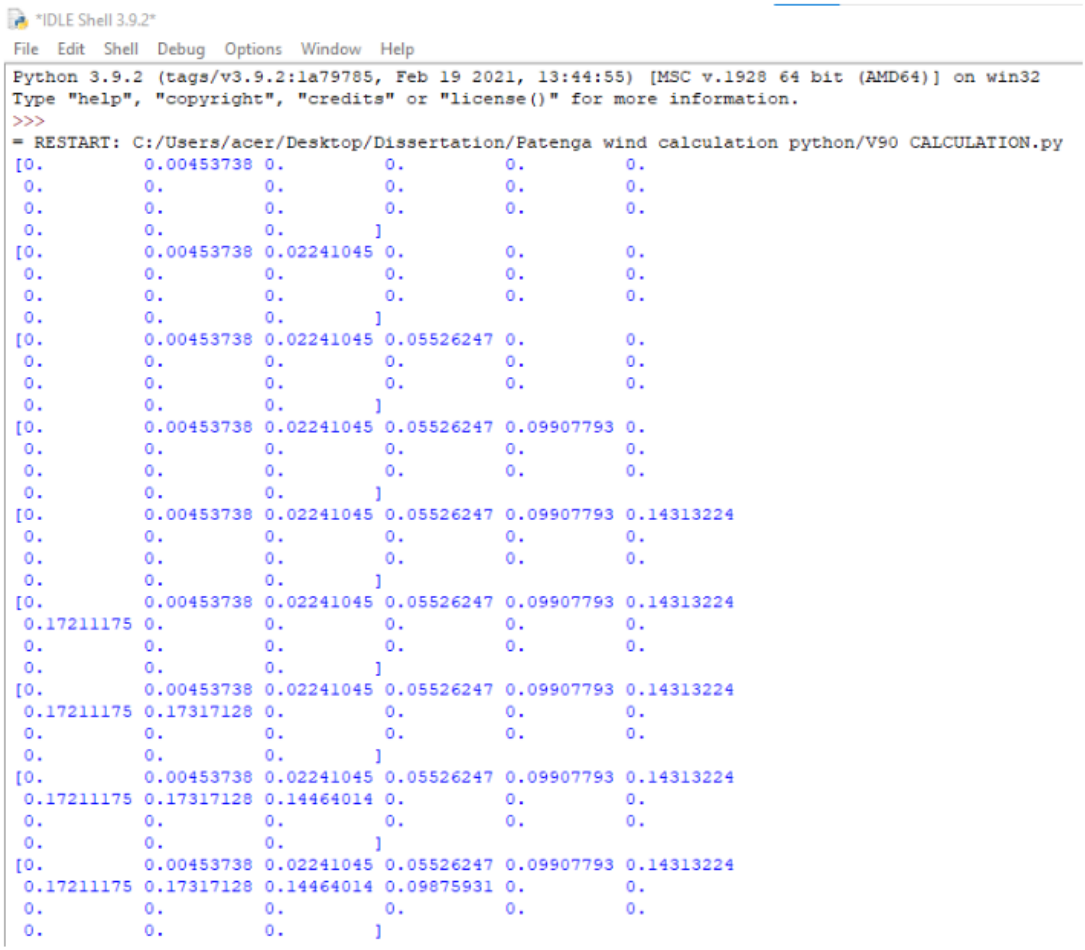

```
 0.          0.          0.          0.          0.          0.
 0.          0.          0.        ]
[0.          0.00453738  0.02241045  0.05526247  0.09907793  0.14313224
 0.17211175  0.17317128  0.14464014  0.09875931  0.05403016  0.
 0.          0.          0.          0.          0.          0.
 0.          0.          0.        ]
[0.          0.00453738  0.02241045  0.05526247  0.09907793  0.14313224
 0.17211175  0.17317128  0.14464014  0.09875931  0.05403016  0.0231395
 0.          0.          0.          0.          0.          0.
 0.          0.          0.        ]
[0.00000000e+00 1.71766433e+03 1.37413147e+04 4.63769370e+04
 1.09930517e+05 2.14708042e+05 3.71015496e+05 5.89158866e+05
 8.79444138e+05 1.25217730e+06 1.71766433e+06 2.00000000e+06
 0.00000000e+00 0.00000000e+00 0.00000000e+00 0.00000000e+00
 0.00000000e+00 0.00000000e+00 0.00000000e+00 0.00000000e+00
 0.00000000e+00]
[0.          0.00453738  0.02241045  0.05526247  0.09907793  0.14313224
 0.17211175  0.17317128  0.14464014  0.09875931  0.05403016  0.0231395
 0.00756111  0.          0.          0.          0.          0.
 0.          0.          0.        ]
[0.00000000e+00 1.71766433e+03 1.37413147e+04 4.63769370e+04
 1.09930517e+05 2.14708042e+05 3.71015496e+05 5.89158866e+05
 8.79444138e+05 1.25217730e+06 1.71766433e+06 2.00000000e+06
 2.00000000e+06 0.00000000e+00 0.00000000e+00 0.00000000e+00
 0.00000000e+00 0.00000000e+00 0.00000000e+00 0.00000000e+00
 0.00000000e+00]
[0.          0.00453738  0.02241045  0.05526247  0.09907793  0.14313224
 0.17211175  0.17317128  0.14464014  0.09875931  0.05403016  0.0231395
 0.00756111  0.0018339   0.          0.          0.          0.
 0.          0.          0.        ]
[0.00000000e+00 1.71766433e+03 1.37413147e+04 4.63769370e+04
 1.09930517e+05 2.14708042e+05 3.71015496e+05 5.89158866e+05
 8.79444138e+05 1.25217730e+06 1.71766433e+06 2.00000000e+06
 2.00000000e+06 2.00000000e+06 0.00000000e+00 0.00000000e+00
 0.00000000e+00 0.00000000e+00 0.00000000e+00 0.00000000e+00
 0.00000000e+00]
[0.          0.00453738  0.02241045  0.05526247  0.09907793  0.14313224
 0.17211175  0.17317128  0.14464014  0.09875931  0.05403016  0.0231395
 0.00756111  0.0018339   0.00032071  0.          0.          0.
 0.          0.          0.        ]
```

```
 0.          0.          0.          ]
[0.00000000e+00 1.71766433e+03 1.37413147e+04 4.63769370e+04
 1.09930517e+05 2.14708042e+05 3.71015496e+05 5.89158866e+05
 8.79444138e+05 1.25217730e+06 1.71766433e+06 2.00000000e+06
 2.00000000e+06 2.00000000e+06 2.00000000e+06 0.00000000e+00
 0.00000000e+00 0.00000000e+00 0.00000000e+00 0.00000000e+00
 0.00000000e+00]
[0.00000000e+00 4.53738039e-03 2.24104499e-02 5.52624699e-02
 9.90779283e-02 1.43132237e-01 1.72111749e-01 1.73171282e-01
 1.44640141e-01 9.87593073e-02 5.40301645e-02 2.31395009e-02
 7.56110839e-03 1.83390033e-03 3.20707292e-04 3.92292193e-05
 0.00000000e+00 0.00000000e+00 0.00000000e+00 0.00000000e+00
 0.00000000e+00]
[0.00000000e+00 1.71766433e+03 1.37413147e+04 4.63769370e+04
 1.09930517e+05 2.14708042e+05 3.71015496e+05 5.89158866e+05
 8.79444138e+05 1.25217730e+06 1.71766433e+06 2.00000000e+06
 2.00000000e+06 2.00000000e+06 2.00000000e+06 2.00000000e+06
 0.00000000e+00 0.00000000e+00 0.00000000e+00 0.00000000e+00
 0.00000000e+00]
[0.00000000e+00 4.53738039e-03 2.24104499e-02 5.52624699e-02
 9.90779283e-02 1.43132237e-01 1.72111749e-01 1.73171282e-01
 1.44640141e-01 9.87593073e-02 5.40301645e-02 2.31395009e-02
 7.56110839e-03 1.83390033e-03 3.20707292e-04 3.92292193e-05
 3.25249536e-06 0.00000000e+00 0.00000000e+00 0.00000000e+00
 0.00000000e+00]
[0.00000000e+00 1.71766433e+03 1.37413147e+04 4.63769370e+04
 1.09930517e+05 2.14708042e+05 3.71015496e+05 5.89158866e+05
 8.79444138e+05 1.25217730e+06 1.71766433e+06 2.00000000e+06
 2.00000000e+06 2.00000000e+06 2.00000000e+06 2.00000000e+06
 2.00000000e+06 0.00000000e+00 0.00000000e+00 0.00000000e+00
 0.00000000e+00]
[0.00000000e+00 4.53738039e-03 2.24104499e-02 5.52624699e-02
 9.90779283e-02 1.43132237e-01 1.72111749e-01 1.73171282e-01
 1.44640141e-01 9.87593073e-02 5.40301645e-02 2.31395009e-02
 7.56110839e-03 1.83390033e-03 3.20707292e-04 3.92292193e-05
 3.25249536e-06 1.76943983e-07 0.00000000e+00 0.00000000e+00
 0.00000000e+00]
```

```
 0.00000000e+00]
[0.00000000e+00 1.71766433e+03 1.37413147e+04 4.63769370e+04
 1.09930517e+05 2.14708042e+05 3.71015496e+05 5.89158866e+05
 8.79444138e+05 1.25217730e+06 1.71766433e+06 2.00000000e+06
 2.00000000e+06 2.00000000e+06 2.00000000e+06 2.00000000e+06
 2.00000000e+06 2.00000000e+06 0.00000000e+00 0.00000000e+00
 0.00000000e+00]
[0.00000000e+00 4.53738039e-03 2.24104499e-02 5.52624699e-02
 9.90779283e-02 1.43132237e-01 1.72111749e-01 1.73171282e-01
 1.44640141e-01 9.87593073e-02 5.40301645e-02 2.31395009e-02
 7.56110839e-03 1.83390033e-03 3.20707292e-04 3.92292193e-05
 3.25249536e-06 1.76943983e-07 6.10915956e-09 0.00000000e+00
 0.00000000e+00]
[0.00000000e+00 1.71766433e+03 1.37413147e+04 4.63769370e+04
 1.09930517e+05 2.14708042e+05 3.71015496e+05 5.89158866e+05
 8.79444138e+05 1.25217730e+06 1.71766433e+06 2.00000000e+06
 2.00000000e+06 2.00000000e+06 2.00000000e+06 2.00000000e+06
 2.00000000e+06 2.00000000e+06 2.00000000e+06 0.00000000e+00
 0.00000000e+00]
[0.00000000e+00 4.53738039e-03 2.24104499e-02 5.52624699e-02
 9.90779283e-02 1.43132237e-01 1.72111749e-01 1.73171282e-01
 1.44640141e-01 9.87593073e-02 5.40301645e-02 2.31395009e-02
 7.56110839e-03 1.83390033e-03 3.20707292e-04 3.92292193e-05
 3.25249536e-06 1.76943983e-07 6.10915956e-09 1.29362677e-10
 0.00000000e+00]
[0.00000000e+00 1.71766433e+03 1.37413147e+04 4.63769370e+04
 1.09930517e+05 2.14708042e+05 3.71015496e+05 5.89158866e+05
 8.79444138e+05 1.25217730e+06 1.71766433e+06 2.00000000e+06
 2.00000000e+06 2.00000000e+06 2.00000000e+06 2.00000000e+06
 2.00000000e+06 2.00000000e+06 2.00000000e+06 2.00000000e+06
 0.00000000e+00]
[0.00000000e+00 4.53738039e-03 2.24104499e-02 5.52624699e-02
 9.90779283e-02 1.43132237e-01 1.72111749e-01 1.73171282e-01
 1.44640141e-01 9.87593073e-02 5.40301645e-02 2.31395009e-02
 7.56110839e-03 1.83390033e-03 3.20707292e-04 3.92292193e-05
 3.25249536e-06 1.76943983e-07 6.10915956e-09 1.29362677e-10
 1.62233471e-12]
```

2. PV-GIS SARAH irradiance data for February 2016 for Chittagong

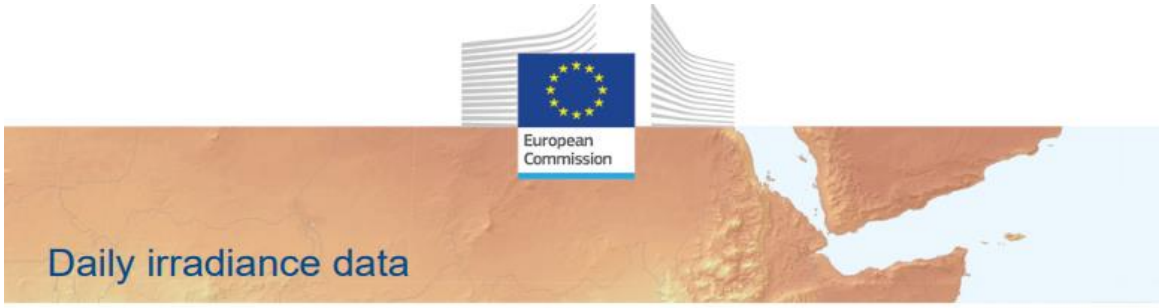

PVGIS-5 geo-temporal irradiation database

Provided inputs

Latitude/Longitude:	22.313, 91.808
Horizon:	Calculated
Database used	PVGIS-SARAH
Month:	February

Outline of horizon at chosen location:

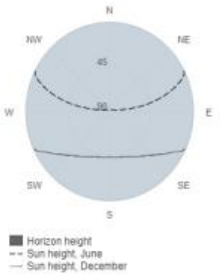

Daily average irradiance on fixed plane with slope 35° and azimuth 0°

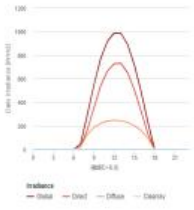

Irradiance on a fixed plane

Time	00:45	01:45	02:45	03:45	04:45	05:45	06:45	07:45	08:45	09:45	10:45	11:45	12:45	13:45	14:45	15:45	16:45	17:45	18:45	19:45	20:45	21:45	22:45	23:45
G(i)	0	0	0	0	0	0	0	42	286	544	769	917	987	986	891	716	491	229	0	0	0	0	0	0
Gb(i)	0	0	0	0	0	0	0	19	161	350	538	664	727	730	650	505	323	132	0	0	0	0	0	0
Gd(i)	0	0	0	0	0	0	0	22	121	186	221	240	246	242	228	200	161	94	0	0	0	0	0	0
Gcs(i)	0	0	0	0	0	0	0	0	0	0	0	0	0	0	0	0	0	0	0	0	0	0	0	0

G(i): Global irradiance on a fixed plane [W/m2].
Gb(i): Direct irradiance on a fixed plane [W/m2].
Gd(i): Diffuse irradiance on a fixed plane [W/m2].

Daily average irradiance on sun-tracking plane

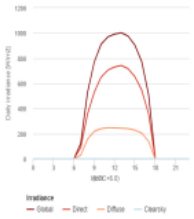

Irradiance on sun-tracking plane

Time	00:45	01:45	02:45	03:45	04:45	05:45	06:45	07:45	08:45	09:45	10:45	11:45	12:45	13:45	14:45	15:45	16:45	17:45	18:45	19:45	20:45	21:45	22:45	23:45
G(n)	0	0	0	0	0	0	0	122	526	770	910	969	991	1001	974	902	772	511	0	0	0	0	0	0
Gb(n)	0	0	0	0	0	0	0	90	355	530	649	704	730	742	716	652	546	359	0	0	0	0	0	0
Gd(n)	0	0	0	0	0	0	0	29	156	218	240	247	246	244	239	228	204	140	0	0	0	0	0	0
Gcs(n)	0	0	0	0	0	0	0	0	0	0	0	0	0	0	0	0	0	0	0	0	0	0	0	0

G(n): Global irradiance on a 2-axis tracking plane [W/m2].
Gb(n): Direct normal irradiance [W/m2].
Gd(n): Diffuse irradiance on a 2-axis tracking plane [W/m2].
Gcs(n): Global Clear-sky irradiance on a 2-axis tracking plane [W/m2].

Daily average temperature

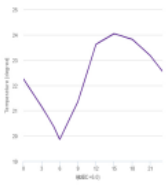

Daily average temperature

Time	00:45	01:45	02:45	03:45	04:45	05:45	06:45	07:45	08:45	09:45	10:45	11:45	12:45	13:45	14:45	15:45	16:45	17:45	18:45	19:45	20:45	21:45	22:45	23:45
T2m	22.25	21.88	21.52	21.16	20.77	20.37	19.86	20.36	20.85	21.35	22.1	22.86	23.62	23.76	23.9	24.04	23.97	23.89	23.82	23.6	23.39	23.17	22.86	22.56

T2m: Daily average temperature [°C].

Joint Research Centre

Report generated on 2021/05/19

2. 1. PV-GIS SARAH irradiance data for March 2016 for Chittagong

PVGIS-5 geo-temporal irradiation database

Provided inputs

Latitude/Longitude:	22.313, 91.808
Horizon:	Calculated
Database used	PVGIS-SARAH
Month:	March

Outline of horizon at chosen location:

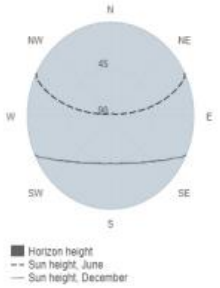

Daily average irradiance on fixed plane with slope 35° and azimuth 0°

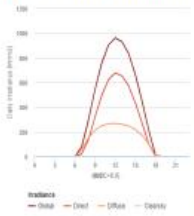

Irradiance on a fixed plane

Time	00:45	01:45	02:45	03:45	04:45	05:45	06:45	07:45	08:45	09:45	10:45	11:45	12:45	13:45	14:45	15:45	16:45	17:45	18:45	19:45	20:45	21:45	22:45	23:45
G(i)	0	0	0	0	0	0	0	79	291	544	757	904	960	931	835	664	450	213	11	0	0	0	0	0
Gb(i)	0	0	0	0	0	0	0	22	135	321	496	623	676	654	574	434	270	104	2	0	0	0	0	0
Gd(i)	0	0	0	0	0	0	0	56	151	213	249	265	268	262	247	220	172	105	9	0	0	0	0	0
Gcs(i)	0	0	0	0	0	0	0	0	0	0	0	0	0	0	0	0	0	0	0	0	0	0	0	0

G(i): Global irradiance on a fixed plane [W/m2].
Gb(i): Direct irradiance on a fixed plane [W/m2].
Gd(i): Diffuse irradiance on a fixed plane [W/m2].
Gcs(i): Global Clear-sky irradiance on a fixed plane [W/m2].

Daily average irradiance on sun-tracking plane

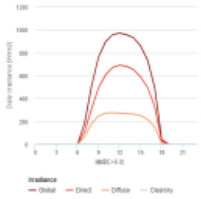

Irradiance on sun-tracking plane

Time	00:45	01:45	02:45	03:45	04:45	05:45	06:45	07:45	08:45	09:45	10:45	11:45	12:45	13:45	14:45	15:45	16:45	17:45	18:45	19:45	20:45	21:45	22:45	23:45
G(n)	0	0	0	0	0	0	0	179	504	761	895	957	971	957	930	859	735	495	41	0	0	0	0	0
Gb(n)	0	0	0	0	0	0	0	109	308	494	606	671	691	680	652	589	496	330	31	0	0	0	0	0
Gd(n)	0	0	0	0	0	0	0	64	180	247	272	275	272	268	263	250	218	151	9	0	0	0	0	0
Gcs(n)	0	0	0	0	0	0	0	0	0	0	0	0	0	0	0	0	0	0	0	0	0	0	0	0

G(n): Global irradiance on a 2-axis tracking plane [W/m2].
Gb(n): Direct normal irradiance [W/m2].
Gd(n): Diffuse irradiance on a 2-axis tracking plane [W/m2].
Gcs(n): Global Clear-sky irradiance on a 2-axis tracking plane [W/m2].

Daily average temperature

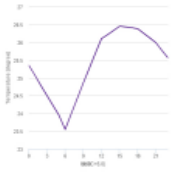

Daily average temperature

Time	00:45	01:45	02:45	03:45	04:45	05:45	06:45	07:45	08:45	09:45	10:45	11:45	12:45	13:45	14:45	15:45	16:45	17:45	18:45	19:45	20:45	21:45	22:45	23:45
T2m	25.35	25.07	24.78	24.5	24.22	23.94	23.55	23.99	24.42	24.86	25.27	25.69	26.1	26.21	26.33	26.45	26.43	26.41	26.38	26.25	26.12	25.99	25.77	25.56

T2m: Daily average temperature [°C].

Report generated on 2021/05/19

3. PV-GIS SARAH irradiance data for April 2016 for Chittagong port

PVGIS-5 geo-temporal irradiation database

Provided inputs

Latitude/Longitude:	22.313, 91.808
Horizon:	Calculated
Database used	PVGIS-SARAH
Month:	April

Outline of horizon at chosen location:

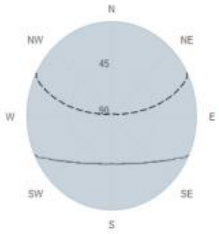

Daily average irradiance on fixed plane with slope 35° and azimuth 0°

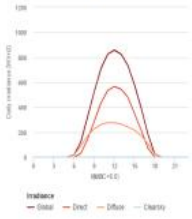

Irradiance on a fixed plane

Time	00:45	01:45	02:45	03:45	04:45	05:45	06:45	07:45	08:45	09:45	10:45	11:45	12:45	13:45	14:45	15:45	16:45	17:45	18:45	19:45	20:45	21:45	22:45	23:45
G(i)	0	0	0	0	0	0	19	119	319	523	708	825	857	825	735	576	390	181	25	0	0	0	0	0
Gb(i)	0	0	0	0	0	0	0	29	142	286	435	533	566	545	480	349	212	71	0	0	0	0	0	0
Gd(i)	0	0	0	0	0	0	18	88	171	227	260	276	276	265	242	216	171	106	24	0	0	0	0	0
Gcs(i)	0	0	0	0	0	0	0	0	0	0	0	0	0	0	0	0	0	0	0	0	0	0	0	0

G(i): Global irradiance on a fixed plane [W/m2].
Gb(i): Direct irradiance on a fixed plane [W/m2].
Gd(i): Diffuse irradiance on a fixed plane [W/m2].
Gcs(i): Global Clear-sky irradiance on a fixed plane [W/m2].

Daily average irradiance on sun-tracking plane

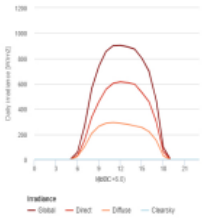

Irradiance on sun-tracking plane

Time	00:45	01:45	02:45	03:45	04:45	05:45	06:45	07:45	08:45	09:45	10:45	11:45	12:45	13:45	14:45	15:45	16:45	17:45	18:45	19:45	20:45	21:45	22:45	23:45
G(n)	0	0	0	0	0	0	58	266	561	739	855	901	903	892	873	802	699	471	96	0	0	0	0	0
Gb(n)	0	0	0	0	0	0	31	153	337	458	556	603	614	608	596	530	457	302	64	0	0	0	0	0
Gd(n)	0	0	0	0	0	0	25	103	207	263	287	293	287	279	266	254	222	154	30	0	0	0	0	0
Gcs(n)	0	0	0	0	0	0	0	0	0	0	0	0	0	0	0	0	0	0	0	0	0	0	0	0

G(n): Global irradiance on a 2-axis tracking plane [W/m2].
Gb(n): Direct normal irradiance [W/m2].
Gd(n): Diffuse irradiance on a 2-axis tracking plane [W/m2].
Gcs(n): Global Clear-sky irradiance on a 2-axis tracking plane [W/m2].

Daily average temperature

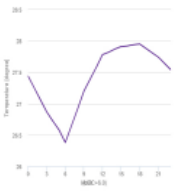

Daily average temperature

Time	00:45	01:45	02:45	03:45	04:45	05:45	06:45	07:45	08:45	09:45	10:45	11:45	12:45	13:45	14:45	15:45	16:45	17:45	18:45	19:45	20:45	21:45	22:45	23:45
T2m	27.44	27.25	27.06	26.87	26.72	26.58	26.38	26.65	26.92	27.2	27.39	27.58	27.78	27.82	27.87	27.91	27.92	27.94	27.95	27.88	27.81	27.74	27.64	27.54

T2m: Daily average temperature [°C].

Report generated on 2021/05/19

4. PV-GIS SARAH daily irradiance data for May 2016 CTG port

PVGIS-5 geo-temporal irradiation database

Provided inputs

Latitude/Longitude:	22.313, 91.808
Horizon:	Calculated
Database used	PVGIS-SARAH
Month:	May

Outline of horizon at chosen location:

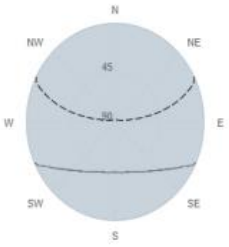

Daily average irradiance on fixed plane with slope 35° and azimuth 0°

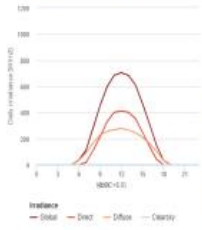

Irradiance on a fixed plane

Time	00:45	01:45	02:45	03:45	04:45	05:45	06:45	07:45	08:45	09:45	10:45	11:45	12:45	13:45	14:45	15:45	16:45	17:45	18:45	19:45	20:45	21:45	22:45	23:45
G(i)	0	0	0	0	0	0	37	111	281	453	598	684	704	684	612	469	312	148	35	0	0	0	0	0
Gb(i)	0	0	0	0	0	0	0	18	109	215	330	402	412	402	355	249	142	42	0	0	0	0	0	0
Gd(i)	0	0	0	0	0	0	36	90	166	229	256	269	278	269	245	211	164	103	34	0	0	0	0	0
Gcs(i)	0	0	0	0	0	0	0	0	0	0	0	0	0	0	0	0	0	0	0	0	0	0	0	0

G(i): Global irradiance on a fixed plane [W/m2].
Gb(i): Direct irradiance on a fixed plane [W/m2].
Gd(i): Diffuse irradiance on a fixed plane [W/m2].
Gcs(i): Global Clear-sky irradiance on a fixed plane [W/m2].

Daily average irradiance on sun-tracking plane

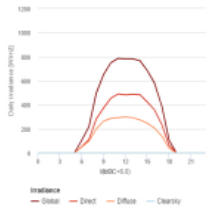

Irradiance on sun-tracking plane

Time	00:45	01:45	02:45	03:45	04:45	05:45	06:45	07:45	08:45	09:45	10:45	11:45	12:45	13:45	14:45	15:45	16:45	17:45	18:45	19:45	20:45	21:45	22:45	23:45
G(n)	0	0	0	0	0	0	104	218	496	650	750	786	782	782	767	686	581	391	106	0	0	0	0	0
Gb(n)	0	0	0	0	0	0	52	111	282	372	455	490	483	488	484	424	357	237	63	0	0	0	0	0
Gd(n)	0	0	0	0	0	0	48	98	199	264	287	293	299	292	275	248	207	141	39	0	0	0	0	0
Gcs(n)	0	0	0	0	0	0	0	0	0	0	0	0	0	0	0	0	0	0	0	0	0	0	0	0

G(n): Global irradiance on a 2-axis tracking plane [W/m2].
Gb(n): Direct normal irradiance [W/m2].
Gd(n): Diffuse irradiance on a 2-axis tracking plane [W/m2].
Gcs(n): Global Clear-sky irradiance on a 2-axis tracking plane [W/m2].

Daily average temperature

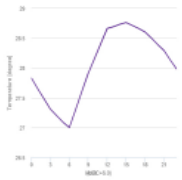

Daily average temperature

Time	00:45	01:45	02:45	03:45	04:45	05:45	06:45	07:45	08:45	09:45	10:45	11:45	12:45	13:45	14:45	15:45	16:45	17:45	18:45	19:45	20:45	21:45	22:45	23:45
T2m	27.83	27.65	27.48	27.31	27.2	27.09	27	27.3	27.61	27.91	28.16	28.41	28.66	28.69	28.73	28.76	28.71	28.66	28.6	28.5	28.39	28.29	28.13	27.98

T2m: Daily average temperature [°C].

Report generated on 2021/05/19

5. PV-GIS SARAH daily irradiance data June 2016 Chittagong port

PVGIS-5 geo-temporal irradiation database

Provided inputs

Latitude/Longitude:	22.313, 91.808
Horizon:	Calculated
Database used	PVGIS-SARAH
Month:	June

Outline of horizon at chosen location:

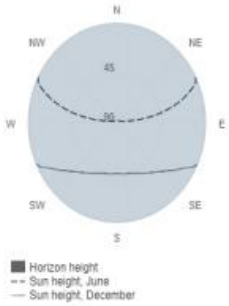

Daily average irradiance on fixed plane with slope 35° and azimuth 0°

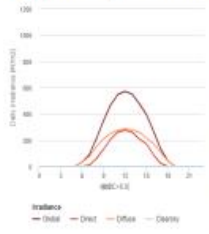

Irradiance on a fixed plane

Time	00:45	01:45	02:45	03:45	04:45	05:45	06:45	07:45	08:45	09:45	10:45	11:45	12:45	13:45	14:45	15:45	16:45	17:45	18:45	19:45	20:45	21:45	22:45	23:45
G(i)	0	0	0	0	0	0	33	88	211	348	469	548	572	550	478	396	267	133	42	0	0	0	0	0
Gb(i)	0	0	0	0	0	0	0	9	58	131	207	261	274	261	209	170	89	23	0	0	0	0	0	0
Gd(i)	0	0	0	0	0	0	32	77	149	209	251	275	285	278	259	217	172	107	41	0	0	0	0	0
Gcs(i)	0	0	0	0	0	0	0	0	0	0	0	0	0	0	0	0	0	0	0	0	0	0	0	0

G(i): Global irradiance on a fixed plane [W/m2].
Gb(i): Direct irradiance on a fixed plane [W/m2].
Gd(i): Diffuse irradiance on a fixed plane [W/m2].

Daily average irradiance on sun-tracking plane

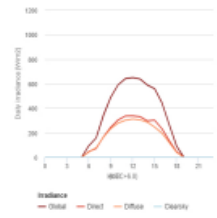

Irradiance on sun-tracking plane

Time	00:45	01:45	02:45	03:45	04:45	05:45	06:45	07:45	08:45	09:45	10:45	11:45	12:45	13:45	14:45	15:45	16:45	17:45	18:45	19:45	20:45	21:45	22:45	23:45
G(n)	0	0	0	0	0	0	94	158	344	490	590	641	650	638	589	559	444	266	92	0	0	0	0	0
Gb(n)	0	0	0	0	0	0	47	72	167	246	305	337	338	331	297	302	233	135	47	0	0	0	0	0
Gd(n)	0	0	0	0	0	0	43	78	165	234	279	302	312	305	286	246	197	120	41	0	0	0	0	0
Gcs(n)	0	0	0	0	0	0	0	0	0	0	0	0	0	0	0	0	0	0	0	0	0	0	0	0

G(n): Global irradiance on a 2-axis tracking plane [W/m2].
Gb(n): Direct normal irradiance [W/m2].
Gd(n): Diffuse irradiance on a 2-axis tracking plane [W/m2].
Gcs(n): Global Clear-sky irradiance on a 2-axis tracking plane [W/m2].

Daily average temperature

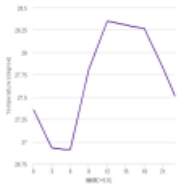

Daily average temperature

Time	00:45	01:45	02:45	03:45	04:45	05:45	06:45	07:45	08:45	09:45	10:45	11:45	12:45	13:45	14:45	15:45	16:45	17:45	18:45	19:45	20:45	21:45	22:45	23:45
T2m	27.36	27.22	27.07	26.93	26.92	26.91	26.91	27.21	27.51	27.81	27.99	28.17	28.35	28.34	28.32	28.31	28.29	28.28	28.27	28.12	27.98	27.83	27.67	27.51

T2m: Daily average temperature [°C].

Joint Research Centre

Report generated on 2021/05/19

6. PV-GIS SARAH daily irradiance data July 2016 Chittagong port

PVGIS-5 geo-temporal irradiation database

Provided inputs

Latitude/Longitude:	22.313, 91.808
Horizon:	Calculated
Database used	PVGIS-SARAH
Month:	July

Outline of horizon at chosen location:

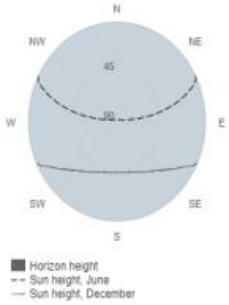

Daily average irradiance on fixed plane with slope 35° and azimuth 0°

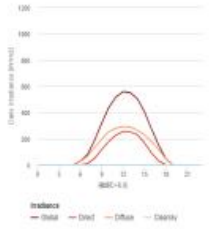

Irradiance on a fixed plane

Time	00:45	01:45	02:45	03:45	04:45	05:45	06:45	07:45	08:45	09:45	10:45	11:45	12:45	13:45	14:45	15:45	16:45	17:45	18:45	19:45	20:45	21:45	22:45	23:45
G(i)	0	0	0	0	0	0	28	78	189	319	439	518	558	551	504	405	271	149	46	0	0	0	0	0
Gb(i)	0	0	0	0	0	0	0	9	51	116	178	227	254	252	230	168	88	29	0	0	0	0	0	0
Gd(i)	0	0	0	0	0	0	28	67	134	196	252	280	293	288	264	229	177	116	45	0	0	0	0	0
Gcs(i)	0	0	0	0	0	0	0	0	0	0	0	0	0	0	0	0	0	0	0	0	0	0	0	0

G(i): Global irradiance on a fixed plane [W/m2].
Gb(i): Direct irradiance on a fixed plane [W/m2].
Gd(i): Diffuse irradiance on a fixed plane [W/m2].
Gcs(i): Global Clear-sky irradiance on a fixed plane [W/m2].

Daily average irradiance on sun-tracking plane

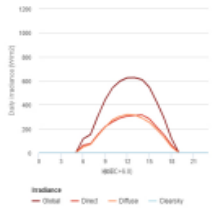

Irradiance on sun-tracking plane

Time	00:45	01:45	02:45	03:45	04:45	05:45	06:45	07:45	08:45	09:45	10:45	11:45	12:45	13:45	14:45	15:45	16:45	17:45	18:45	19:45	20:45	21:45	22:45	23:45
G(n)	0	0	0	0	0	0	115	151	305	443	541	597	625	626	610	546	422	288	119	0	0	0	0	0
Gb(n)	0	0	0	0	0	0	64	75	151	218	259	289	306	311	315	282	214	149	65	0	0	0	0	0
Gd(n)	0	0	0	0	0	0	48	69	144	214	275	305	319	314	289	253	195	128	49	0	0	0	0	0
Gcs(n)	0	0	0	0	0	0	0	0	0	0	0	0	0	0	0	0	0	0	0	0	0	0	0	0

G(n): Global irradiance on a 2-axis tracking plane [W/m2].
Gb(n): Direct normal irradiance [W/m2].
Gd(n): Diffuse irradiance on a 2-axis tracking plane [W/m2].
Gcs(n): Global Clear-sky irradiance on a 2-axis tracking plane [W/m2].

Daily average temperature

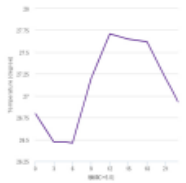

Daily average temperature

Time	00:45	01:45	02:45	03:45	04:45	05:45	06:45	07:45	08:45	09:45	10:45	11:45	12:45	13:45	14:45	15:45	16:45	17:45	18:45	19:45	20:45	21:45	22:45	23:45
T2m	26.8	26.69	26.58	26.47	26.47	26.47	26.46	26.71	26.95	27.2	27.37	27.54	27.71	27.69	27.67	27.65	27.64	27.63	27.62	27.48	27.34	27.2	27.07	26.93

T2m: Daily average temperature [°C].

Joint Research Centre

Report generated on 2021/05/19

7. PV-GIS SARAH daily irradiance data August 2016 Ctg port

PVGIS-5 geo-temporal irradiation database

Provided inputs

Latitude/Longitude:	22.313, 91.808
Horizon:	Calculated
Database used	PVGIS-SARAH
Month:	August

Outline of horizon at chosen location:

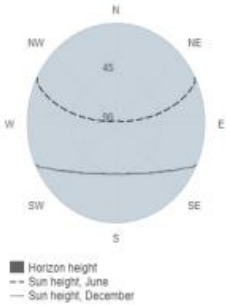

Daily average irradiance on fixed plane with slope 35° and azimuth 0°

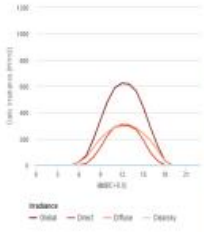

Irradiance on a fixed plane

Time	00:45	01:45	02:45	03:45	04:45	05:45	06:45	07:45	08:45	09:45	10:45	11:45	12:45	13:45	14:45	15:45	16:45	17:45	18:45	19:45	20:45	21:45	22:45	23:45
G(i)	0	0	0	0	0	0	23	72	195	342	485	588	623	617	563	439	285	147	35	0	0	0	0	0
Gb(i)	0	0	0	0	0	0	0	11	59	133	226	291	297	297	271	189	94	32	0	0	0	0	0	0
Gd(i)	0	0	0	0	0	0	22	60	132	202	250	285	314	308	281	241	186	111	34	0	0	0	0	0
Gcs(i)	0	0	0	0	0	0	0	0	0	0	0	0	0	0	0	0	0	0	0	0	0	0	0	0

G(i): Global irradiance on a fixed plane [W/m2].
Gb(i): Direct irradiance on a fixed plane [W/m2].
Gd(i): Diffuse irradiance on a fixed plane [W/m2].
Gcs(i): Global Clear-sky irradiance on a fixed plane [W/m2].

Daily average irradiance on sun-tracking plane

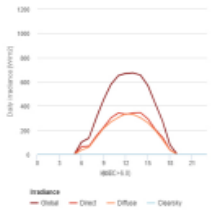

Irradiance on sun-tracking plane

Time	00:45	01:45	02:45	03:45	04:45	05:45	06:45	07:45	08:45	09:45	10:45	11:45	12:45	13:45	14:45	15:45	16:45	17:45	18:45	19:45	20:45	21:45	22:45	23:45
G(n)	0	0	0	0	0	0	102	134	301	452	579	651	669	673	655	569	420	275	79	0	0	0	0	0
Gb(n)	0	0	0	0	0	0	63	68	151	224	302	342	332	341	345	294	207	141	40	0	0	0	0	0
Gd(n)	0	0	0	0	0	0	36	60	139	217	269	306	335	329	303	262	200	123	35	0	0	0	0	0
Gcs(n)	0	0	0	0	0	0	0	0	0	0	0	0	0	0	0	0	0	0	0	0	0	0	0	0

G(n): Global irradiance on a 2-axis tracking plane [W/m2].
Gb(n): Direct normal irradiance [W/m2].
Gd(n): Diffuse irradiance on a 2-axis tracking plane [W/m2].
Gcs(n): Global Clear-sky irradiance on a 2-axis tracking plane [W/m2].

Daily average temperature

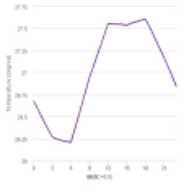

Daily average temperature

Time	00:45	01:45	02:45	03:45	04:45	05:45	06:45	07:45	08:45	09:45	10:45	11:45	12:45	13:45	14:45	15:45	16:45	17:45	18:45	19:45	20:45	21:45	22:45	23:45
T2m	26.68	26.54	26.4	26.27	26.24	26.22	26.21	26.45	26.7	26.95	27.15	27.35	27.56	27.55	27.55	27.54	27.57	27.59	27.61	27.47	27.32	27.17	27.01	26.84

T2m: Daily average temperature [°C].

Report generated on 2021/05/19

8. PV-GIS SARAH daily irradiance data September 2016 Ctg port

PVGIS-5 geo-temporal irradiation database

Provided inputs

Latitude/Longitude:	22.313, 91.808
Horizon:	Calculated
Database used	PVGIS-SARAH
Month:	September

Outline of horizon at chosen location:

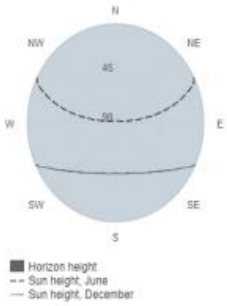

Daily average irradiance on fixed plane with slope 35° and azimuth 0°

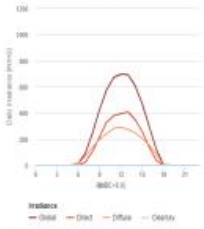

Irradiance on a fixed plane

Time	00:45	01:45	02:45	03:45	04:45	05:45	06:45	07:45	08:45	09:45	10:45	11:45	12:45	13:45	14:45	15:45	16:45	17:45	18:45	19:45	20:45	21:45	22:45	23:45
G(i)	0	0	0	0	0	0	15	90	245	425	579	672	696	692	608	471	292	118	4	0	0	0	0	0
Gb(i)	0	0	0	0	0	0	0	23	103	218	329	379	393	407	349	257	135	36	0	0	0	0	0	0
Gd(i)	0	0	0	0	0	0	14	65	137	199	240	281	291	273	248	205	152	80	4	0	0	0	0	0
Gcs(i)	0	0	0	0	0	0	0	0	0	0	0	0	0	0	0	0	0	0	0	0	0	0	0	0

G(i): Global irradiance on a fixed plane [W/m2].
Gb(i): Direct irradiance on a fixed plane [W/m2].
Gd(i): Diffuse irradiance on a fixed plane [W/m2].
Gcs(i): Global Clear-sky irradiance on a fixed plane [W/m2].

Daily average irradiance on sun-tracking plane

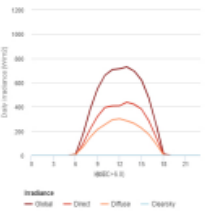

Irradiance on sun-tracking plane

Time	00:45	01:45	02:45	03:45	04:45	05:45	06:45	07:45	08:45	09:45	10:45	11:45	12:45	13:45	14:45	15:45	16:45	17:45	18:45	19:45	20:45	21:45	22:45	23:45
G(n)	0	0	0	0	0	0	10	170	380	550	659	706	713	729	694	620	471	251	12	0	0	0	0	0
Gb(n)	0	0	0	0	0	0	0	94	217	321	395	407	408	438	420	380	284	149	8	0	0	0	0	0
Gd(n)	0	0	0	0	0	0	8	68	150	215	254	293	301	284	263	224	172	93	4	0	0	0	0	0
Gcs(n)	0	0	0	0	0	0	0	0	0	0	0	0	0	0	0	0	0	0	0	0	0	0	0	0

G(n): Global irradiance on a 2-axis tracking plane [W/m2].
Gb(n): Direct normal irradiance [W/m2].
Gd(n): Diffuse irradiance on a 2-axis tracking plane [W/m2].
Gcs(n): Global Clear-sky irradiance on a 2-axis tracking plane [W/m2].

Daily average temperature

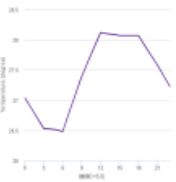

Daily average temperature

Time	00:45	01:45	02:45	03:45	04:45	05:45	06:45	07:45	08:45	09:45	10:45	11:45	12:45	13:45	14:45	15:45	16:45	17:45	18:45	19:45	20:45	21:45	22:45	23:45
T2m	27.04	26.87	26.7	26.53	26.52	26.51	26.48	26.79	27.09	27.39	27.64	27.88	28.12	28.1	28.09	28.07	28.07	28.07	28.07	27.9	27.74	27.58	27.4	27.22

T2m: Daily average temperature [°C].

Report generated on 2021/05/19

9. PV-GIS SARAH daily irradiance data October 2016 Ctg port

PVGIS-5 geo-temporal irradiation database

Provided inputs

Latitude/Longitude:	22.313, 91.808
Horizon:	Calculated
Database used	PVGIS-SARAH
Month:	October

Outline of horizon at chosen location:

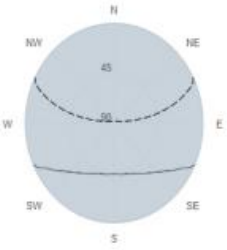

Daily average irradiance on fixed plane with slope 35° and azimuth 0°

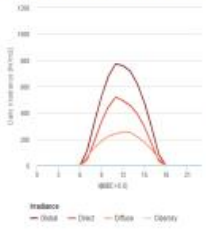

Irradiance on a fixed plane

Time	00:45	01:45	02:45	03:45	04:45	05:45	06:45	07:45	08:45	09:45	10:45	11:45	12:45	13:45	14:45	15:45	16:45	17:45	18:45	19:45	20:45	21:45	22:45	23:45
G(i)	0	0	0	0	0	0	1	111	323	522	682	771	758	717	621	478	292	85	0	0	0	0	0	0
Gb(i)	0	0	0	0	0	0	0	43	183	332	448	519	492	456	393	295	165	34	0	0	0	0	0	0
Gd(i)	0	0	0	0	0	0	1	66	135	182	223	240	254	250	218	176	123	49	0	0	0	0	0	0
Gcs(i)	0	0	0	0	0	0	0	0	0	0	0	0	0	0	0	0	0	0	0	0	0	0	0	0

G(i): Global irradiance on a fixed plane [W/m2].
Gb(i): Direct irradiance on a fixed plane [W/m2].
Gd(i): Diffuse irradiance on a fixed plane [W/m2].
Gcs(i): Global Clear-sky irradiance on a fixed plane [W/m2].

Daily average irradiance on sun-tracking plane

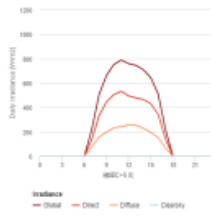

Irradiance on sun-tracking plane

Time	00:45	01:45	02:45	03:45	04:45	05:45	06:45	07:45	08:45	09:45	10:45	11:45	12:45	13:45	14:45	15:45	16:45	17:45	18:45	19:45	20:45	21:45	22:45	23:45
G(n)	0	0	0	0	0	0	0	216	505	662	752	788	760	745	708	644	510	212	0	0	0	0	0	0
Gb(n)	0	0	0	0	0	0	0	134	332	447	505	533	494	479	465	430	344	140	0	0	0	0	0	0
Gd(n)	0	0	0	0	0	0	0	75	157	198	232	244	256	254	228	196	151	66	0	0	0	0	0	0
Gcs(n)	0	0	0	0	0	0	0	0	0	0	0	0	0	0	0	0	0	0	0	0	0	0	0	0

G(n): Global irradiance on a 2-axis tracking plane [W/m2].
Gb(n): Direct normal irradiance [W/m2].
Gd(n): Diffuse irradiance on a 2-axis tracking plane [W/m2].
Gcs(n): Global Clear-sky irradiance on a 2-axis tracking plane [W/m2].

Daily average temperature

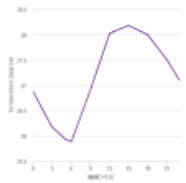

Daily average temperature

Time	00:45	01:45	02:45	03:45	04:45	05:45	06:45	07:45	08:45	09:45	10:45	11:45	12:45	13:45	14:45	15:45	16:45	17:45	18:45	19:45	20:45	21:45	22:45	23:45
T2m	26.88	26.64	26.4	26.17	26.06	25.94	25.88	26.22	26.57	26.91	27.28	27.65	28.02	28.08	28.13	28.18	28.12	28.06	28	27.83	27.67	27.5	27.3	27.09

T2m: Daily average temperature [°C].

Report generated on 2021/05/19

10. PV-GIS SARAH daily irradiance data November 2016 Ctg port

PVGIS-5 geo-temporal irradiation database

Provided inputs

Latitude/Longitude:	22.313, 91.808
Horizon:	Calculated
Database used	PVGIS-SARAH
Month:	November

Outline of horizon at chosen location:

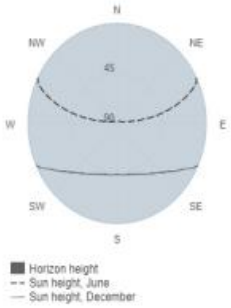

Daily average irradiance on fixed plane with slope 35° and azimuth 0°

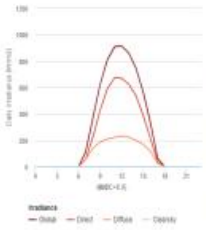

Irradiance on a fixed plane

Time	00:45	01:45	02:45	03:45	04:45	05:45	06:45	07:45	08:45	09:45	10:45	11:45	12:45	13:45	14:45	15:45	16:45	17:45	18:45	19:45	20:45	21:45	22:45	23:45
G(i)	0	0	0	0	0	0	0	115	370	623	810	908	914	859	745	565	335	64	0	0	0	0	0	0
Gb(i)	0	0	0	0	0	0	0	58	225	428	590	673	669	624	537	388	213	36	0	0	0	0	0	0
Gd(i)	0	0	0	0	0	0	0	56	141	187	209	222	231	223	199	170	118	27	0	0	0	0	0	0
Gcs(i)	0	0	0	0	0	0	0	0	0	0	0	0	0	0	0	0	0	0	0	0	0	0	0	0

G(i): Global irradiance on a fixed plane [W/m2].
Gb(i): Direct irradiance on a fixed plane [W/m2].
Gd(i): Diffuse irradiance on a fixed plane [W/m2].
Gcs(i): Global Clear-sky irradiance on a fixed plane [W/m2].

Daily average irradiance on sun-tracking plane

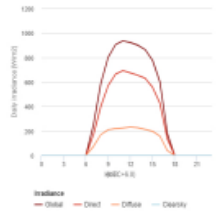

Irradiance on sun-tracking plane

Time	00:45	01:45	02:45	03:45	04:45	05:45	06:45	07:45	08:45	09:45	10:45	11:45	12:45	13:45	14:45	15:45	16:45	17:45	18:45	19:45	20:45	21:45	22:45	23:45
G(n)	0	0	0	0	0	0	0	245	584	802	905	936	923	901	865	776	601	178	0	0	0	0	0	0
Gb(n)	0	0	0	0	0	0	0	167	398	570	664	693	674	655	631	557	428	135	0	0	0	0	0	0
Gd(n)	0	0	0	0	0	0	0	72	169	210	220	225	231	227	213	198	157	40	0	0	0	0	0	0
Gcs(n)	0	0	0	0	0	0	0	0	0	0	0	0	0	0	0	0	0	0	0	0	0	0	0	0

G(n): Global irradiance on a 2-axis tracking plane [W/m2].
Gb(n): Direct normal irradiance [W/m2].
Gd(n): Diffuse irradiance on a 2-axis tracking plane [W/m2].
Gcs(n): Global Clear-sky irradiance on a 2-axis tracking plane [W/m2].

Daily average temperature

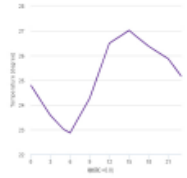

Daily average temperature

Time	00:45	01:45	02:45	03:45	04:45	05:45	06:45	07:45	08:45	09:45	10:45	11:45	12:45	13:45	14:45	15:45	16:45	17:45	18:45	19:45	20:45	21:45	22:45	23:45
T2m	24.8	24.39	23.98	23.58	23.3	23.02	22.87	23.34	23.8	24.27	25.01	25.75	26.49	26.66	26.83	27.01	26.79	26.58	26.37	26.2	26.03	25.86	25.51	25.15

T2m: Daily average temperature [°C].

Joint Research Centre

Report generated on 2021/05/19

11. PV-GIS SARAH daily irradiance data December 2016 Ctg port

PVGIS-5 geo-temporal irradiation database

Provided inputs

Latitude/Longitude:	22.313, 91.808
Horizon:	Calculated
Database used	PVGIS-SARAH
Month:	December

Outline of horizon at chosen location:

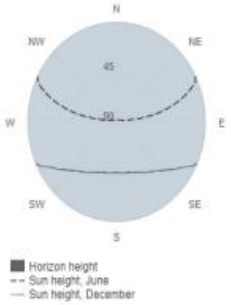

Daily average irradiance on fixed plane with slope 35° and azimuth 0°

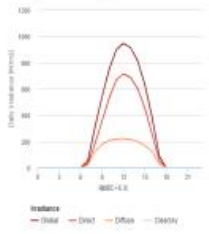

Irradiance on a fixed plane

Time	00:45	01:45	02:45	03:45	04:45	05:45	06:45	07:45	08:45	09:45	10:45	11:45	12:45	13:45	14:45	15:45	16:45	17:45	18:45	19:45	20:45	21:45	22:45	23:45
G(i)	0	0	0	0	0	0	0	52	305	539	748	899	947	913	811	629	385	87	0	0	0	0	0	0
Gb(i)	0	0	0	0	0	0	0	30	180	355	531	669	713	686	601	452	257	55	0	0	0	0	0	0
Gd(i)	0	0	0	0	0	0	0	22	122	178	207	218	221	215	199	169	123	31	0	0	0	0	0	0
Gcs(i)	0	0	0	0	0	0	0	0	0	0	0	0	0	0	0	0	0	0	0	0	0	0	0	0

G(i): Global irradiance on a fixed plane [W/m2].
Gb(i): Direct irradiance on a fixed plane [W/m2].
Gd(i): Diffuse irradiance on a fixed plane [W/m2].
Gcs(i): Global Clear-sky irradiance on a fixed plane [W/m2].

Daily average irradiance on sun-tracking plane

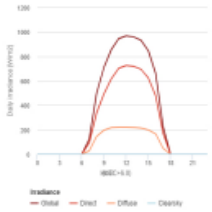

Irradiance on sun-tracking plane

Time	00:45	01:45	02:45	03:45	04:45	05:45	06:45	07:45	08:45	09:45	10:45	11:45	12:45	13:45	14:45	15:45	16:45	17:45	18:45	19:45	20:45	21:45	22:45	23:45
G(n)	0	0	0	0	0	0	0	122	497	711	857	946	967	960	932	846	659	223	0	0	0	0	0	0
Gb(n)	0	0	0	0	0	0	0	93	338	494	617	703	725	719	695	624	478	171	0	0	0	0	0	0
Gd(n)	0	0	0	0	0	0	0	27	146	197	218	222	222	219	214	199	165	48	0	0	0	0	0	0
Gcs(n)	0	0	0	0	0	0	0	0	0	0	0	0	0	0	0	0	0	0	0	0	0	0	0	0

G(n): Global irradiance on a 2-axis tracking plane [W/m2].
Gb(n): Direct normal irradiance [W/m2].
Gd(n): Diffuse irradiance on a 2-axis tracking plane [W/m2].
Gcs(n): Global Clear-sky irradiance on a 2-axis tracking plane [W/m2].

Daily average temperature

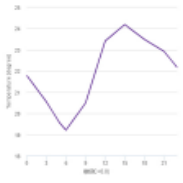

Daily average temperature

Time	00:45	01:45	02:45	03:45	04:45	05:45	06:45	07:45	08:45	09:45	10:45	11:45	12:45	13:45	14:45	15:45	16:45	17:45	18:45	19:45	20:45	21:45	22:45	23:45
T2m	21.79	21.38	20.96	20.55	20.06	19.57	19.21	19.64	20.06	20.49	21.47	22.44	23.41	23.67	23.83	24.19	23.95	23.72	23.49	23.3	23.11	22.92	22.55	22.17

T2m: Daily average temperature [°C].

Report generated on 2021/05/19

12. PV-GIS SARAH daily irradiance data January 2016 Ctg port

PVGIS-5 geo-temporal irradiation database

Provided inputs

Latitude/Longitude:	22.313, 91.808
Horizon:	Calculated
Database used	PVGIS-SARAH
Month:	January

Outline of horizon at chosen location:

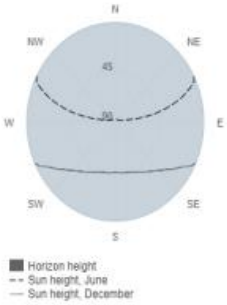

Daily average irradiance on fixed plane with slope 35° and azimuth 0°

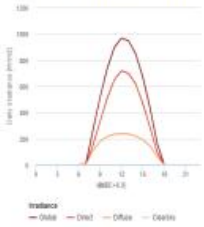

Irradiance on a fixed plane

Time	00:45	01:45	02:45	03:45	04:45	05:45	06:45	07:45	08:45	09:45	10:45	11:45	12:45	13:45	14:45	15:45	16:45	17:45	18:45	19:45	20:45	21:45	22:45	23:45
G(i)	0	0	0	0	0	0	0	6	263	515	735	895	968	947	848	669	440	166	0	0	0	0	0	0
Gb(i)	0	0	0	0	0	0	0	3	149	330	508	649	718	698	617	468	289	98	0	0	0	0	0	0
Gd(i)	0	0	0	0	0	0	0	2	111	179	217	234	237	236	219	193	145	66	0	0	0	0	0	0
Gcs(i)	0	0	0	0	0	0	0	0	0	0	0	0	0	0	0	0	0	0	0	0	0	0	0	0

G(i): Global irradiance on a fixed plane [W/m2].
Gb(i): Direct irradiance on a fixed plane [W/m2].
Gd(i): Diffuse irradiance on a fixed plane [W/m2].
Gcs(i): Global Clear-sky irradiance on a fixed plane [W/m2].

Daily average irradiance on sun-tracking plane

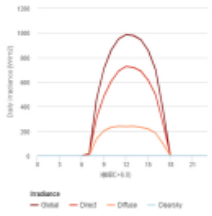

Irradiance on sun-tracking plane

Time	00:45	01:45	02:45	03:45	04:45	05:45	06:45	07:45	08:45	09:45	10:45	11:45	12:45	13:45	14:45	15:45	16:45	17:45	18:45	19:45	20:45	21:45	22:45	23:45
G(n)	0	0	0	0	0	0	0	16	459	708	861	950	984	978	944	856	700	373	0	0	0	0	0	0
Gb(n)	0	0	0	0	0	0	0	14	309	484	607	689	726	718	690	614	496	266	0	0	0	0	0	0
Gd(n)	0	0	0	0	0	0	0	2	137	203	232	240	238	239	231	219	185	99	0	0	0	0	0	0
Gcs(n)	0	0	0	0	0	0	0	0	0	0	0	0	0	0	0	0	0	0	0	0	0	0	0	0

G(n): Global irradiance on a 2-axis tracking plane [W/m2].
Gb(n): Direct normal irradiance [W/m2].
Gd(n): Diffuse irradiance on a 2-axis tracking plane [W/m2].
Gcs(n): Global Clear-sky irradiance on a 2-axis tracking plane [W/m2].

Daily average temperature

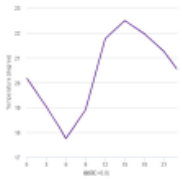

Daily average temperature

Time	00:45	01:45	02:45	03:45	04:45	05:45	06:45	07:45	08:45	09:45	10:45	11:45	12:45	13:45	14:45	15:45	16:45	17:45	18:45	19:45	20:45	21:45	22:45	23:45
T2m	20.18	19.8	19.41	19.03	18.61	18.2	17.75	18.13	18.52	18.9	19.85	20.8	21.75	22	22.24	22.49	22.31	22.14	21.96	21.72	21.49	21.25	20.9	20.54

T2m: Daily average temperature [°C].

Report generated on 2021/05/19